

Doctoral Thesis

Functionalized biodegradable co-polyesters for medical applications

Funkcionalizované biologicky rozložitelné kopolyestery pro lékařské aplikace

Author: **M.E. Maliheh Amini Moghaddam**

Degree programme: P2808 Chemistry and Materials Technology

Degree course: 2808v006 Technology of Macromolecular Compounds

Supervisor: Prof. Ing. Vladimír Sedlařík, Ph.D.

Zlín, March 2021

© Maliheh Amini Moghaddam

Published by **Tomas Bata University in Zlín** in the Edition **Doctoral Thesis**.
The publication was issued in the year 2021.

Key words: polyesters, biodegradable polymers, medical application, modification, porous materials, polylactic acid.

Klíčová slova: polyester, biodegradovatelné polymery, aplikace v medicince, modifikace, porézní materiály, polylaktid.

Full text of the doctoral thesis is available in the Library of TBU in Zlín

ISBN 978-80-.....

TABLE OF CONTENT

ABSTRACT	6
ABSTRAKT	6
INTRODUCTION	7
1. THEORETICAL BACKGROUND	8
1.1. BIODEGRADABLE POLYESTERS	8
1.1.1. Aliphatic polyesters	8
1.1.2. Aromatic polyesters.....	15
1.2. BIODEGRADATION ROUTES OF POLYESTERS	15
1.3. MODIFICATIONS OF BIODEGRADABLE POLYESTERS	18
1.3.1. Bulk modifications of polyesters.....	18
1.3.2. Surface modifications of polyesters	19
1.4. APPLICATIONS OF BIODEGRADABLE POLYESTERS	21
1.4.1. Biomedical applications	22
1.4.2. Non-biomedical applications.....	28
AIMS OF WORK.....	30
2. EXPERIMENTAL PART	31
2.1. Preparation and characterization of microcellular antibacterial polylactide-based systems prepared by additive extrusion with ALUM	31
2.2. Preparation and characterization of polylactide-based porous systems mat for wound dressing application	47
SUMMARY OF WORK	64
CONTRIBUTION TO SCIENCE AND PRACTICE	65
REFERENCES	66
LIST OF FIGURES	74
LIST OF TABELS.....	76
LIST OF SYMBOLS AND ABBREVIATIONS.....	77
CURRICULUM VITAE	79
LIST OF PUBLICATIONS.....	81

ACKNOWLEDGEMENTS

With many thanks to my supervisor prof. Vladimír Sedlařík for his guidance during this research.

To all people from Tomas Bata University and people from my internship in Australia, Monash University who helped me during this journey.

To my parents and brothers, without their supports and everlasting encouragement, I could not have completed my Ph.D.

DEDICATION

To my parents and my brothers.

To Ph.D. students in flight (ps752) who were unable to defend their doctoral dissertation. Rest in peace.

ABSTRACT

This doctoral thesis is aimed at development and characterizations of novel biodegradable polylactid acid based systems for medical applications. The first part of this work is dedicated to preparation and characterization of novel biodegradable micro structured antibacterial systems where the antibacterial activity of the prepared materials was ensured by incorporation of the inorganic additive based on double sulfates of aluminium. The second part is focused on preparation and characterization of 3D polymer structures. The antibiotic gentamicin sulfate was used as model bioactive agent suitable for wound dressing applications. Both experimental parts were also comprised of the detailed structural and degradation studies that bring novel insights into the field of biodegradable polyesters medical research.

ABSTRAKT

Tato disertační práce je zaměřena na vývoj a charakterizaci nových biologicky odbouratelných systémů na bázi kyseliny polymléčné pro lékařské aplikace. První část této práce je věnována přípravě a charakterizaci mikrostrukturovaných antibakteriálních systémů, kde byla antibakteriální aktivita připravených materiálů zprostředkována pomocí anorganického aditiva na bázi hlinitých podvojných solí kyseliny sírové. Druhá část je zaměřena na přípravu a charakterizaci 3D polymerních struktur pro krytí ran. Jako modelovou bioaktivní látku bylo použito antibiotikum gentamicin sulfát. Obě experimentální studie obsahují detailní popis strukturních a degradačních vlastností vyvinutých systémů a přináší tak nové poznatky do oblasti materiálového výzkumu biorozložitelných polyesterů pro medicínské aplikace.

INTRUDUCTION

Aliphatic polyesters were firstly used in medical applications as sutures in 1971. Since then, research in biodegradable aliphatic polyesters has gained considerable attention due to the increasingly attractive biomedical, environmental, and agricultural applications [1]. Especially, biodegradable polyesters have highly desirable applications due to their biocompatibility, biodegradability and bioresorbability properties in biomedical areas, such as pharmaceutical industry and tissue engineering scaffolds. All these applications mainly rely on the fact that the polymers ultimately disappear after providing the desired functionalities. In this respect, the mechanism of polyesters' degradation and erosion in aqueous media has drawn great attention [2, 3]. Although, polyesters combine relatively intrinsic properties (as mentioned above) with easy synthetic methods and acceptable production costs, they often have poor mechanical and physical properties. Therefore, augmented mechanical and physical properties can be achieved by tailoring the chemistry of polyesters [4, 5]. Modification is one of the promising ways to enhance the mechanical properties and improve the capabilities of existing biodegradable polyesters for desired biomedical applications [4].

The presented thesis is devoted to the preparation of biodegradable aliphatic polyesters and biopolymers for biomedical applications. The first section summarizes the development of microcellular antibacterial polylactide-based systems prepared by additive extrusion with ALUM. The second section focuses on polylactide-polyvinyl alcohol-based porous systems loaded with gentamicin for wound dressing applications.

1. THEORETICAL BACKGROUND

1.1. BIODEGRADABLE POLYESTERS

The term polyester refers to a polymer containing repeated units of ester within its backbone. They can be obtained by different types of reactions. However, polyesterifications between diols and dibasic acids are the most important types of reactions [6]. Ester functional groups are involved in the main chain or through a short side-chain [7]. Their general formula is:

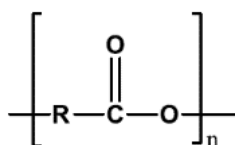


Figure 1. Scheme of chemical structure of ester group [7].

In most cases, polyester is synthesized by either polycondensation or by ring-opening polymerization. Each method gives different degrees of molecular weight, stereochemical structure, and molecular weight distribution. Polyesters produced by polycondensation show poor control of molecular weight, and broad polydispersity index. Nevertheless, the low-price of production, low sensitivity to water and air and eco-friendly experimental conditions make this method favourable. High-molecular weight with high crystallinity polyesters is synthesized by a catalytic ring-opening procedure. Besides, enzymatic and bacterial synthesis are available as well. For instance, polyhydroxyalkanoates (PHA) are a group of polyesters produced by microbial fermentation [5, 8-10].

1.1.1. Aliphatic polyesters

Aliphatic polyesters are mostly biodegradable and biocompatible, and some of them are bioresorbable. The bioresorbable was introduced to qualify compounds through elimination of degradation by-products by natural pathways (metabolization or kidney filtration). Hence, bioresorption is elimination of the initial foreign material with no residual side effects. Bioresorbable polyesters have benefits to certain medical applications. The polymers can be altered to degrade at a specified rate, useful in cases where the body needs temporary support in tissue healing [11-13].

Intrinsic properties of polyesters and their adjustable mechanical properties result in the broadening of their application in the biomedical field[8, 14-16]. Aliphatic polyesters mainly are high-melting and semicrystalline. Their physical properties mostly depend on the flexibility of the chain, degree of branching, the composition of repeat units, molecular mass, presence of polar groups, and crystallinity. The physical properties of aliphatic polyesters can be tailored by copolymerization, blending, and change in the macromolecular architecture [3]. In table 1., mechanical performance of cartilage, cardiovascular tissues, and bone, which have been treated with polyester-based implants, are summarized.

Table 1. Mechanical properties of the biodegradable polyesters and a few tissues and commercially available biomaterials [8].

Material	Type	Tensile modulus (E, MPa)	Ultimate tensile strength (σ_m , MPa)	Elongation at break (ϵ_m , %)	Reference
Tissues	Bone (Trabecular)	483	2	2.5	[17]
	Cartilage	10-100	210-40	15-20	[18]
	Cardiovascular	2-6	1	1200	[19]
Medical devices	Mg-based orthopaedic screw	Not reported	~200	~9	[20]
	suture	~850	~37	~70	[21]
	Medical mesh (Vicryl®)	4.6±0.6 (stiffness N/ mm)	78.2±10.5 (maximum force N/ cm)	150 ± 6	[22]
Polyesters	PGA	7000-8400	890	30	[23]
	PLGA(50:50)	~2000	63.6	3-10	[24, 25]
	PLA	3500	55	30-240	[26]
	PHB	3500	~40	5-8	[27]
	PPF	2000-3000	3-35	20.3	[28-30]
	PCL	~700	4-28	700-1000	[23, 24]
	PPC	830	21.5	330	[31]
	PBS	~700	~17.5	~6	[32]

Poly(lactic acid) (PLA)

Poly(lactic acid) is one of the most promising biodegradable, biocompatible, and bioresorbable aliphatic polyesters (Figure 2). PLA is synthesized from bio-based renewable resources such as corn, however, it can also be produced from petrochemicals. PLA is obtained by direct condensation, ring-opening polymerization and by direct methods like azeotropic dehydration and enzymatic through a lactide intermediate, as illustrated in Figure 3 [10, 14, 33-35].

As a bioabsorbable polymer, PLA has a proven potential to replace conventional petrochemical-based polymers for industrial applications [36]. PLA is a thermoplastic polyester which can be synthesized in either amorphous or crystalline form. This is caused by the stereoregularity of the monomer (lactic acid or cyclic dimer lactide), therefore there are 3 different PLA forms, PDLA, PLLA, and PDLLA. These three forms of PLA have different properties depending on their isomer composition. While PDLLA is completely amorphous, PLLA is a crystalline polymer. For example owing to crystallinity of poly(L-lactide) possesses better mechanical properties than poly(DL-lactide)[37, 38].

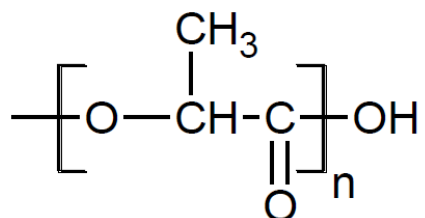


Figure 2 - Chemical structure of PLA [37]

Generally, PLA is a brittle and hard polymer with high mechanical properties and glass transition temperature between 55°C-65°C and a melting point around 160°C-170°C. It has low extension, good tensile strength, high modulus, which can also form high strength fibres. It degrades homogeneously by hydrolytic erosion as well as random scission of the ester linkages. The degradation time depends on the porosity, molecular weight, and crystallinity [7, 37].

PLA is considered a versatile polymer that has been used in numerous applications. In 1970, PLA based materials have been approved by US Food and Drug Administration (FDA) for direct contact with biological fluids and also for producing materials in contact with food [23, 39-41]. A variety of PLA blends have been employed for various biomedical applications such as drug delivery, sutures, implants, and tissue engineering.

PLA is also the only member of the polyester family that has been employed for load-bearing applications such as orthopedic plates and screws [8].

In addition, due to having a very favourable eco-friendly image and recycling, the rate of consumption is enhancing in environmental applications such as packaging and consumer goods [6, 15, 42]. Moreover, PLA becomes an adequate candidate for the application of packaging for short service life goods or fresh food, including lamination filming, overwrapping, and blister packaging [43]. The appropriate properties of PLA and the demand to find a commercially viable degradable plastics has led to the large-scale production of PLA for a broad range of compostable materials [23, 40, 41].

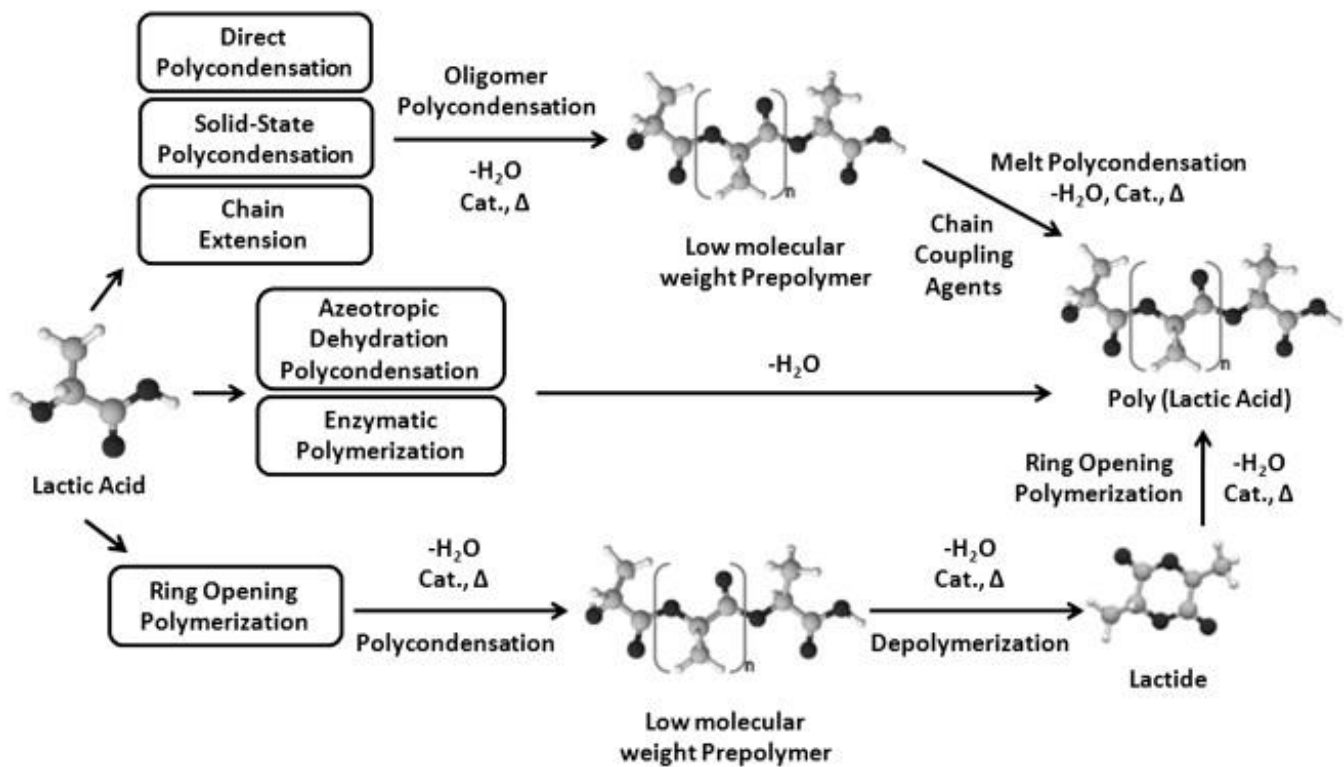


Figure 3. Main routes for the synthesis of PLA [14].

Polyglycolic acid (PGA)

PGA is the first biodegradable synthetic polymer employed in biomedical applications. It is biocompatible and bioresorbable aliphatic polyester which has gained FDA (US Food and Drug Administration) approval for clinical use (Figure 4). PGA is a hydrophobic polyester, highly crystalline, which has a high melting point and relatively

low solubility in organic solvents. It is degraded through bulk erosion with random hydrolysis of ester linkages. The hydrolysis starts by the amorphous phase, followed by the degradation of the crystallized section. Degradation products eventually eliminated from the body in the form of water and carbon dioxide [7, 28, 37, 44]

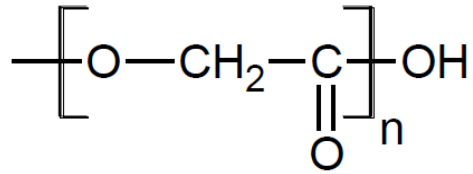


Figure 4 - Chemical structure of PGA [37].

Ring-opening polymerization of the cyclic diesters glycolide is most commonly used to synthesize high-molecular-weight PGA. However, the low-molecular-weight of PGA has also been synthesized by direct polycondensation in the presence of water [45].

PGA-based biomaterials are mainly used for the fabrication of absorbable sutures and drug delivery carriers due to its fast degradation in vivo. It is widely used as a polymer for scaffold due to relatively hydrophilic nature and also employed for tissue engineering [8, 28, 44].

Poly (lactic-co-glycolic acid) (PLGA)

The physical and mechanical properties of the PLGA are controlled by the comonomers (glycolide and lactide). Both the DL- and the L-lactides were employed for co-polymerization (Figure 5). Different ratio of monomers results in polyesters of tailor-made properties. While PLA and PGA tend to be crystalline, their copolymers are highly amorphous, owing to chain irregularity caused by the presence of a second component [7, 37].

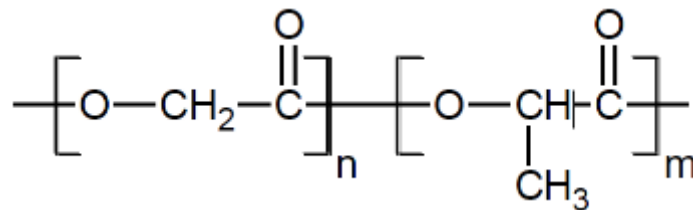


Figure 5 - Chemical structure of PLGA [7].

The PLGA undergo bulk erosion by hydrolysis of the ester bonds and degradation rate could be reduced by increasing the lactic acid ratio. It is interesting that, for instance, a copolymer containing DL-lactide and glycolide (1:1) degrades faster than either homopolymer [7, 37].

Indeed, PLGA has become a promising option for the production of absorbable medical devices, drug carriers, and drug-eluting stents, due to the excellent stents and drug carriers and compatibility with the human body [46].

Poly(ϵ -caprolactone) (PCL)

PCL is biodegradable petroleum-based polyester with a low glass transition temperature (T_g) of $-60\text{ }^\circ\text{C}$ and melting point ($60\text{ }^\circ\text{C}$). It is partially-crystalline with rubbery and highly processable structure (Figure 6); it dissolves in a broad range of organic solvents and can form miscible blends with a broad range of polymers. PCL is an interesting polyester as the monomer is cheap, it is synthesized by ring-opening polymerization of (ϵ -caprolactone) using a catalyst such as an octoate [7, 8, 37, 38, 47].

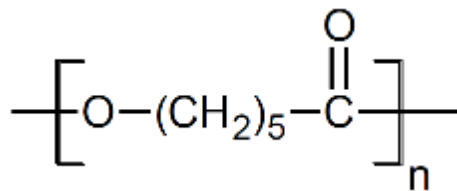


Figure 6 - Chemical structure of PCL [7]

The degradation occurs owing to the presence of a hydrolytically labile aliphatic ester bond, however, the degradation rate is slow. Moreover, the actions of the bacteria broadly distributed in the ecosystem highly impact the environmental degradation of PCL. Some published papers suggest that some yeasts and filamentous fungi can hydrolyse PCL into products that are soluble in water. For instance, according to the literature, *Pullularia pullulans* can effectively degrade the lower molecular weight of PCL film ($M_w=1,250$). However, the extent of the decomposition of a PCL film with M_w above 15,000 by the fungus was negligible. In order to efficiently degrade PCL with higher M_w s, *Penicillium sp.* yeast and strain can be used [7, 8, 47, 48].

PCL has been broadly considered for biomedical field including drug delivery and tissue engineering and it also has remarkable drug permeability. Its compatibility with a great number of drugs enables uniform drug distribution in the formulation matrix, and its long-term degradation takes several months. PCL was studied commonly for tissue engineering applications too, such as scaffold for bone tissue engineering [7, 8, 46, 47].

Poly(hydroxylalkanoates) (PHAs)

PHAs are synthetic biodegradable and biocompatible polyesters that can be chemically synthesized and, can also be biosynthesized with the fermentation of microorganisms (Figure 7) [8, 49, 50].

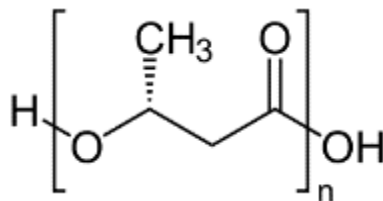


Figure 7 - Chemical structure of PHAs [50].

PHB and PHBV are the most researched forms of the PHA family for biomedical applications owing to their adjustable mechanical properties. The slower hydrolysis rates of microbially produced polyesters confirm that PHB and PHBV can be employed to extend the range of drug delivery systems. PHBV has been used for drug delivery both as microcapsules and as a tablet. Generally, PHAs have been used to develop various devices, such as cardiovascular patches, and orthopaedic pins, sutures, tendon, and articular cartilage, tissue engineered nerve, repair patches, and adhesion barriers [5, 8, 44].

The main limiting factors for the medical applications of the PHA family are 1) minimal cell interaction capacity, 2) low ultimate tensile strain. To tackle these issues, these polymers have been blended with numerous synthetic and other natural polymers [5, 8, 49].

The biodegradation of PHB and other PHA derivatives arises through the hydrolysis of the ester linkage. PHB degradation mechanisms are enzymatic or hydrolytic, and thermal. Hydrolytic degradation of PHB releases 3HB, which is a normal metabolite in human blood; hence, in the absence of endotoxin, the biodegradation of PHB produced by bacteria does not cause any physiological reaction [8, 50].

Polydioxanone (PDO)

PDO is poly(ether-ester), it is not a pure polyester (there is an ether bond in the main chain). PDO is a semi-crystalline polymer (up to 55%) with a melting point around $T_m \sim 60^\circ\text{C}$ and glass transition point $T_g \sim 0^\circ\text{C}$ [37] (Figure 8).

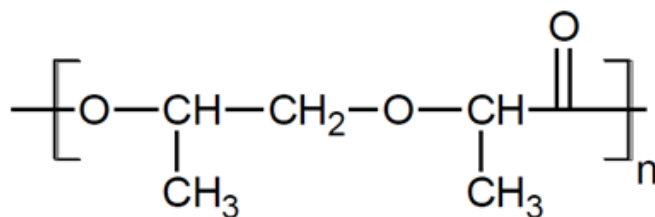


Figure 8 - Chemical structure of PDO [37].

PDO degradation is through non-specific scission of the ester backbone. Owing to the high hydrophobicity and crystallinity, it is a moderately degrading polymer. It is frequently used as a suture in surgical applications [7, 37].

1.1.2. Aromatic polyesters

This polyester group constitutes amorphous glass transition temperature (high- T_g) co-polyesters, entitled amorphous polyarylates, and semicrystalline polyesters that frequently show anisotropic liquid crystalline (LC) melts. Aromatic polyesters that do not have any flexible structure units are very high melting polymers or frequently nonmelttable, which cannot be processed. Wholly aromatic co-polyesters show excellent mechanical properties and heat resistance, therefore, they are used as high-performance thermoplastics.

Wholly aromatic liquid crystalline polyesters degrade at 450-550 °C by the homolytic scission of ester bonds and emit CO, CO₂, and phenol [6, 51, 52].

1.2. BIODEGRADABLE ROUTES OF POLYESTERS

Biodegradable polymers refer to polymers, which degrade in the biological environment, such as any condition where biochemical or biological processes take place, irrespective of the degradation mechanism [7]. The biodegradability of polymers depends mostly on its main chain structure and the presence of hydrolysable or oxidizable linkages. The concept of biodegradation is illustrated in Figure 9.

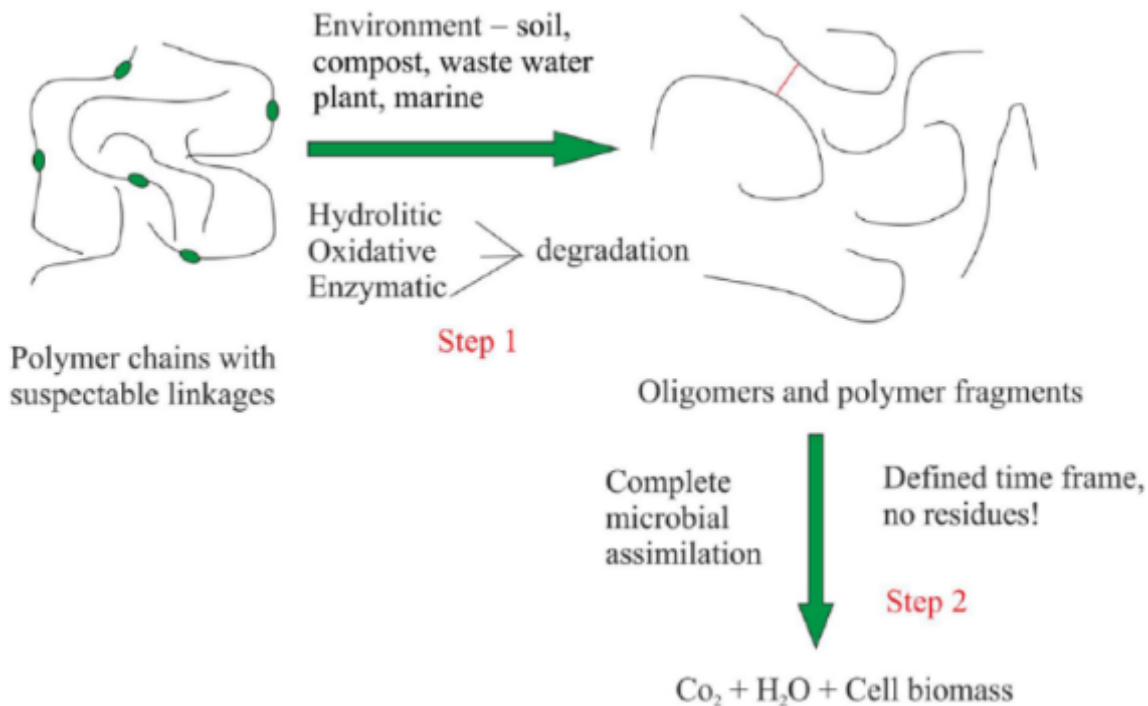


Figure 9. Diagrammatic representation of the chemistry of biodegradation [40].

Polymers containing hydrolysable groups, like esters, are more susceptible to biodegradation by hydrolysis. When polyesters are placed in an aqueous medium, the cleavable ester bonds of polymer hydrolyse into the carboxylic acid group (COOH) and a hydroxyl group (OH), as shown in Figure 10 [8, 9, 53]. The biodegradation in polyesters is affected by different factors including repetitive units' type, sequence length, molecular weight, molecular geometry, compositions, hydrophilicity, morphology (e.g., crystallinity, size of spherules, orientation), surface area, and additives [3].

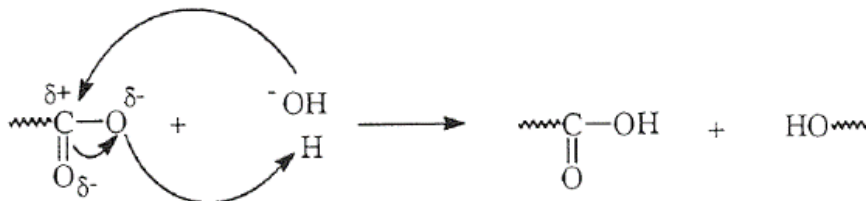
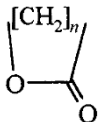


Figure 10. Hydrolytic degradation of polyesters [9].

Biodegradable polymers for ecological applications are defined polymers maintained mechanical strength and other properties similar to non-biodegradable polymers, but they are finally degraded to low-molecular-weight compounds such as CO₂, H₂O and non-toxic by-products by microorganisms living in the environments. While, bioresorbable polymeric biomaterials are adsorbed by the body and then disappear when the device is no longer needed through natural pathways [54-56].

The polyesters are the most extensively investigated category of biodegradable polymers. They are important, because of the synthetic versatility, as well as of the numerous monomers that build the polyesters [1]. Table 2. Summarizes the range of monomers for synthesizing polyesters, and polymerizations which can be carried out either in the bulk or in the solution [44].

Table 2. Biodegradable polyesters [44].

Type	Monomers	Examples of polymers
Poly(a-ester)s	a-Hydroxy acid e.g. HO—C(R)H—COOH. Dimeric cyclic lactide or glycolide undergoes ROP	Poly (glycolic acid) (PGA) (R ¹ /4H). Poly (lactic acid) or polylactide (PLA or PL) (R ¹ /4CH ₃). Copolymers poly(lactic acid-co -glycolic acid) (PLGA)
Poly(b-ester)s or poly(3-hydroxyalkanoate)s (PHAs)	b-Hydroxy acid e.g. HO—C(R)H—CH ₂ —COOH, or cyclic lactone	Poly(3-hydroxybutanoate) (P3HB) (R=CH ₃). Poly(3-hydroxyvalerate) (PHV) (R=C ₂ H ₅) Copolymers poly(hydroxybutyrate-co -hydroxyvalerate) mol% HV defined (PHBV (8% HV))
Poly(c-ester)s	HO—C(R)H—(CH ₂) ₂ —COOH or cyclic lactone	Poly(4-hydroxybutanoate) (P4HB) (R=H)
Other polyesters or polylactones	 cyclic lactone	Poly (ε-caprolactone), n=5 Poly (valerolactone), n =4

1.3. MODIFICATIONS OF BIODEGRADABLE POLYESTERS

Polyesters have been widely used in biomedical applications. However, for many applications, they are not ideal materials due to high crystallinity, hydrophobicity, brittleness, thermal instability, and lack of total absorption. Therefore, for the fabrication of polyesters with tailored properties to meet the specific requirements, modifications is needed to be diversified and improved. Moreover, surface properties of biomaterials are significantly important, while they influence the biological interactions with the host tissue. For example, in tissue engineering, cell surface has different receptors, which bind with surrounding specific proteins or other cells [50, 57-61].

The most common strategies to increase the versatility of polyesters and overcome the limitations is through bulk or surface modifications [37, 60, 62].

1.3.1. Bulk modifications of polyesters

Bulk modification has an effect on the chemical composition and structure of polymers by chemical functionalization, copolymerization with other monomers or blending with other polymers [37, 63].

Copolymerization

Copolymerization is polymerization of two or more monomers, in which the copolymer is prepared. The copolymers usually have considerably different properties from each homopolymer. Regarding biodegradable polymer, different types of copolymer with a wide range of properties have been synthesized. For example, PLGA is suggested for improving biodegradability with stronger solubility and lower melting point, therefore it has been introduced as the best-defined biomaterial with high performance in drug release application [37, 63].

Blending

In the polymer industry, one of the typical technique in bulk modification is blending. Polymer blends are physical mixtures of two or more polymers or introducing a low molecular weight component to the polymer matrix. For biodegradable and biocompatible polyesters, plasticizers and various stabilizers are supplemented.

By blending polyesters with naturally derived compounds (starch, proteins) and synthetic polymers (PEG, PVA) a new kind of biodegradable material/polymers could be obtained. For example, blending of PLA with PCL has been reported with increased flexibility but decreased toughness. There are two different blending strategies, first is

combining of the components in a molten state (in an extruder), second is mixing in a suitable solvent [37, 63].

Chemical functionalization

Chemical functionalization refers to the introducing of new functional groups into the polymer backbone or altering the nature of those that are already present in order to add reactive groups along the main chain or promote fixation, and adhesion of active molecules. Chemical functionalization can be achieved by two approaches [61, 64, 65].

A) Polymerization of substituted monomers

Attaching the cyclic monomers to the polymer backbone by ring opening polymerization is called substituted cyclic monomers polymerization. Various functional groups especially unsaturated, hydrophilic and halogenated groups are attached to aliphatic polyester back bone.

B) Post-polymerization reactions

Reactions carry on along the polymers or on the end groups. However, there are no reactive side groups in the simple homopolymer [37, 60].

1.3.2. Surface modifications of polyesters

The main aim of surface treatment is to alter the outermost layer of a polyester by attaching some functional groups onto the surface for improving its barrier properties, wettability, sealability, printability and dye uptake, its adhesion to other materials, its resistance to glazing, or its interaction with a biological environment while maintaining the desirable bulk properties of the polyesters. Surface-modification methods are classified as chemical methods and physical methods [37, 62].

Coating

Coating is one of the simplest and cost-effective surface modification methods. Generally, the coating materials get ready in solutions and the coatings are prepared by brushing, soaking, or spraying techniques. Surface coating method is a physical treatment and the coating has relatively weak bond to the surface by Van Der Waals force. Moreover, it is based on absorption or deposition of the modifying agent to the polymer surface [37, 66, 67].

Plasma treatment

Plasma treatment is a widely and straight-forward used technique to modify the surface of materials for improving wettability and cell affinity of cell scaffolds. Plasma is a complex system composed of excited states or neutral of atoms, molecules, electronics, ions, free radicals, and a radiant photon with high energy.

The surface parts of the materials are exposed to energies higher than the characteristic bonding energy of polymers, these parts undergo scission reactions and form new bonding configurations on the surface. Plasma treatment using non-deposition gases such as ammonia, oxygen, hydrogen oxide and so on, can be used to graft functional groups including -NH_2 , -OH , and -COOH . However, the main drawback of this method is that it partially reduces the effectiveness of the surface modification owing to surface rearrangement. Figure 11. Illustrates the attachment of certain functional groups on the surface of polyester. [37, 66, 67].

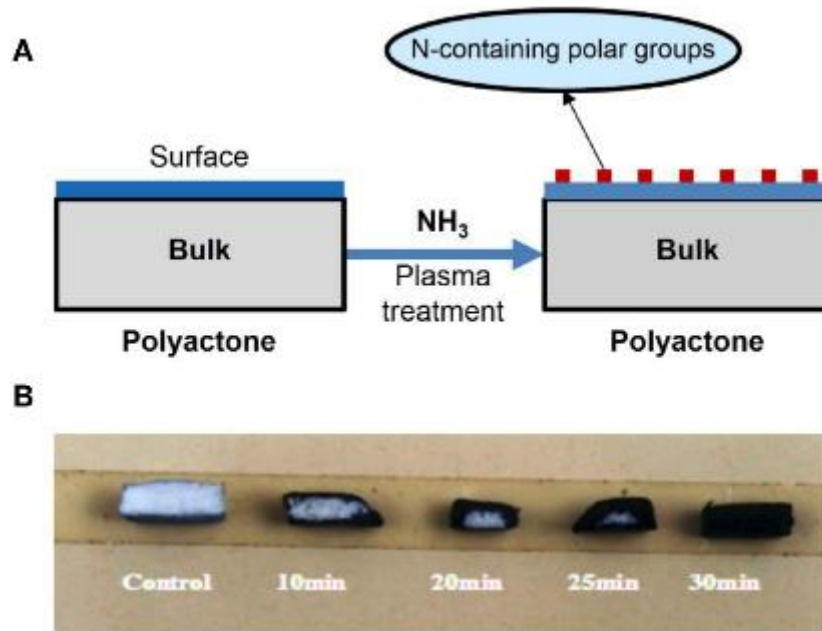


Figure 11. (A) Scheme of formation of N-containing polar groups on surface of polylactone-type polymer using ammonia plasma treatment; (B) the influence of plasma-treating time under power 20W and 30 Pa of NH₃ atmosphere on treated depth of PLGA scaffold [67].

Entrapment

The biomaterial surface in this method can be non-covalently but stably modified with water-soluble polymers. Exposing the polymer surface to the solvent/non-solvent

mixture leads to gelation of the polymer at the surface, allowing the modifier to diffuse inside. The swelling is reversed upon exposure to a non-solvent. This technique improves hydrophilicity and blood compatibility of biomaterial surfaces. The scheme of this method is presented in figure 12 [37, 61].

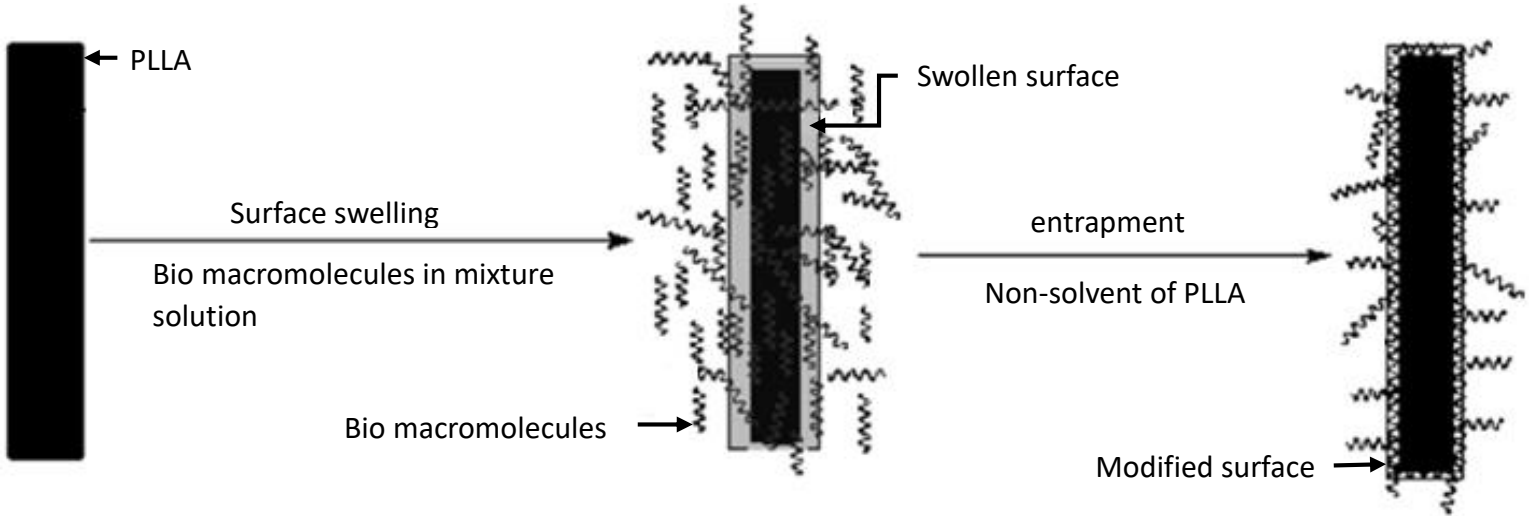


Figure 12. The modification of PLLA by the entrapment method [61].

Chemical modification

Chemical modification is based on the reaction of reactive groups on the surface of the polymers with a modifying agent. For example, in biodegradable polyesters after surface hydrolysis, hydrophilic carboxyl and hydroxyl can be formed by cleaving the ester bond, by treating with NaOH solution. The resulting groups can also be employed to conjugate the bioactive molecules, such as L-lysine, collagen and Arg-Gly-Asp peptide [37, 66].

1.4. APPLICATIONS OF BIODEGRADABLE POLYESTERS

The polyester category is extremely large and, depending on the nature of radicals (R^1 and R^2) which was presented in Figure 13, exhibits a vast variety of structures, properties, architectures, and as a result, applications.

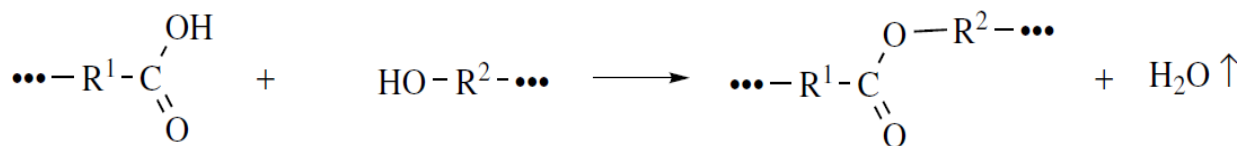


Figure 13. Esterification between carboxylic acid and alcoholic group [6].

Polyesters are one of the most economically important groups of polymers. The production of polyesters is expected to increase rapidly over the next decade, due to their highly favourable properties such as environmental friendliness, recyclability, and biodegradability [6, 8, 68].

The abundance of monomers used in polyester synthesis causes the preparation of an extensive variety of materials possessing special characteristics for a broad range of applications, which is divided into biomedical and non-biomedical applications.

1.4.1. Biomedical applications

Aliphatic polyesters are considered as biodegradable, bioresorbable and biocompatible polymers which have been broadly employed in medical applications over the past several decades. Both synthetic and natural polyesters have been used as components of biomedicines owing to distinctive chemical structures. Table 3 presents the commercially available polyester-based products.

Table 3. Commercial products made from biodegradable polyesters and their applications [8].

Polymers	Applications	Commercial products
PLA	Fracture fixation, interference screws, suture anchors, meniscus repair, reconstructive surgeries, Vasculargrafts, Adhesion Barriers, Articular cartilage repair, Bone graft substitute, Dural substitutes,	Proceed™ Surgical Mesh (Ethicon Inc.) , Artisorb™ Bioabsorbable GTR Barrier (Atrix laboratories, Fort Collins, CO, USA)

	Skin substitutes, Tissue augmentation, Scaffolds	
PLGA	(Composition 85:15): Interference screws, plates, suture anchors, Stents/(Composition 50:50):Suture, drug delivery, Articular cartilage repair/(Composition 90:10):Artificial skin, wound healing, hernia repair, suture, tissue engineered vascular grafts	Rapidsorb® plates (DePuy Synthes CMF, West Chester, PA, USA), Lactosorb® TraumaPlatingSystem (Biomet, Inc., Warsaw, IN, USA) [L-lactide/glycolide= 82/18], RFS™ Screw System (Tornier), RFS™ (Resorbable Fixation System) Pin System (Tornier), Xinsorb BRS™ stent (Huaan Biotechnology Group, Gansu, China) REF1, Dermagraft®, Vicryl® woven mesh (Ethicon Inc.) (Composition 90:10)
PCL	Suture coating, dental orthopaedic implants, Tissue repair, hybrid tissue-engineered heart valves, Surgical meshes, cardiac patches, Vascular grafts, Adhesion Barriers, Dural substitutes, Stents, Ear implants, Tissue engineering scaffolds	Tissue repair patches (Ethicon Inc.), Bulking and Filling agents (Angelo, 1996), DermaGraft™ (Organogenesis Inc., Canton, MD, USA
PPF	Orthopedic implants, dental, foam coatings, drug delivery, Scaffolds	—
PPC	Scaffolds	—
PHB	Sutures (P4HB polymer), screw fasteners for meniscal cartilage repair, Scaffold for tendon repair, Reconstructive surgeries (Surgical	Phantom Fiber™ suture (Tornier Co.), MonoMax® suture (Braun Surgical Co.), BioFiber™ scaffold (P4HB polymer) (Tornier Co.),

	meshes), Vascular grafts, Nerve repair, Bone tissue scaffold (P3HB), Wound dressing (P3HB), hemostats (P4HB), Stents	TephaFlex® mesh (Tepha Inc.) (P4HB polymer), GalaFLEX mesh (Galatea Corp.), Tornier® surgical mesh (Tornier Co.)
PHBV	Scaffolds	—
PBS	Stents, Sterilization wrap, Diagnostic or Therapeutic Imaging	Disposable Medical Products-Bionolle® 1000 and 3000 (Showa Highpolymer Co. Ltd.)

Pharmaceutical use

For the purpose of delivering therapeutically active drug molecules to sites of disease in the body in a less invasive and effective way, a new dosage form technology, called drug delivery systems (DDS), by using polymer has been developed. The goal of DDS is sustained release of drugs for a favourable time at an optimal dose, targeting of drugs to the site of action, controlled release of drugs and delivery of bioactive compounds mainly through mucous membranes and skin. DDS is the main and highly versatile application for polyesters. Generally, polyesters have been employed to form nanoparticles, polymeric dendrimers, micelles, and polymersomes. Figure 14 illustrates the common nanocarriers used for drug delivery.

Furthermore, polyester-based DDS have been employed for cancer treatment and diagnosis, via loading different types of bioactive compounds and imaging probes over the past decades. So far, different types of polyester-based DDS have been used for clinical applications. For example, Genexol-PM, Zoladex and Signifor LAR, especially for polyester-based micelles which have a proven high performance in cancer therapy [8, 44, 54, 69, 70].

Up till now, several types of polyesters including PLA, PGA, PLGA, PCL, and poly (dioxanone)s (PDO) have been the most widely used polyesters in commercial application in the DDS area [8, 71].

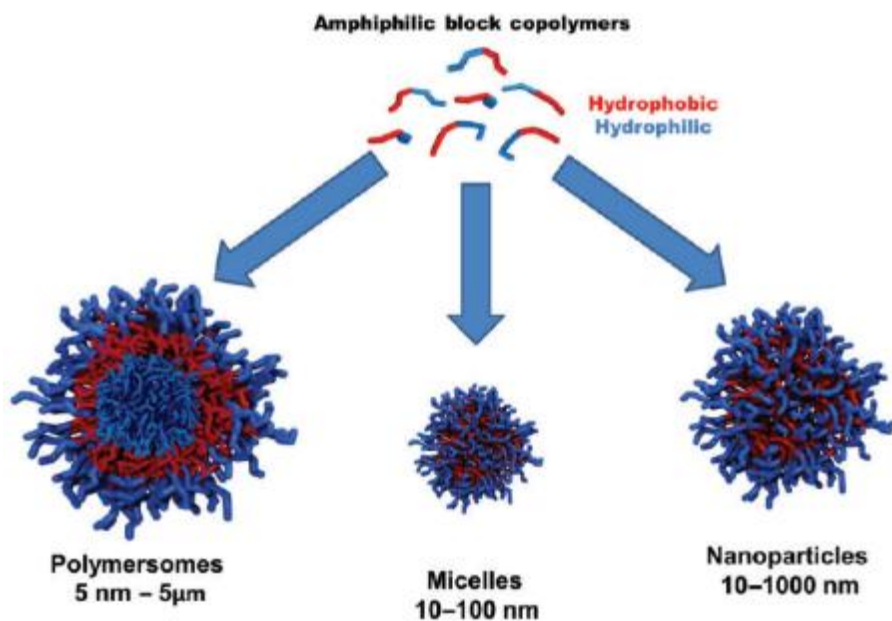


Figure 14. Type and sizes of common nanocarriers used for drug delivery [70].

Use for tissue engineering

Tissue engineering is an emerging technology to repair tissue defects or regenerate biological tissues to replace the defective or lost tissues by employing cells and cell growth factors. To fulfill this aim, three-dimensional (3D) constructs which are called scaffolds, are made of biodegradable and biocompatible materials and cell cultures are grown inside of that. Aliphatic polyesters are the most frequently used synthetic biodegradable polymers for fabrication scaffolds due to their properties in tissue regeneration. The properties of the ideal scaffold are shown in the table 4.

Table 4. Summary of scaffold design criteria and related functions in tissue engineering [72].

Scaffold design criteria	Resulting function in engineered tissue
Biologic compatibility	Non-toxic/minimal inflammatory response
3D matrix architecture	Physiologically relevant environment for cell function
Void space	Highly porous and interconnected pores to allow cell infiltration, transport of nutrients, humoral factors and waste products
Surface chemistry and topography	Cell attachment and cell-matrix interactions
Appropriate mechanical behavior	Seamless integration with surrounding tissue(s) able to withstand in vivo forces and avoid stress shielding
Degradation rate	Scaffold lead to the formation of a functionalized matrix
Structural anisotropy	Anisotropic mechanical behavior Influence orientation of cells and ECM deposition

Over the last decades, the tissue engineering field has been developing the testing and fabrication of artificial cartilage, blood vessels, heart valves, bone, breast, bowel, lung, liver, nerves, kidney, trachea, and pancreas. The basic steps of tissue engineering are illustrated in Figure. 15 [18, 54, 72-76]. PCL, PLA, PGA, and their copolymer PLGA is commonly used in tissue engineering application [8, 76].

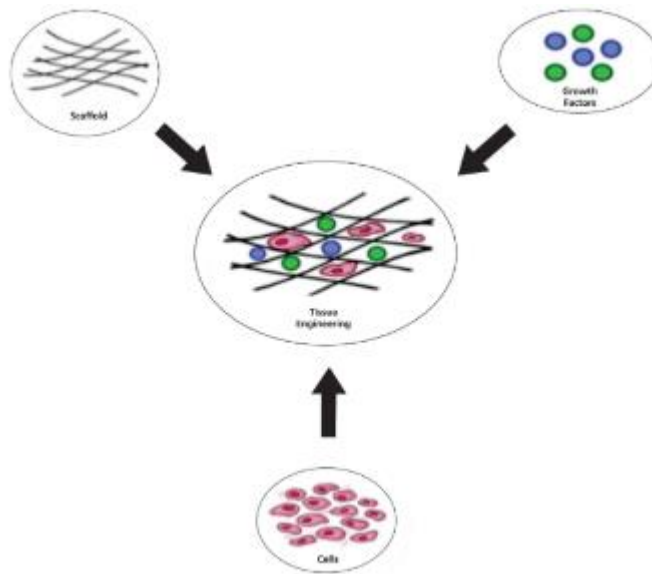


Figure 15. Basic steps in tissue engineering [75].

Surgical use

Polymeric materials have also been used in surgical applications, frequently in situations where there is intimate contact with living tissues, therefore it is a fundamental requirement to display adequate biocompatibility so as not to have any adverse effects on the tissue. Generally, polymeric materials for surgical use are divided into three categories: bioabsorbable (biodegradable or resorbable), biostable and partially biodegradable. Therefore, aliphatic polyesters appear at the moment to be one of the most promising and attractive options [13, 54, 77, 78].

The use of synthetic polymers for sutures is one of the largest consumption in the category of surgical use. As sutures remain in the tissue, it can cause inflammation in a variety of ways such as foreign body reaction, degradation or allergic reaction. Hence, the new generation of absorbable suture materials may decrease inflammation. Dexon (Polyglycolic acid) and Dexon II (Dexon coated with polycaprolate) are commercially available for absorbable sutures. The other applications of polyesters in surgical use are displayed in Table 5 [54, 79, 80].

Table 5. Representative synthetic biodegradable polymers currently used or under investigation for medical application [54, 80-83].

Polymer	Application
PLLA/PGA	Surgical mesh coatings
Photocrosslinkable PGS derivatives	Surgical sealants
PCL, PLLA, PLGA, PCL-PEG, PLACL	Scaffolds for the treatment of cutaneous wounds
PU- polyester	Wound dressing
Poly(glycolic acid- <i>co</i> -L-lactic acid)	Suture, Fracture fixation, Oral implant
Poly(ϵ -caprolactone)	Contraceptive delivery implant
Poly(L-lactide)	Fracture fixation, Ligament augmentation

1.4.2. Non-biomedical applications

In addition to the biomedical area, the other major application of biodegradable polyesters is in plastic industries for replacing biostable plastics for keeping our earth environments clean. If biodegradation by-products do not exert adverse impacts on plants and animals on the earth, biodegradable plastics can be considered as environmentally friendly or ecological materials. Hence, much attention has been focused on producing biodegradable plastics which, however, should solve several requirements. They are to be cost-effective, satisfactory in mechanical properties and have an eco-friendly image. Applications of biodegradable polyesters in plastic industries are listed in Table. 6 [54, 84].

The applications cover a broad spectrum of industries including agriculture, fishery, civil engineering, construction, outdoor leisure, food, toiletry, cosmetics, and other consumer products. when plastics are used indoors as food containers that are difficult to separate from the food remaining after use, the waste can be utilized as compostable if it is biodegradable [50, 84].

Table. 6. Ecological applications of biodegradable polymers [54].

Application	Fields	Examples
Industrial applications	Agriculture, Forestry	Mulch films, Temporary replanting pots, Delivery system for fertilizers and pesticides
	Fisheries	Fishing lines and nets, Fishhooks, Fishing gears
	Civil engineering and construction industry	Forms, Vegetation neets and sheets, Water retention sheets
	Outdoor sports	Golf tees, Disposable plates, cups, bags, and cutlery
Composting	Food packaging	Package, Containers, Wrappings, Bottles, Bags, Films, Retail bags, Six-pack rings
	Toiletry	Diapers, Feminine hygiene products
	Daily necessities	Refuge bags, Cups

AIMS OF WORK

Aliphatic polyesters combine the rarely met properties of biocompatibility, bioresorbability, and biodegradability, which accounts for their broad use as biomaterials and as environmentally friendly thermoplastics. However, the lack of functional groups along the backbone and poor mechanical properties induce an intense limitation to extend new applications. It is highly desirable to implement efficient processes in order to modify biodegradable polyesters and tailor properties including crystallinity, hydrophilicity, and biodegradation rate. Therefore, the aim of the doctoral thesis is based on the state of the art study, and conclusions resulting from that are the following:

- Preparation and characterization of microcellular antibacterial poly lactide-based systems prepared by additive extrusion with ALUM.
- Poly lactide-polyvinyl alcohol-based porous systems loaded with gentamicin for wound dressing applications.

2. EXPERIMENTAL PART

2.1. Preparation and characterization of microcellular antibacterial polylactide-based systems prepared by additive extrusion with ALUM

Introduction

In recent years, polylactide (PLA), an environmentally friendly biopolymer, has been widely applied in the biomedical sphere (eg, as sutures, implants, and porous scaffolds) due to its exceptional mechanical, biodegradable, and biocompatible properties [85-88]. The three-dimensional porous structures of these materials make them suitable for use in tissue engineering as implants for regenerating certain types of tissue, such as skin and bones [89, 90].

Fundamentally, PLA has the potential to be processed into microcellular form through various conventional techniques, including compression moulding, extrusion, and injection molding [85, 86, 91, 92]. Microcellular extrusion is considered one of the most promising procedures for decreasing density for biomedical application [87, 93]. Essentially, two methods for manufacturing microcellular materials exist. The first approach utilizes supercritical fluids (SCF_s) typified by CO₂ and N₂, while the other pertains to chemical blowing agents (CBA_s), such as carbonated salts; the latter results in creation of CO₂ because of the occurrence of thermal decomposition [90]. In the first approach, SCF_s are commonly employed due to their nontoxicity and nonflammability properties [89]. Nonetheless, maintaining a critical condition is not a simple matter, since it is necessary to apply an accurate and precise pressure of CO₂ to control the expansion and structure of products in the extruder barrel [94]. In contrast, CBA_s possess the advantages of being used without such consideration of pressure and it is more cost-efficient as compared with utilizing SCF_s [90]. It is only recently that studies have appeared in the literature on the microcellular extrusion of PLA. The majority of these describe the process of utilizing supercritical CO₂ for this purpose [95, 96]; hence, there is a significant lack of research on CBA_s. Moreover, attention in such works should be paid to investigating the change in hydrolytic degradability that often accompanies formation of a microcellular structure. Indeed, the kinetics of degradation (bioresorption) of the implant material constitute a key factor in medical applications [97].

In recent years, it has become a commonplace to prevent the spread of microbial infections associated with medical devices through antimicrobial treatment of materials. In addition, due to the rise in drug-resistant pathogens witnessed over the past few decades, enhancing the antimicrobial properties of materials is a matter that has gained importance. Inhibiting microbial growth on the surface of a polymer and its surroundings is achievable by mixing an organic or inorganic agent into the polymer matrix [98-100].

Several papers have been published on the subject in the literature, wherein organic agents are added into a PLA matrix; examples of the former include cellulose, chitosan, and silver [94, 101]. Turalija et al showed that incorporating silver or chitosan into PLA resulted in them acting as antimicrobial agents effective against gram-positive and gram-negative bacteria.

Out of all the possible antimicrobial additives, aluminium potassium sulfate (ALUM) stands out due to its particularly advantageous characteristics, including ease of availability and low price. In addition, it is environmentally friendly and has been approved by the Food and Drug Administration (FDA). Indeed, ALUM has been frequently employed for medical application as a consequence of it not being absorbed by the body; thus, it is considered a harmless substance [102]. Bnyan *et. al.* reported that ALUM inhibits the growth of gram-positive and gram-negative bacteria and exhibits a level of antimicrobial activity comparable with cefotaxime (a commercial antibiotic) [102]. Despite all its undeniable advantages, ALUM has largely been overlooked by researchers as an additive for antimicrobial maintenance of a polymeric device [98].

The investigation presented herein focused on the effect of the microcellular structure of PLA on the properties of the given material, as well as its hydrolysis, antimicrobial properties, and the release of an antimicrobial agent from the PLA matrix. Antimicrobial PLA foam was processed via the microcellular extrusion method, with a mixture of monobasic sodium salt (sodium hydrogen carbonate + another salt, at the ratio 1:1) applied as the CBA, and hydrated potassium aluminium sulfate (ALUM) as the antimicrobial agent. Study was made as to the thermal, tensile, and antimicrobial properties of the prepared microcellular PLA incorporated with ALUM. The hydrolytic degradation and release of the antimicrobial agent were studied in biological buffer solutions at pH 7 by gel permeation chromatography (GPC) and elemental analysis, respectively.

Materials

PLA semicrystalline PLA4042D with an average molecular weight (M_w) of 120 000 g mol⁻¹ was purchased from NatureWorks Ingeo, Minnetonka, Minnesota. Antimicrobial potassium aluminium sulfate dodecahydrate (ALUM) and monobasic sodium salts (MSS), based on sodium hydrogen carbonate in a mixture with sodium dihydrogen phosphate (ratio 1:1) and applied as a foaming agent, were supplied by Sigma-Aldrich, St. Louis, Missouri.

Preparation of PLA mixtures

Prior to being compounded, PLA pellets were dried at 80°C under reduced pressure (300 mbar) for at least 8 hours. A co-rotating twin screw micro compounder (HAAKE MiniLab II, Thermo Scientific, Waltham, Massachusetts) which was equipped with two stainless steel screws and a bypass valve was utilized. This allowed continuous recirculation of the material at 190°C; with the screw speed set to 50 rpm for compounding operations without the bypass valve. The compositions of the resultant samples are shown in Table. 7.

Table. 7. Compositions of the investigated samples

Component content (wt.%)/sample designation	PLA	ALUM	MSS
PLA	100	-	-
PLA/ALUM	99	1	-
PLA/ALUM/MSS3	97	1	3
PLA/ALUM/MSS5	94	1	5
PLA/MSS3	97	-	3
PLA/MSS5	95	-	5

Characterization

Changes in molecular weight during hydrolysis by GPC

GPC analysis was conducted on an HT-GPC 220 chromatographic system (Agilent, Santa Clara, California), equipped with a dual detection set-up (refractive index and viscometric response detectors). The samples were dissolved in tetrahydrofuran (THF; approximately 3 mg mL⁻¹) overnight. Separation and detection took place on PL gel-mixed bed columns (1× Mixed-A, 300 × 7.8 mm, 15 μm particles + 1× Mixed-B, 300 × 7.8 mm, 10 μm particles + 1× Mixed-D, 300 × 7.8 mm, 5 μm particles) at 40°C in THF; the flow rate equaled 1.0 mL min⁻¹ and injection volume was 100 μL. The GPC system was calibrated through universal calibration, with narrow polystyrene standards ranging from 580 to 271 000 g mol⁻¹ (Polymer Laboratories Ltd, UK). The weight average molar mass (M_w), number average molar mass (M_n), and molar-mass dispersity ($\mathcal{D} = M_w/M_n$) of the tested samples were discerned from peaks corresponding to the relevant polymer fractions. All data processing was carried out in Cirrus software.

Thermal properties—differential scanning calorimetry (DSC)

Thermal properties were investigated by DSC on a DSC1 STAR system (Mettler Toledo, Greifensee, Switzerland). Samples with approximately 5 mg in weight were placed in aluminium pans. Nitrogen flow was set to 50 mL min⁻¹, and the following heating program was applied: an initial heating cycle from 0°C to 200°C (10°C min⁻¹),

maintaining the same for 2 minutes, and subsequent cooling to 0°C (20°C min⁻¹). Afterward, the temperature of 0°C was held for 2 minutes and a further heating scan performed at 200°C. Melting point temperature (T_m) and exothermal response relating to cold crystallization (T_c) were obtained from the first heating cycle. The region of glass-transition temperature (T_g) was determined from the second heating scan. The degree of crystallinity χ_c was calculated according to Equation (1) [99].

$$\chi_c = \left(\frac{\Delta H_m - \Delta H_c}{\Delta H_m^0} \right) * 100\% \quad (1)$$

where ΔH_m is the enthalpy of fusion, ΔH_c represents cold crystallization enthalpy, and ΔH_m^0 is the tabulated enthalpy of fusion for a theoretically 100% crystalline PLA homopolymer (93.1 J g⁻¹) [99].

Porosity

The porosity of the microcellular samples was calculated from the bulk density (ρ_B) of the microcellular polymers, which was computed from the weight to volume ratio (ρ_{Th}) of individual samples and the theoretical density, according to the following equation

$$Porosity (\%) = \left(1 - \frac{\rho_B}{\rho_{Th}} \right) * 100 \quad (2)$$

Morphology

The morphology of the prepared material was determined by thermionic emission scanning electron microscopy (ESEM) (VEGA II LMU, TESCAN, Brno, Czech Republic) in order to visualize the size and distribution of particles in the PLA matrix. The specimens were prepared by cryogenically fracturing the samples in liquid nitrogen and then coating them with a thin layer of Au/Pd. A microscope, equipped with an SE detector, was operated in high-vacuum mode at an acceleration voltage of 10 kV.

Tensile test

Investigations into the mechanical properties of the samples were carried out on a universal tensile testing device, an M350-5 CT Materials Testing Machine (Testometric Company, Lancashire, UK), at a crosshead speed of 5 mm min⁻¹ in accordance with ČSN EN ISO 527-1-4. The dimensions of dog-bone form specimens cut from compression moulded plates measured 60 × 4 × 0.1 mm. Prior to testing, the samples were conditioned at 25°C, 50% RH for 24 hours. A minimum of eight specimens from each group were tested.

Statistical analysis was applied to process the results of mechanical properties evaluation. In order to eliminate extraneous results, the Dean-Dixon test was carried out (Q-test;

confidence level $\alpha = .95$). After eliminating peripheral figures, corresponding averages and standard deviations (SD) were calculated.

Abiotic hydrolysis

The extent and rate of PLA hydrolysis were monitored for 140 days at 37°C. The PLA samples (50 mg) were cut into 0.5 × 0.5 cm specimens and then suspended in 50 mL of sodium phosphate buffer (0.1 mol L⁻¹, pH 7) amended with a microbial growth-inhibiting substance (NaN₃, 2% w/w). The experiment was carried out in three replications for each type of samples. The samples were withdrawn at appropriate intervals and analyzed by GPC and DSC.

Release test

The individual samples (approximately 100 mg) were immersed in 10 mL of phosphate buffer saline (PBS, 7.4 pH) and incubated at 37°C. All experiments were carried out in triplicates. The volume of 1 mL was removed at predetermined intervals, the used PBS was replaced with 1 mL of fresh PBS, and then filtration took place through a 0.22 μm syringe PTFE filter for subsequent analysis. The concentration of the Al related to the ALUM released was determined by atomic absorption spectroscopy (AAS).

Atomic absorption spectroscopy (AAS)

The exact concentration of Al release into the buffer medium was determined by AAS, on an Agilent DUO 240FS/240Z/UltrAA unit (Agilent Technologies, Santa Clara, California) equipped with a hollow cathode lamp (Al: I = 10 mA and wavelength = 396.2 nm) and a deuterium lamp for background correction. A mixture of gasses, acetylene, and air was applied in the flame at flow rates of 2.0 and 13.5 L min⁻¹, respectively. Concentration was calculated according to a calibration gauged by standards with specified concentrations (Ag: 1000 mg/L, Agilent Technologies; Zn: 1000 mg/L, Fluka Analytical).

Antimicrobial test

Antibacterial testing was carried out according to a procedure based on ISO 22196: 2007 “Measurement of antibacterial activity on plastic surfaces”. The bacteria employed in this study were *Staphylococcus aureus* CCM 4516 (gram-positive) and *Escherichia coli* CCM 4517 (gram-negative). Bacterial suspensions were prepared at concentrations of 1.0 10⁶ CFU mL⁻¹ and 1.5 10⁷ CFU mL⁻¹ for *E. coli* and *S. aureus*, respectively. The dimensions of each specimen and the polyethylene film were 25 mm x 25 mm, a 20 mm × 20 mm respectively.

Number of the colony forming units (CFU) was determined, and its reduction (CR) was expressed by diminishment in the number of colonies formed per cm² in percent, according to Equation 3:

$$CR = \left(-\frac{N_s}{N_B} \right) * 100 (\%) \quad (3)$$

where NB is the number of viable colonies per cm² recovered from the material without the additive (blank) after 24 hours and NS is the number of viable colonies per cm² recovered from samples containing the antimicrobial agents after 24 hours.

Results and discussions

Characterization of materials

Materials properties including molecular weight, thermal and mechanical properties and morphology of specimens prepared from neat PLA and microcellular PLA expanded by sodium bicarbonate and Alum as antimicrobial compound were investigated. Recognized as being environmentally friendly and cheap CBA, MSS decomposes at low temperature and releases CO₂ easily. Antibacterial modification was mediated by another inexpensive and widely available additive, ALUM. Papers in the literature highlight that PLA degrades during melting process methods such as extrusion [95], a phenomenon that could be accelerated by enhancing the material with additives [100, 103]. Therefore, the effect of agents on the properties of the PLA was researched after the preparation process had ended, and these findings were compared with characteristics prior to commencement of said process.

Morphology

Scanning electron microscopy (SEM) was utilized to investigate the morphology of samples, especially to gain data on the microstructure of the microcellular specimens. As can be observed from Figure 16, adding ALUM to neat PLA caused the specimens to develop more fracture-like characteristics than evidenced in neat PLA. As expected, the gases formed by the decomposition of MSS in the PLA during extrusion gave rise to an expanded pore structure in the majority of pores, measuring in the order of hundreds of micrometers. The higher expansion ratio and density discerned of the pores were achieved by employing a greater amount of the blowing agent: (5 wt% of MSS) in the samples PLA/MSS5 (Figure 16D) and PLA/ALUM/MSS5 (Figure 16F). Additionally, incorporating ALUM and combining it with the expansion process induced by the greater concentration of MSS led to decrease in cell size and increase in the cell density of the polymer matrix, in comparison with the PLA/MSS5 sample; notably, a more uniform cell structure was also obtained. The pores in the PLA/ALUM/MSS5 specimen were roughly comparable in size with the morphological characteristics of a microcellular PLA reported in a study [104], which had been formed by nitrogen in a supercritical state through injection moulding experiments.

Table 8 summarizes the percentage of porosity of the microcellular PLA samples. In accordance with findings from the SEM images, free space volume was at its highest level when the greater concentration of MSS was utilized. Nevertheless, if applied in tandem with ALUM, porosity significantly diminished because of the less porous substructures formed, in addition to which the average pore size of the specimens reduced. These phenomena had been anticipated because of the number of bubbles nucleated, which is fully dependent on the concentration of the blowing agent dissolved in the polymer matrix [105].

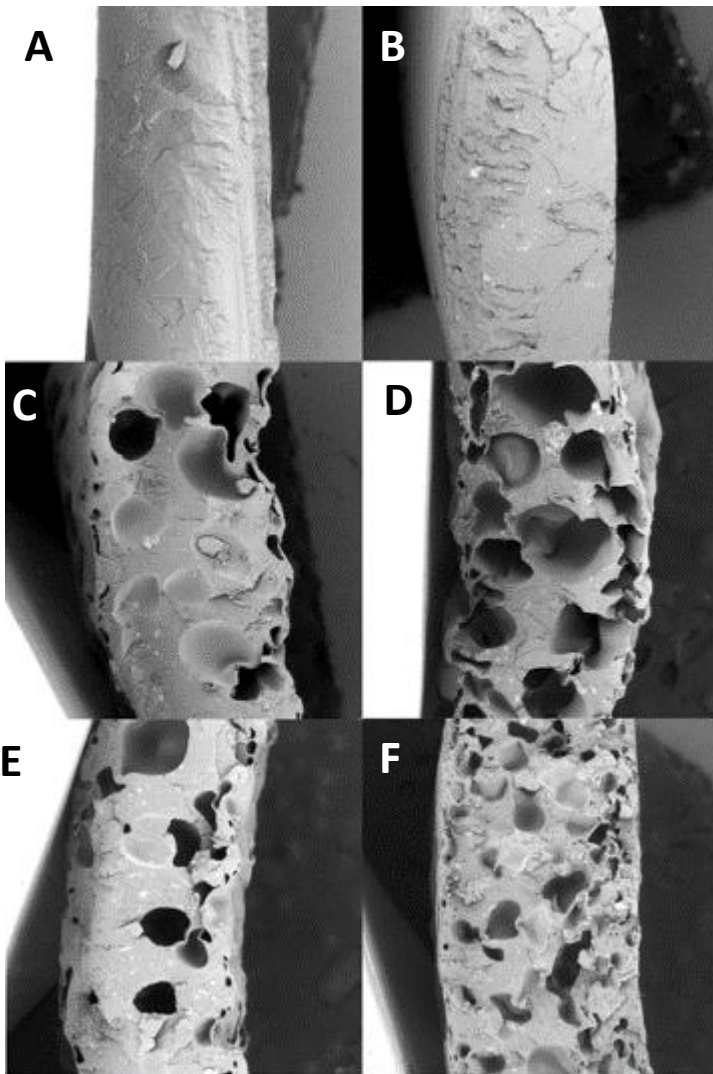


Figure 16. SEM micrographs of the microstructures of (A) PLA, (B) PLA-ALUM, (C) PLA/MSS3, (D) PLA/MSS5, (E) PLA/ALUM/MSS3, (F) PLA/ALUM/MSS5.

Molecular weight and distribution

The average molecular weights of all samples, measured by GPC, are listed in Table 8. Neat, unprocessed PLA was used as a reference to compare the results obtained for the final samples. As can be seen, a significant drop in M_w was detected for neat PLA after it had been processed in comparison with the same unprocessed material, caused by thermal degradation. This decline in M_w was much more pronounced for the material incorporating the antimicrobial agent ALUM and the composites expanded by MSS (PLA/ALUM, PLA/ALUM/MSS3, PLA/ALUM/MSS5). The M_w of the neat PLA and PLA with additives dropped by approximately 14% and 43%, respectively, after processing the same.

Potentially, this significant reduction in M_w could be attributed to the acidic nature of ALUM ($KAl(SO_4) \cdot 12H_2O$) and MSS, which were employed in tandem with the expansion agent. These additives act as an acidic catalyst, accelerating the random hydrolysis of the ester bonds in the PLA [106]. Furthermore, water molecules present in the chemical structure of ALUM could promote hydrolysis of the polymer. The concurrent effect exerted by the additives on acceleration of degradation is clearly evidenced in the M_w of the PLA/ALUM/MSS5 material, which contained ALUM and the greatest amount of the blowing agent

Thermal properties

The results of DSC analysis, which are detailed in Table 8, demonstrate that the additives employed to prepare the antimicrobial microcellular PLA did not significantly influence the thermal properties of the given PLA, in comparison with the neat material prior to and after processing. The degree of crystallinity of the specimens, calculated from data obtained by thermal analysis, was very low. This can be attributed to the short time available for crystallization to occur during the preparation of the specimens. However, the slightly higher crystallinity of the PLA with additives potentially indicates their nucleation effect, facilitating PLA crystallization [85].

Table. 8. Selected material-related properties of samples after preparation and before degradation experiments.

Sample/property	Neat PLA prior to processing	Neat PLA after processing	PLA ALUM	PLA/MSS3	PLA/MSS5	PLA ALUM MSS3	PLA ALUM MSS5
Content of ALUM [%]	-	-	1	-	-	1	1
Content of BS [%]	-	-	-	3	5	3	5
M_w^a [kg·mol ⁻¹]	122.9	107.1	86.5	90.1	90.1	91.5	85.5
\bar{D}^b	2.44	2.12	2.43	2.53	2.42	2.34	2.24
T_m^c [°C]	154.1	152.5	153.5	155.0	154.6	154.3	154.0
ΔH_m^d [J·g ⁻¹]	-35.9	-26.9	-24.3	16.1	-27.7	-25.3	-27.8
T_c^e [°C]	-	123.2	123.5	126.2	125.7	126.2	124.5
ΔH_c^f [J·g ⁻¹]	-	26.2	22.0	16.6	24.5	21.1	25.0
T_g^g [°C]	59.8	59.3	59.8	58.4	57.8	59.7	59.8
χ_c^h [%]	38.6	0.7	2.5	0.5	3.5	4.5	3.0
Porosity	-	-	-	22.9	29.8	19.1	17.9

^a weight average molecular weight; ^b molar mass dispersity; ^c melting temperature; ^d enthalpies of melting; ^e crystallization temperature; ^d enthalpies of crystallization; ^g glass transition temperature; ^h calculated crystallinity; ⁱ neat PLA processed under identical conditions to the corresponding blends; ^j value obtained from DMA measurements.

Mechanical properties

Tensile tests were conducted to determine the effect of the additives on mechanical properties of the samples. Table. 9. details the tensile strength, elongation at break and Young modulus of the pure PLA and PLA base samples. Supplementing neat PLA with ALUM subtly enhanced all the mechanical characteristics of the material. As anticipated, the mechanical properties of the expanded samples diminished significantly in a very similar manner, regardless of their exact composition. This decline was more pronounced than the results published elsewhere [104], which investigated the comparable

morphology of microcellular PLA specimens. Such a deterioration occurred primarily because of the free-space volume contained in the expanded samples, thereby deteriorating the integrity of the same, partially reducing their molecular weight and diminishing the resultant mechanical properties

Table. 9. Initial mechanical properties of neat PLA and microcellular PLA.

Sample	Tensile strength (MPa)	Elongation at break (%)	Young's modulus (MPa)
Neat PLA after processing	50.5 ± 2.6	16.7 ± 2.1	788.8 ± 62.9
PLA-ALUM	60.6 ± 2.6	16.8 ± 0.6	907.4 ± 88.1
PLA/MSS3	27.1 ± 0.6	10.2 ± 0.5	382.2 ± 34.3
PLA/MSS5	21.4 ± 0.8	8.2 ± 0.2	321.8 ± 80.0
PLA/ALUM/MSS3	20.9 ± 0.7	9.2 ± 0.7	345.6 ± 67.6
PLA/ALUM/MSS5	21.1 ± 1.0	7.3 ± 0.2	569.2 ± 25.5

Hydrolysis

The effects of the additives and microcellular structure on the rate of hydrolysis of the PLA-based materials were investigated by GPC and DSC in an aqueous environment at 37°C in the presence of a microbial growth inhibiting substance (NaN₃).

Changes in molecular weight during abiotic degradation

GPC measurement was carried out to discern changes in the PLA at a molecular level during hydrolysis (Figure 17). Reductions in M_w occurred because of random chain scission of the ester bonds, an action that participated in such hydrolysis [107]. The M_w reduction rate in the neat PLA was in agreement with a previous investigation [107], which was performed at a temperature beneath the point of glass transition. At this temperature, when PLA is in the glassy state, the polymer chains are tightly bound to one another resulting in a limited mobility. Therefore, making it much harder for water to

penetrate the polymer matrix. Moreover, the kinetics of hydrolytic scission of ester bonds by water are reduced significantly. Herein, the microcellular materials (PLA/MSS3 and PLA/MSS5) showed a slightly accelerated chain scission rate than the neat PLA. This acceleration can be attributed to two factors: the lower M_w in the microcellular samples at the beginning of hydrolysis and their porous structure enabling effective contact of the polymer material with the degradation media. As a result, there was an increase in the effective surface area of the samples, allowing water to penetrate the polymer more readily than in the neat PLA. Interestingly, the M_w of samples incorporated with ALUM remained largely unchanged for about 30 days, after which it decreased at a similar rate as the material without the additive. Hence, although the microcellular samples reached a lower M_w at the end of the observation period of 140 days, the rate of hydrolysis of the microcellular specimens was somewhat comparable with that of the non-expanded PLA material.

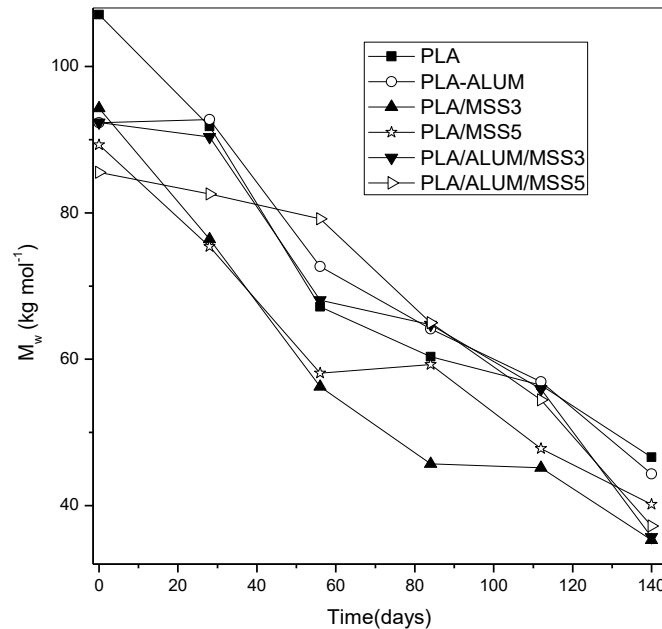


Figure. 17. Molecular weight evolution of the materials during abiotic hydrolysis

Changes in thermal properties during abiotic degradation

Table. 10. illustrates the effect of abiotic hydrolysis (at 0.1 mol L⁻¹, pH 7) on the thermal properties of the microcellular samples and contrasts them with those of the

nonporous materials. The samples were initially highly amorphous [108, 109], but after 12 weeks, a visible increase in crystallinity was detected in the microcellular samples only. This indicated that some newly formed degradation products possessed sufficient mobility to produce a crystalline lattice [108]. Notably, PLA/MSS5 showed the highest value for the degree of crystallinity, potentially attributable to the highly porous structure of the specimens. The formation of low-molecular-weight fragments, caused by chain scission of the ester bonds entrapped in the polymer matrix, brought about slight reduction in melting and glass transition temperatures. The new oligomers acted as a plasticizer, sufficiently lowering values for T_g [107]. This behaviour was again more pronounced for the microcellular samples, which was in agreement with the findings obtained from GPC analysis. A split in the melting peak also appeared at certain sampling times for all the specimens. In the nonporous samples, this could be attributed to a different rate of chain scission in the cortex of the material, while in the microcellular specimens, the reason is selective degradation of the amorphous phase rather than the crystalline part.

Table. 10. Thermal properties of samples prior to and after abiotic hydrolysis at various times.

Sample	Time of hydrolysis (weeks)	$T_{m_1}^a$ [°C]	$\Delta H_{m_1}^b$ [J·g ⁻¹]	$T_{m_2}^c$ [°C]	$\Delta H_{m_c}^d$	T_c^e [°C]	ΔH_c^f [J·g ⁻¹]	T_g^g [°C]	χ_c^h [%]
PLA	0	152.5	-	-	-26.9	123.2	26.2	59.3	0.7
	4	152.2	-	-	-35.9	119.2	34.5	60.0	1.5
	12	149.0	-22.4	156.5	-39.4	110.5	37.9	59.4	1.6
	20	148.1	-14.6	157.3	-40.3	104.6	40.1	58.7	0.2
PLA-ALUM	0	153.5	-	-	-24.3	123.5	22.0	59.8	2.5
	4	152.0	-	-	-33.0	117.7	31.0	59.2	2.2
	12	148.9	-19.7	156.5	-38.6	109.0	33.6	59.29	5.4
	20	148.1	-15.4	157.0	-42.5	105.1	37.7	58.93	5.2
PLA/MSS3	0	155.0	-	-	-16.1	126.2	16.6	58.4	0.5
	4	151.1	-24.01	157.4	-36.3	114.7	34.18	59.1	2.3
	12	148.9	-12.33	156.8	-38.5	107.7	30.3	59.1	8.7
	20	155.1	-	-	-41.5	95.4	28.1	56.5	14.4

PLA/MSS5	0	154.6	-	-	-27.7	125.7	24.5	57.8	3.5
	4	152.2	-16.2	158.7	-30.6	114.8	26.2	60.6	4.8
	12	148.6	-17.8	157.1	-41.8	107.7	31.5	58.7	11.1
	20	146.9	-11.0	155.8	-42.8	99.7	28.8	57.7	15.0
PLA/ALUM/MSS3	0	154.3	-	-	-25.3	126.2	21.1	59.7	4.5
	4	151.3	-28.1	157.5	-42.7	119.8	39.7	59.3	3.3
	12	148.9	-12.7	157.3	-38.0	106.5	28.7	58.8	10.0
	20	154.5	-	-	-42.3	94.0	33.4	56.2	9.6
PLA/ALUM/MSS5	0	154.0	-	-	-27.8	124.5	25.0	59.8	3.0
	4	152.2	-	155.7	-33.3	117.7	25.3	59.4	8.6
	12	155.8	-	-	-37.9	103.5	22.6	57.6	16.4
	20	155.7	-	-	-41.8	952	31.9	56.1	10.7

^a melting temperature of first peak; ^b enthalpies of melting of first peak; ^c melting temperature of second peak; ^d total enthalpies of melting; ^e crystallization temperature; ^f enthalpies of crystallization; ^g glass transition temperature; ^h calculated crystallinity;

Release of the antimicrobial compound

Release of the antimicrobial agent from the PLA samples in phosphate buffer solution (pH = 7.4) was investigated to evaluate the effect of the porous structures on the stability of ALUM in the polymer matrix. Samples containing ALUM were incubated at 37 °C for approximately 120 days in the buffer solution. The release of ALUM occurred by the microcellular samples (PLA/ALUM/MSS). Initial rapid release occurred around 10 days and followed by a gradual release. The initial release can be attributed to the release of ALUM located close to the surface. In contrast, nonporous samples exhibited a rapid release of less than 1% of the ALUM over a few days, followed by negligible release in the subsequent period (Figure 18). The more rapid release observed from the porous samples could be attributed to the microcellular morphology of the samples, which possess the larger active surface area; this permits faster penetration of water into the polymer matrix and subsequent diffusion of ALUM onto the polymer surface. Comparing the two porous samples revealed that the initial rapid release of both was almost identical, although the release of ALUM during the following phase was slightly more pronounced for PLA/ALUM/MSS5, as it contained smaller and more numerous

pores in its structure. At the end of the observation period, the cumulative release of ALUM equalled approximately 15% and 10% for PLA/ALUM/MSS5 and PLA/ALUM/MSS3, respectively, whereas for PLA-ALUM, it was only about 1%.

In point of fact, while the release of an antimicrobial agent from a medical implant might diminish the antimicrobial effect of the given material, it could still prevent microbial growth in its surroundings. Note that the tolerance of PLA/ALUM was very low, hence not visible in Figure 18.

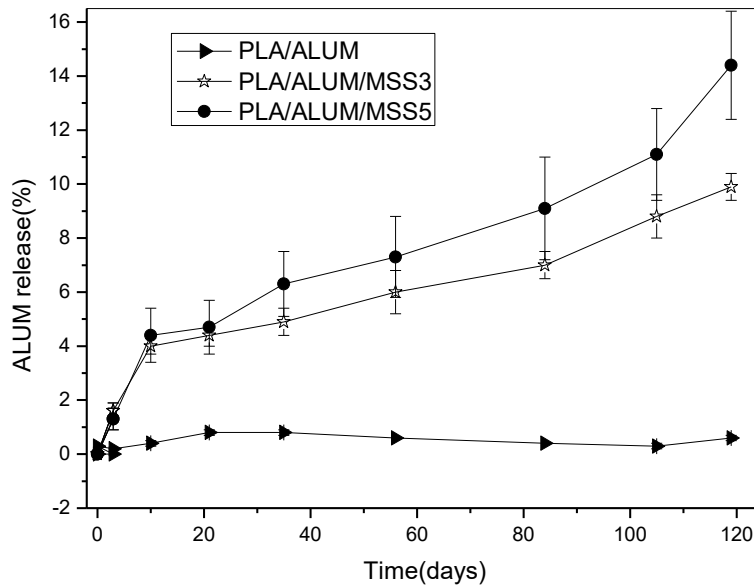


Figure. 18. Release of ALUM in phosphate buffer saline (PBS) buffer (pH = 7.4) at 37°C.

Antimicrobial properties

In order to inhibit microorganism growth effectively, their life cycle has to be interrupted. Table. 11 shows the reduction in bacterial growth of *S. aureus* (gram-positive) and *E. coli* (gram-negative) on the surface of the PLA-ALUM, microcellular PLA/ALUM/MSS3, and microcellular PLA/ALUM/MSS5 specimens after 24 hours of incubation at 35 ± 2 °C. In general, PLA-ALUM specimens showed no alteration in bacterial growth. Whereas, microcellular specimens showed promising results at inhibiting the growth of the tested bacterial strains. As can be seen in the table ALUM shows effective antimicrobial activity against the gram-negative bacteria (*E. coli*), as compared to a gram-positive (*S. aureus*). Gupta *et al*, reported that ALUM could be considered an effective antimicrobial agent against the gram-negative bacteria, in comparison with a gram-positive. This phenomenon occurs because of the differences in

the membrane structure and thickness of the peptidoglycan layer in gram-positive and gram-negative microorganisms [110-113]. Some studies reported that MSS showed antimicrobial activity against *E. coli* and *S. aureus*; therein, the value of CR rose as a consequence of increasing the amount of MSS [114]. This means that synergic effects could be expected from ALUM and MSS. Surprisingly, only PLA/ALUM/MSS5 showed a noticeable drop in reduction of CFU (CR) against *E. coli*. This can be attributed to smaller and more numerous pores of the specimens that may affect the results of the applied testing procedure (ISO 22196). However, the obtained results showed antibacterial effects of both PLA/ALUM/MSS3 and PLA/ALUM/MSS5 samples

Table. 11. Reduction in colony forming units (CR) effected by of pure PLA-ALUM, microcellular PLA/ALUM/MSS3, and microcellular PLA/ALUM/MSS5

sample	CR (%)	
	<i>E. coli</i> CCM 4517	<i>S. aureus</i> CCM 4516
PLA-ALUM	100	100
PLA/ALUM/MSS3	93	98
PLA/ALUM/MSS5	64	97

CONCLUSION

This work focused on preparing and characterizing of antibacterial, microcellular polymeric material based on PLA, utilizing potassium aluminium sulfate dodecahydrate (ALUM) as an antimicrobial agent and monobasic sodium salts as a blowing agent. Morphological analysis of the surface of specimens revealed that adding ALUM instigated greater cell density in the polymer matrix and reduced average cell size. Tests demonstrated that mechanical properties of microcellular PLA were diminished because of microcellular morphology, and hydrolysis acceleration took place due to increasing the effective surface area of the microcellular PLA, thereby evidencing a rapid reduction in molecular weight by approximately 43% in comparison with neat PLA. The microcellular PLA samples exhibited accelerated degradation, primarily due to their microcellular structure, facilitating better penetration of the buffer solution into the structure of samples. Furthermore, the release of an antimicrobial compound and subsequent antimicrobial activity against *S. aureus* and *E. coli* were evaluated. It was confirmed that the rate of release in PLA/ALUM/MSS5 (15 %) was higher than in other samples (10 %, PLA/ALUM/MSS3), as a consequence of its microcellular morphology and more numerous pores in its structure. Finally, it was demonstrated that ALUM

proved effective antimicrobial activity against the gram-positive and gram-negative bacteria utilized, although its effect was greater against the latter of the two.

2.2. Preparation and characterization of polylactide-based porous systems mat for wound dressing application

Introduction

Wound dressings have improved vastly over the past decade, from crude, traditional gauze to tissue-engineered scaffolds. An extensive variety of wound dressing formats based on their application for the wound have been investigated or made commercially available [115, 116]. A desirable wound dressing should provide an optimal healing environment which leads to a rapid wound healing. It should be able to absorb exudates from the wound surface, maintain a proper moist environment in the wound bed, and, crucially, it should be able to gradually release antimicrobial active agents to ensure prolonged antimicrobial activity and sustain a healthy concentration of healing tissues [117, 118]. In recent years, there has been growing attention to fabricate porous structures for wound dressing applications based on natural and synthetic polymers via different techniques. Polylactide (PLA) is one of the biopolymer which has been widely used in wound dressing applications due to its biocompatibility, biodegradability, good mechanical durability, and non-toxicity to the human body[119, 120]. However, PLA is highly hydrophobic which extremely restricts its application in the field of wound dressing due to the limitation of water uptake capacity. Moreover, hydrophobicity of PLA has a great impact on the efficiency of the release of the active agents from the polymer matrix[119, 121-123]. Therefore, porous structure could be one approach in order to tackle these issues. A three-dimensional porous structure can improve the permeability of the wound dressing, and at the same time providing sufficient space for cell growth. It has previously been reported that porous structures promote the skin regeneration and wound healing [119, 124]. Furthermore, porous structures offer a larger surface area that could allow active agents to diffuse out from the matrix in an extremely efficient manner[123].

PVA is synthetic biocompatible polymer widely used in biomedical applications[125]. Ribba *et al.* fabricated PLA-PVA films for wound dressing applications, which exhibited good stability over time, humidity control and, biocompatibility[126]. Hongyan *et al.* developed the PLA-PVA/SA membranes and assessed their in-vivo and vitro wound healing capability. These membranes displayed effective wound healing performance[125].

Surface liquid spraying is a unique and simple method for the preparation of a porous structure (porous mats). It is similar to the emulsion freeze-drying technique. However, the only difference is that in the surface liquid spraying method, the organic phase is sprayed to the aqueous phase, which gives a more porous structure[127, 128]. Generally, emulsion freeze-drying technique is the most widely used method due to its relative ease of use. However, this method has two major restrictions: (1) poor encapsulation

efficiency (EE) and (2) fast release of active agents occurring at the early stages. Several studies have reported that the addition of salts to the polymer could enhance the encapsulation efficiency by depressing drug aqueous solubility, and simultaneously may depress organic solvent solubility in the aqueous phase[129-131]. Pistel *et al.* demonstrated that the addition of inorganic additives such as salts to the aqueous phase causes increasing porosity and the specific surface area of the polymer[132]. One approach to overcome the release in early stages is thermal treatment or heating the polymer matrixes above the (T_g). Thermal treatment above T_g could change the physical-mechanical properties and therefore prolonging the drug release[133-135]. Castro *et al.* reported sustained release of simvastatin from polylactide acid (PLA) membranes after thermal treatment[136].

In this study, PLA-PVA porous mats were fabricated by surface liquid spraying method for potential wound dressing application. Sodium chloride (NaCl) and potassium permanganate ($KMnO_4$) salts were added to the aqueous phase of an oil in water (O/W) emulsion. NaCl is a neutral salt while $KMnO_4$ is a strong oxidizing agent and has mild antiseptic and astringent properties, which traditionally has been used to treat exuding wounds [137, 138]. Finally, after a short thermal treatment (80°C, 2 min) of the mats, the effect of the salts (NaCl, $KMnO_4$) and the thermal treatment on the in-vitro release profile, entrapment efficiency and physicochemical properties of the mats were investigated.

Materials

Poly lactide semi-crystalline PLA6202D was purchased from NatureWorks® Ingeo™ (Minnetonka, Minnesota, USA). Chloroform was purchased from VWR (14 Media Village, Leighton Buzzard, LU7 0GA, UK). Gentamicin sulfate salt and polyvinyl alcohol were supplied by Sigma-Aldrich (St. Louis, Missouri, USA). Sodium chloride was purchased from Mikrochem (Slovak Republic). Potassium permanganate was purchased from Penta Prague (Czech Republic).

Preparation of the porous mats

The organic phase was 2% PLA in chloroform solution and the aqueous phase was 0.1% PVA aqueous solution. Different salt concentrations were added to the aqueous phase (10 g/L NaCl and 0.4 mg/L $KMnO_4$). The resultant organic solution was sprayed onto the PVA aqueous solution at the rate of 4 mL/min under moderate magnetic stirring (600 rpm) and 1 bar air-pressure at room temperature to form an oil in water (O/W) emulsion. Subsequently, stirring was maintained overnight in order to evaporate the chloroform. Next, the product was washed three times with deionized water (DI) and

filtered. The loading of GS was performed by dissolving GS in DI water and dispersing the filtered product into the solution of GS and DI water. The final product was then frozen. In the final step, the frozen sample was lyophilized. Figure 19 shows the schematic diagram of the surface liquid spraying process.

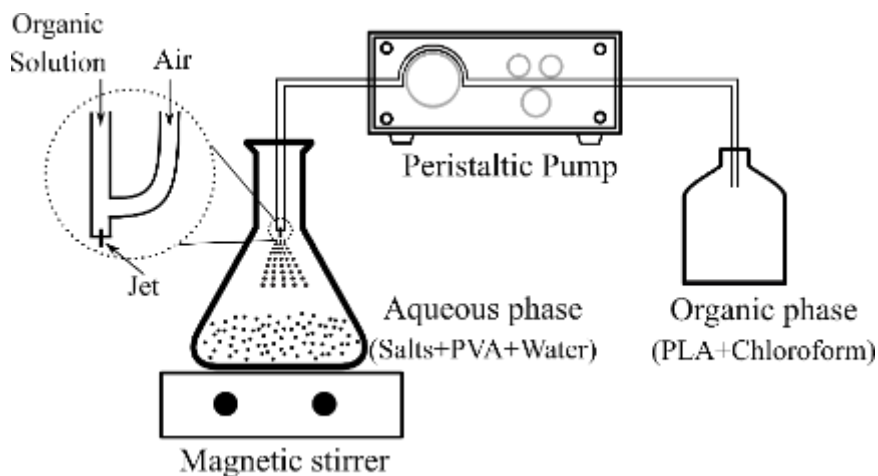


Figure. 19. Scheme of Surface liquid spraying process.

Thermal treatment of the porous mats

In order to study the effect of thermal treatment, the porous mats were placed in an oven (Memmert, Germany) at 80°C for 2 minutes. The mats were then kept in the silica gel containing desiccator. Subsequently, thermal treated mats were then subjected to the various characterization tests as described below.

Characterization of the porous mats

Attenuated Total Reflection Fourier-transform infrared (ATR-FTIR) spectroscopy

The ATR-FTIR test is an appropriate approach to identify functional groups of polymers and molecular structures of the chemicals. The FT-IR spectra were obtained on a Nicolet iS10 instrument equipped with a Zn/Se crystal (Thermo Fisher Scientific, Waltham, MA). The collected spectra in the wavenumber range from 400 to 4000 cm^{-1} represented the average of 64 scans at a spectral resolution of 4 cm^{-1} . The spectra for mats before and after the thermal treatment were recorded.

Differential scanning calorimetry (DSC)

Thermal properties of mats before and after thermal treatment were investigated by DSC on a DSC1 STAR system (Mettler Toledo, Greifensee, Switzerland). The preparation of samples has been adopted from our previous paper [139]. In brief, approximately 5 mg of each mat was placed in an aluminium pan. The following heating

program was applied in the presence of Nitrogen with the flow rate of 50 mL min⁻¹: In an initial heating cycle mats were heated from 25°C to 180°C (10°C min⁻¹), the upper temperature being maintained for 5 minutes. This was followed by a subsequent cooling to -35°C (10°C min⁻¹). The temperature of -35°C was maintained for 5 minutes, and a further heating scan was performed at 220°C (10°C min⁻¹). The melting temperature (T_m) and exothermal response related to cold crystallization temperature (T_c) were obtained from the second heating cycle. The region of glass-transition temperature (T_g) was determined from the second heating scan. The degree of crystallinity (χ_c) was calculated according to the Equation (4) [139]:

$$\chi_c = \left(\frac{\Delta H_m - \Delta H_c}{\Delta H_m^0} \right) * 100\% \quad (4)$$

where, ΔH_m is the heat of fusion ΔH_c represents the enthalpy of cold crystallization and ΔH_m⁰ is the tabulated heat of fusion for a theoretically 100% crystalline PLA homopolymer (93.1 J g⁻¹) [139].

Morphological analysis

The morphology of the mats was investigated by thermionic-emission scanning electron microscopy; (ESEM) (VEGA-II LMU, TESCAN, Brno, Czech Republic) in order to visualize the porosity of the mats. The mats were prepared by cryogenic fracturing of the mats in liquid nitrogen. This was followed by coating mats with a thin layer of Au/Pd. The microscope equipped with an SE detector was operated at an acceleration voltage of 10 kV in the high-vacuum mode [139].

Porosity measurement

The porosity of the mats was determined by liquid displacement method [140]. The weight (W₁) and volume (V) of mats were measured before the immersion into ethanol. After the saturation of mats by absorbing ethanol, the weight of mats were measured again (W₂). The porosity of the mats was calculated according to the Equation (5) (ρ represents the density of the ethanol) [140]. All experiments were performed in triplicate.

$$Porosity (\%) = \left(\frac{W_2 - W_1}{\rho V} \right) * 100 \quad (5)$$

Swelling test

The swelling test was performed by immersing pre-weighted samples (samples were cut into 1 cm² square pieces) in phosphate-buffered saline (PBS) solution of pH 7.4 at 37°C. Subsequently, the samples were removed at specific time intervals and the excess water on the surface was carefully absorbed by using filter paper, after which the samples were weighted. The degree of swelling was calculated according to the following Equation [141]:

$$\text{Degree of swelling (\%)} = (W_t - W_i)/W_i * 100 \quad (6)$$

where, W_t is the weight of the swollen sample, and W_i is the sample at time zero (starting time).

Water solubility

To determine the water solubility of mats, samples (samples were cut into 1 cm² square pieces) were placed in an oven at 37°C for 24 h. Then, the dried mats were immersed in DI water for 24 h and dried again at 37°C for 24 h. The solubility of the mats was evaluated using the following Equation [142]:

$$S = \left(\frac{W_0 - W_d}{W_0} \right) * 100 \quad (7)$$

where, W_0 and W_d represent the weights of the dry sample and the weight of the dried sample at 37°C after immersion in distilled water, respectively [142].

Water vapor transmission rate (WVTR)

The moisture permeability of the mats was determined by measuring the WVTR according to the standard ASTM test method (E96-90), as follows [143]. The samples were cut into discs with a diameter of 15 mm, and mounted on top of a plastic tube containing 10 mL of distilled water. These assemblies were sealed with Teflon tape in order to avoid boundary loss and then placed in a straight position at 37°C inside an oven contained 1 kg of freshly dried silica gel to maintain relatively low humidity conditions. After regular intervals of time, the weights of the assemblies were measured. The WVTR of the samples was calculated according to the Equation (8) [144]:

$$\text{WVTR (gr/m}^2 \cdot \text{Day)} = (W_i - W_f)/A \quad (8)$$

where, A is the exposure area, and W_i and W_f are the initial and final weights of the assemblies, respectively.

Drug loading and in-vitro release study

The gentamicin sulfate (GS) loading efficiency and in-vitro release behaviour of the drug was carried out in the presence of a non-toxic and isotonic release medium, PBS. The entrapment efficiency (EE) and loading capacity (LC) of GS were evaluated by immersing the mats into 50 mL of PBS 10 mM at pH 7.4 in capped glass flasks. The glass flasks were kept in an orbital incubator (Stuart SI500, UK) at $37 \pm 0.5^\circ\text{C}$, set to 40 rpm for 1 h. Equations (9) and (10) were applied to calculate EE (%) and LC (%), respectively [145].

$$EE(\%) = \frac{\text{Total}_{\text{GS}} - \text{Free}_{\text{GS}}}{\text{Total}_{\text{GS}}} \times 100 \quad (9)$$

$$LC(\%) = \frac{\text{Total}_{\text{GS}} - \text{Free}_{\text{GS}}}{\text{matsweight}} \times 100 \quad (10)$$

where, Total_{GS} was the amount of primary GS added to the solution and Free_{GS} was assessed through high-performance liquid chromatography (HPLC), on a Dionex UltiMate 3000 Series device (Thermo Fisher Scientific, Germany) using o-phthalaldehyde (OPA) as a derivatizing agent. The methodology was adapted from Smělá *et al.*, [146] with minor modification, as described below. The reducing solution was prepared by adding 250 μL of 2-mercaptoethanol and 10 mL of 0.04 M sodium borate (pH~11). Separately, a solution of OPA was prepared by dissolving 2.5 g of OPA in a mixture composed of 400 μL methanol, 200 μL reducing solution and 4.4 mL of 0.04 M sodium borate (pH~11). The OPA solution was stored in the dark and utilized within 24 h after preparation. The separation after OPA in needle derivatization was performed on a reversed-phase column XSELECT CSH C18 5 μm (4.6 x 250 mm; Waters, USA), equipped with a security guard column (Phenomenex, USA) at 30 $^\circ\text{C}$. A mixture of 100 mM Acetate buffer (A; pH 5.8) and HPLC grade Acetonitrile (ACN; B) was applied as the mobile phase (55:45, v/v) at a flow rate of 0.4 mL/min. The volume of the injection was defined by user defined program (UDP) settings, a volume of 10 μL was injected into the column originating from a drawn sample volume of 1 μL . The eluted OPA derivatives were detected by fluorescence using 330 nm and 440 nm as excitation and emission wavelengths, respectively. All measurements were performed in triplicate.

In the next stage, to evaluate the in-vitro release rate, the medium was replaced with 50 mL fresh PBS 10mM (pH 7.4), and glass flasks were kept in an orbital incubator at

37 ± 0.5 °C, 40 rpm. At predefined time intervals, 2 mL of the medium was taken, and the same volume of the fresh medium was replaced in the glass flasks. The amount of GS in the medium was evaluated by HPLC apparatus, and OPA was used as a derivatizing agent [146]. The cumulative percentage release of GS from the mats was calculated and plotted against time (n= 3).

Results and discussion

Attenuated Total Reflection Fourier-transform infrared (ATR-FTIR) spectroscopy

The ATR-FTIR spectroscopy analysis was carried out to investigate the structural changes of mats based on PLA, PVA, and different salts before and after thermal treatment at the molecular level. The FT-IR spectra of mats are shown in Figure. 20. The PLA-PVA mats show some characteristic peaks identified by the strong infrared absorption band in the region of $1650\text{--}1754\text{ cm}^{-1}$, which corresponds to the stretching vibration of the carbon-oxygen double bond. The band at 1187 cm^{-1} is assigned to the stretching vibration of the carbon-oxygen bond. The two peaks around 1448 and 1373 cm^{-1} correspond to the methyl groups of the PLA-PVA mats. Moreover, the high intensive peak that is positioned at 3399 cm^{-1} corresponds to the stretching vibration of the oxygen-hydrogen bond[147-149]. Figure. 20. illustrates that the intensity and position of the absorption peak of the hydroxyl group changed with the addition of salts and the thermal treatment. Addition of KMnO_4 to the mat caused the disappearance of the OH peak in the FT-IR spectra, which indicates the oxidation of PVA to polyvinyl ketone (PVK). The formation of corresponding ketone is due to the fact that KMnO_4 is a strong oxidizing agent[150-152].

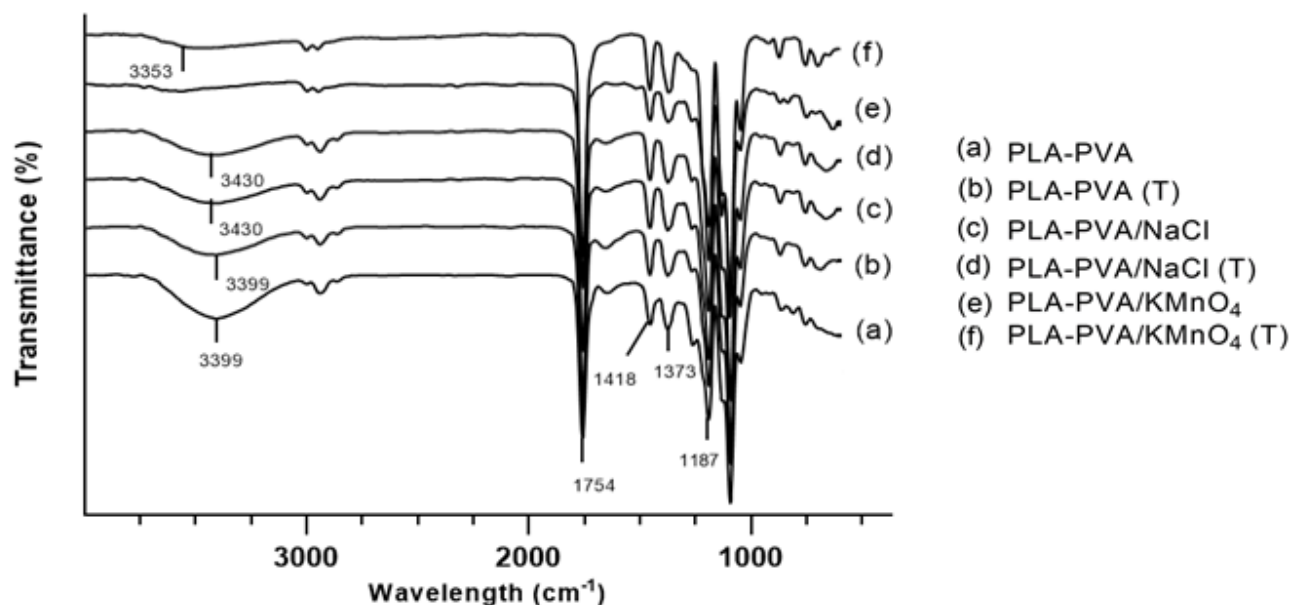


Figure. 20. FT-IR spectra of PLA-PVA (a), PLA-PVA (T) (b), PLA-PVA/KMnO₄ (c), PLA-PVA/KMnO₄ (T) (d), PLA-PV/NaCl (e), PLA-PVA/NaCl (T) (f) mats.

In the case of the addition of NaCl, the hydroxyl peak in PLA-PVA/NaCl mat is weaker than it is in PLA-PVA mat and its position was shifted slightly toward a higher frequency (3430 cm⁻¹). This can be attributed to a higher degree of hydrogen bonding in the PLA-PVA mat, because hydrogen bonding is disrupted by the addition of NaCl [153]. The thermal treated PLA-PVA and PLA-PVA/NaCl mats show that the hydroxyl peak has a lower intensity in comparison with the non-thermal treated mats [154]. In case of the thermal treated PLA-PVA/KMnO₄ mat, the OH peak in the FT-IR spectra appear and it is shifted to a higher wavelength from (3353 cm⁻¹). This can be explained by the partially formation of the carboxylic acid group due to the elevated temperature in the presence of KMnO₄ [155, 156].

Thermal properties

DSC analysis of the porous mats was carried out to study the effects of the thermal treatment and salts on the thermal behaviour of the mats. The correlated thermal properties of the mats are summarized in Table. 12. As expected, crystallinity (χ_c) increased after the thermal treatment of the mats [136]. The T_g of the mats did not demonstrate any significant changes after the thermal treatment as shown in Figure. 21. Furthermore, T_m , and T_c values were not affected by the thermal treatment and were in agreement with the published literature values [136, 157]. Increase in the concentration of NaCl caused significant reduction in crystallinity, which could be attributed to the fact that high NaCl content impedes PLA chain mobility and thereby prohibits crystallization [158]. According to the literature, the oxidation of PLA and PVA by

KMnO₄ caused a decrease in crystallinity [159, 160]. Moreover, the addition of salts induced a decrease in T_c, an increase in T_m (consistent with the results given in[161]), and showed no difference in the T_g values.

Table. 12. Selected material-related properties of the mats before and after thermal treatment.

Sample/property	Untreated			After thermal treatment		
	PLA-PVA	PLA-PVA/KMnO ₄	PLA-PVA/NaCl	PLA-PVA	PLA-PVA/KMnO ₄	PLA-PVA/NaCl
χ _c	5.1	4.9	0.7	8.8	5.3	3.0
T _g	61.9	62.0	62.0	61.1	61.7	61.2
T _c	129.9	118.3	115.4	130.4	118.1	114.4
T _m	164.3	167.4	168.0	164.6	167.5	167.0

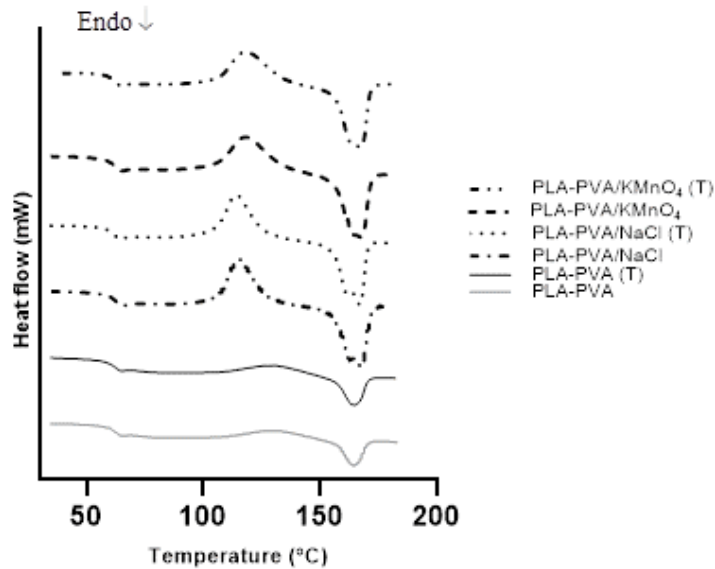


Figure. 21. DSC curves of porous PLA mats.

Measurement of porosity

The study of the porosity of wound dressing is a very important factor as it affects the absorption capacity of exudates from the wound, which can reduce the probability of infection[162]. As shown in Table. 13, all the mats showed a porosity ranging between

68 - 94 %. These results indicate that the porosity was increased with the addition of the salts. A higher salt concentration led to increase in the porous structure, resulting in an irregular and spongier shape[132]. However, the total porosity of the mats slightly decreased after the thermal treatment[134, 135, 163]. The graph clearly shows that non-thermal treated mats with the highest concentration (10 g/L) of NaCl possessed the highest porosity (94%), whereas there was a reduction of porosity (92%) for thermal treated mat with the same concentration of NaCl. Addition of KMnO₄ to the mat also followed the same trend as NaCl in terms of porosity. It is worth noting that the thermal treated mat without salt (neat mat) showed the lowest levels of porosity (68%).

Table. 13. Porosity measurements of porous mats after 24 h of immersion in ethanol at room temperature.

	Untreated			After thermal treatment		
Sample	PLA-PVA	PLA-PVA/KMnO ₄	PLA-PVA/NaCl	PLA-PVA	PLA-PVA/KMnO ₄	PLA-PVA/NaCl
Porosity	69.87±2.1	78.77±4.2	94.1±1.5	68.1±1.2	75±0.94	92.86±0.54

Morphology of the porous mats

The optical photographs PLA-PVA porous mat is shown in Figure. 22. PLA-PVA has white appearance with a smooth surface. Scanning electron microscopy (SEM) was used to investigate the effects of the addition of salts and thermal treatment on the morphology of porous mats. As can be observed from Figure. 23, the PLA-PVA mat show a disordered, interconnected pore-like structure with a rough surface. However, high resolution SEM analysis shows (Figure. 24 (a)) that the neat PLA-PVA mat, has fracture-like characteristics with almost no holes or pores. The addition of 10 g/L NaCl to the mats led to formation of more porous structures with interconnected pores with varying pore size in the range of 0.2 - 7 μm (Figure. 24 (b)). As can be seen from Figure. 24 (c), the addition of 0.4 mg/L KMnO₄ to the mat led to formation of a porous structure in a range of 0.4 - 4 μm. However, comparing Figures 24 (b) and 24 (c) leads to two main observations: (1) the addition of 10 g/L NaCl to the mats led to formation of more porous structures compared to the addition of 0.4 mg/L KMnO₄ to the mats; and (2) the addition of different salts leads to the formation of different shapes and sizes of the pores. It is likely that the size and shape of the pores are different due to the oxidation of PVA by KMnO₄ (discussed in FT-IR analysis section) in the case of PLA-PVA/KMnO₄. Pore formation of the mats containing salts can be attributed to its osmotic properties in aqueous phase, which has already been demonstrated by other authors[132, 164]. The

mats that have been subjected to thermal treatment present smoother surfaces with fewer fractures and less porosity (Figure. 24). These results were consistent with other studies[135, 163].

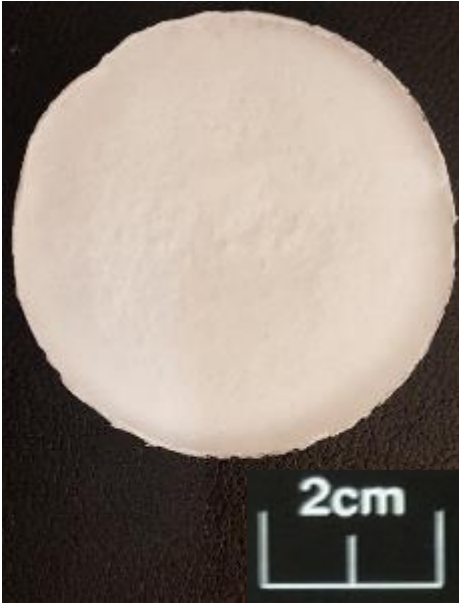


Figure. 22. Photographic appearance of PLA-PVA porous mat.

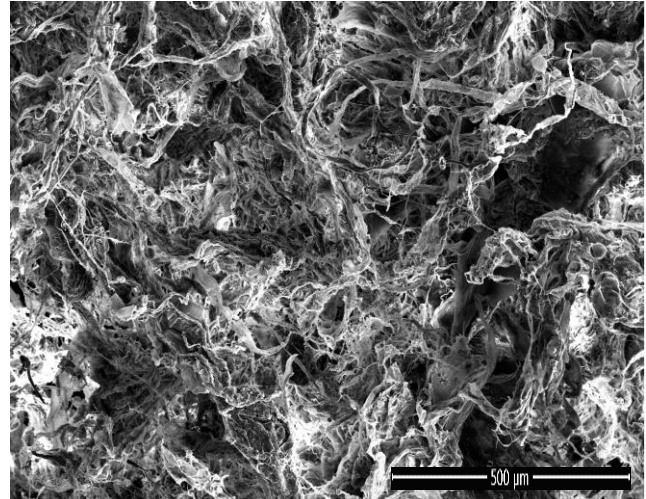


Figure. 23. SEM image of PLA-PVA porous mat

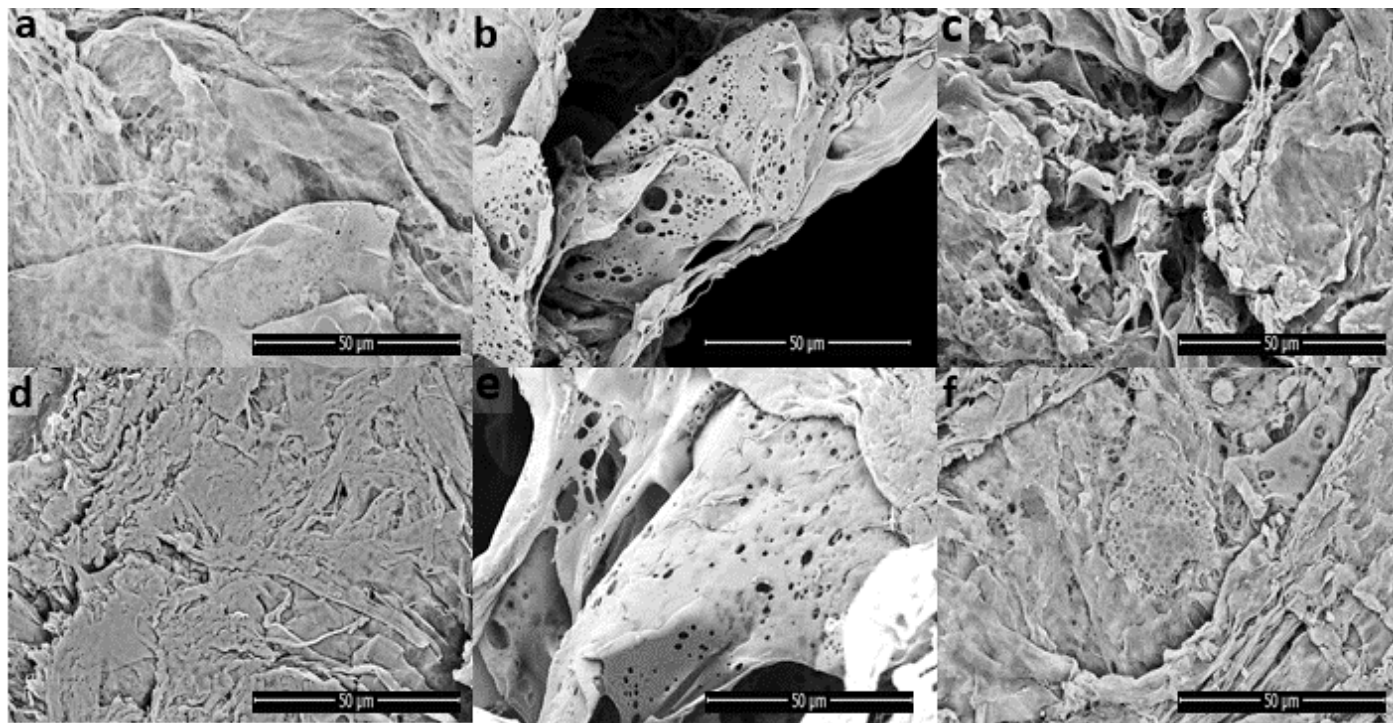


Figure. 24. SEM images of the porous mats: (a) PLA-PVA, (b) PLA-PVA/NaCl, (c) PLA-PVA/KMnO₄, (d) PLA-PVA (T), (e) PLA-PVA/NaCl (T), and (f) PLA-PVA/KMnO₄ (T).

Swelling test

The degree of swelling is mainly dependent on the porosity and hydrophilicity of the mats[140, 165]. This property of the mats plays an important role in acceleration of wound healing as it absorbs exudates and fluids secreted from the wound and provides a moist environment in the wound area[117, 122]. Figure. 25 shows the swelling behaviour of the mats. It was observed that increasing porosity led to an increase in the swelling degree. The highest swelling degree obtained by the non-thermal treated PLA-PVA/NaCl mat. This can be attributed to the high porosity percentage of PLA-PVA/NaCl compared to other mats (Table. 13). The lowest swelling degree was obtained from thermal treated neat PLA-PVA mat due to its lowest porosity and relative high crystallinity[166]. The higher swelling degree of thermal treated PLA-PVA/KMnO₄ mat compared to non-thermal treated PLA-PVA/KMnO₄ mat may be attributed to the formation of carboxylic acid group by oxidation of PVK in the presence of KMnO₄ at an elevated temperature (80°C). Therefore, the higher swelling degree of thermal treated PLA-PVA/KMnO₄ mat is attributed to the higher polarity and hydrophilic character of the carboxylic acid[161, 167, 168].

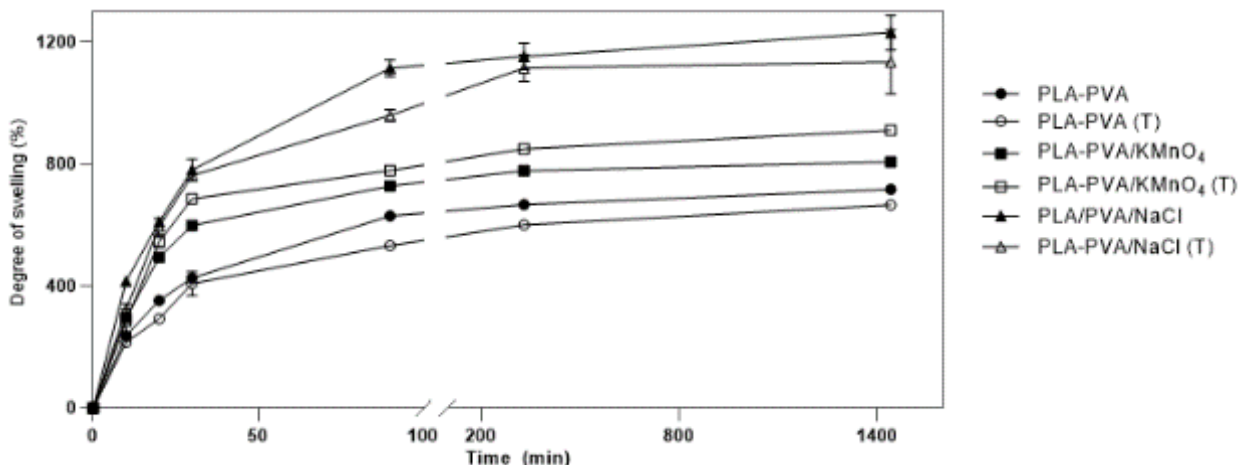


Figure. 25. Swelling studies of the porous mats in PBS with pH 7.4 at 37°C.

Water solubility

The water solubility of a polymer is a key factor in wound dressing applications, as the rate of degradation or hydrolysis takes place simultaneously with the wound healing process. If the degradation of the wound dressing occurs before the completion of the wound healing process, the wound dressing will need to be applied on the patient several times. This will not only cause discomfort but will also impose extra costs on the patient [169]. The water solubility assessment was performed by calculating the weight loss of the mats in DI water after 24 h using Equation 4. Water solubility of the mats ranges from 2% for thermal treated PLA-PVA and 10% for non-thermal treated PLA-PVA/NaCl as indicated in Table. 14. These results reveal that water solubility increases by increasing the amount of the salts in the mats. This increase in water solubility can be attributed to an increase in the porosity of the mats by the addition of salts. More porous structures allow and retain a higher number of water molecules in their structure [142, 169]. It is worth noting that all the mats kept their initial shape even after 24 h. Notably, the thermal treatment of the mats did not significantly affect the values of water solubility.

Table. 14. Water solubility measurements of the porous mats in DI water after 24 h at 37°C.

	Untreated			After thermal treatment		
Sample	PLA-PVA	PLA-PVA/KMnO ₄	PLA-PVA/NaCl	PLA-PVA	PLA-PVA/KMnO ₄	PLA-PVA/NaCl
Water solubility	4.09±0.00	6.50±0.20	10.87±0.18	2.67±0.25	7.36±0.18	9.41±0.50

Water vapour transmission rate (WVTR)

Water vapour transmission rate is the measurement of the amount of water lost through the dressing material [162]. An ideal wound dressing material should protect the wound from dehydration, which will occur due to high WVTR. It should also protect the wound from accumulation of exudate and the risk of bacterial growth caused by low WVTR [170, 171]. To maintain a moist environment for better wound healing the optimal range of WVTR for wound dressing material is 2000 - 2500 (g/m².day) [144, 172]. As shown in Table. 15, the measured value WVTR of the mats were in the range of 2115 - 2287 g/m².day. As previously mentioned, the addition of salts increased the porosity of the mats. This increase in the porosity is the main reason for the observed increase in values of the WVTR in PLA-PVA/NaCl and PLA-PVA/KMnO₄ mats. The thermal treatment of the mats did not affect the values of WVTR. The obtained WVTR results demonstrate that the mats are suitable for wound dressing applications [144, 172].

Table. 15. Water vapour transmission rate of the porous mats.

	Untreated			After thermal treatment		
Sample	PLA-PVA	PLA-PVA/KMnO ₄	PLA-PVA/NaCl	PLA-PVA	PLA-PVA/KMnO ₄	PLA-PVA/NaCl
WVTR	2146.01±19.48	2214.16±20.94	2287.61±25.31	2077±18.65	2207.08±24.45	2259.3±21.35

In-vitro drug release studies

An ideal antimicrobial wound dressing should sustain a long period of controlled drug release in order to accelerate the healing process and to avoid frequent changing of the

dressing [155]. Gentamicin sulfate as an antibiotic agent was loaded into the PLA-PVA mats. The effect of the addition of different types of salts and thermal treatment on entrapment efficiency (EE), loading capacity (LC), and in-vitro were studied. Tang *et al.* reported that the EE of drugs in the surface liquid spraying method is higher than the EE of drugs in traditional emulsion solvent evaporation method [127]. Therefore, liquid spraying method was used to obtain a higher EE. As shown in Table. 16, the surface liquid spraying method resulted in a high entrapment efficiency of the drug (90.11%). Furthermore, the addition of salts increased the EE. This could be attributed to changing the aqueous solubility of the organic solvent by salt [131, 173]. This could also be explained by increasing the porosity of the mats due to the addition of salts as mentioned in the porosity measurement section [132, 174]. While the thermal treatment did not significantly impact the EE, this was not the case for the PLA-PVA/NaCl. This could be attributed to the reduced porosity of PLA-PVA/NaCl due to the thermal treatment. Table 16 demonstrates that the addition of salts and thermal treatment did not affect LC (%), which can be attributed to the strong dependency of LC on the polymer weight ratio in accordance with Equation 10.

Table. 16. EE and LC of the porous mats before and after thermal treatment.

	Untreated treatment			After thermal treatment		
	PLA-PVA	PLA-PVA/KMnO ₄	PLA-PVA/NaCl	PLA-PVA	PLA-PVA/KMnO ₄	PLA-PVA/NaCl
EE (%)	90.11±0.21	92.08±0.06	97.57±0.03	92.38±0.49	93.52±0.46	86.7±0.4
LC (%)	4.5±0.01	4.6±0.003	4.8±0.001	4.6±0.02	4.7±0.02	4.32±0.02

The addition of salts to the polymer has a crucial effect on the initial burst release and the porosity of the mats. The initial burst release and the porosity of the mats varies depending on the salt concentration [132]. The in-vitro release profiles of antibiotics from the wound dressings are displayed in Figure. 26. PLA-PVA/NaCl mat exhibited the highest initial burst release due to the highest salt concentration and porosity. The cumulative drug release was around 82 %. The burst release rate during the first 24 hours in PLA-PVA/NaCl mat can be attributed to the fact that the aqueous environment washed all the drug from the surface and other nearby drug and was removed through the pores of the polymer matrix [174, 175]. In comparison with PLA-PVA/NaCl mat, thermal treated PLA-PVA/NaCl mat, showed an initial burst release of drugs during the first 6 hours of around 11%. This clearly showed a reducing initial burst release followed by a

gradual release in a decreasing rate over time with around 50% release of the drug during 14 days. These results are consistent with the results of other groups where thermal treatment was employed as a tool for prolonging the release of the drug. Moreover, thermal treatment of polymer at temperatures above T_g reduced the drug release rate [133, 176]. This can be attributed to the fact that thermal treatment increases the crystallinity of the polymer, in which crystalline domains function as a physical barrier, leading to slower diffusion of the drug [136]. As a result, thermal treatment of the PLA-PVA/NaCl mat causes the sustained release of GS. However due to the heating of the mats above T_g (80°C) the drug release rate was reduced.

As shown in Figure. 26, for PLA-PVA/ KMnO_4 mat, the initial burst release of drugs during the first 24 hours was only approximately 20%, followed by a gradual and constant release of GS over 14 days. The cumulative drug release was 33%. However, thermal treated PLA-PVA/ KMnO_4 mat showed an initial burst release of around 12 % during the first 6 hours followed by a fast sustained release profile around 61% over 14 days. As can be seen in the Figure, the cumulative drug release rate of heat treated PLA-PVA/ KMnO_4 mat had a higher release rate in comparison with PLA-PVA/ KMnO_4 mat. This could be explained by the formation of PVK as the result of the interaction between KMnO_4 and PVA. Thermal treating of PLA-PVA/ KMnO_4 mat caused partial oxidation of the formed PVK by KMnO_4 , and as a result formation of carboxylic acid groups. Carboxylic acids have a higher polarity and hydrophilic character in comparison with ketones (PVK) [161, 167, 168]. Therefore, thermally treated PLA-PVA/ KMnO_4 mat have a relatively higher hydrophilicity as compared to non-thermal treated PLA-PVA/ KMnO_4 mat. This higher hydrophilicity causes PBS to permeate more freely into thermal treated PLA-PVA/ KMnO_4 mat than it can permeate into the PLA-PVA/ KMnO_4 mat. Hence, although thermal treatment of the PLA-PVA/ KMnO_4 mat led to a decrease in the porosity, its higher relative hydrophilic character caused the higher cumulative release rate.

For the neat PLA-PVA mat, the initial burst release occurred during the first 6 hours followed by a slow and gradual release at around 58% over 14 days (Figure. 26). The thermally treated neat PLA-PVA mat exhibited the initial burst release in the first 6 hours at around 14% and the cumulative drug release was 20%. This means that the thermally treated neat PLA-PVA mat could not release the drugs and kept the drug inside the mat. This can be attributed to the less porous structure and relatively higher crystallinity of the mat [177].

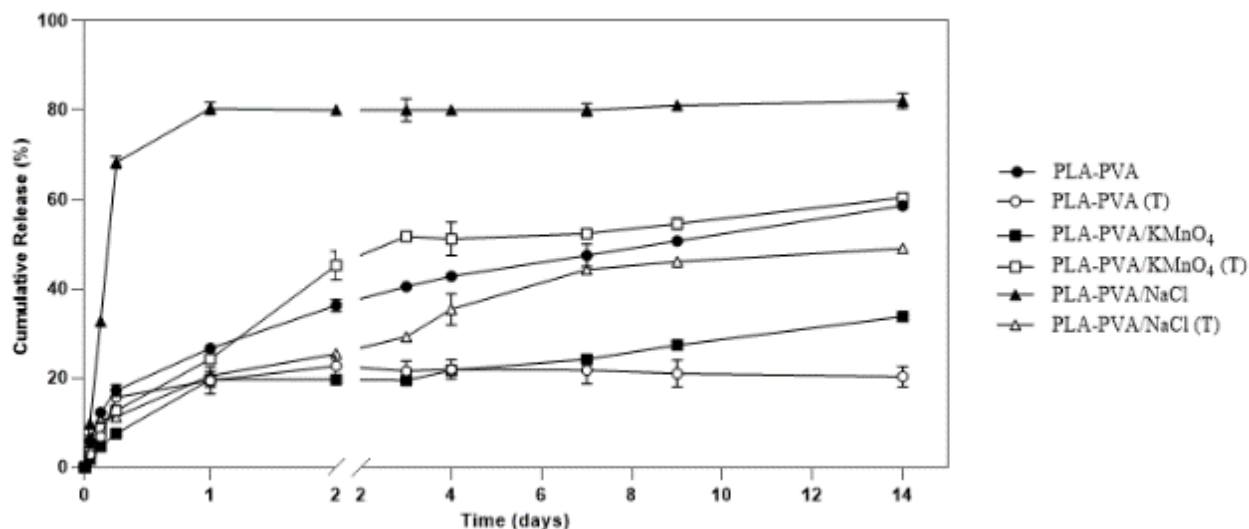


Figure. 26. In-vitro release profiles of porous mats loaded GS in pH 7.4 at 37°C.

CONCLUSIONS

Polymeric porous mats of PLA-PVA were prepared in this study by a slightly modified form of surface liquid spraying method. The effects of the addition of different salts (NaCl and KMnO₄) and thermal treatment (80 °C for 2 min) on the mats were investigated. The SEM results indicated that prepared mats had interconnected porous structures and the addition of salts considerably enhanced the porosity of the mats. Moreover, the swelling degree and water solubility of mats were increased due to the increase in porosity. The in-vitro release of gentamicin sulfate was studied and it was shown that a higher entrapment efficiency and initial burst release was achieved by the addition of salt to the aqueous phase. Additionally, the thermal treatment of the polymer above T_g reduced the initial burst release and prolonged the release of the drug. Finally, it worth noting that the procedure suggested in this study to prepare mats is cost-efficient and non-toxic, since all the solvents can be easily and completely removed. Therefore, the novel PLA-PVA mats developed in this work could be a potential candidate for wound dressing applications in the future.

SUMMARY OF WORK

Polyesters are widely used biodegradable polymers in biomedical applications such as drug delivery, cancer therapy, wound dressing, surgical use, and more. However, due to their intrinsic properties, such as hydrophobicity, polyesters should be modified in order to fine tune their use in some applications. Poly (lactic acid) is an environmentally-friendly polyester that has drawn attention over the past few decades owing to its suitable biocompatible, biodegradable and bioactive properties. PLA is highly hydrophobic polymer, therefore, one approach to address this issue is blending with another material to make porous structure. In this way porosity is increased and this in turn, increases the contact surface of the polymer.

According to the current state of knowledge, the overview of hydrophobic issue was drawn in the theoretical part, and research aims of work were defined. On the basis of this, the experimental part was devoted to the preparation of different PLA-based porous system for biomedical applications.

In this thesis, the first project focused on preparing and characterizing antibacterial, microcellular polymeric material based on PLA, utilizing potassium aluminium sulfate dodecahydrate (ALUM) as an antimicrobial agent and monobasic sodium salts as a blowing agent. Morphological analysis of the surface of specimens revealed that adding ALUM instigated greater cell density in the polymer matrix and reduced average cell size. The results showed increasing porosity in the polymer matrix led to an increase in release of ALUM. Moreover, porous samples showed effective antimicrobial activity against *E. coli* in comparison with *S. aureus*.

In the second project polymeric porous mats of PLA-PVA were prepared by surface liquid spraying technique. The SEM results indicated that mats had interconnected porous structures and the addition of salts considerably enhanced the porosity of the mats. The in-vitro release of gentamicin sulfate was studied and it was shown that a higher entrapment efficiency was achieved by the addition of salt to the aqueous phase.

CONTRIBUTIONS TO SCIENCE AND PRACTICE

The presented doctoral thesis brings new insights into the field of biodegradable polymers based on poly (lactic acid), which are highly potential for biomedical applications.

The main contribution to the science of the reported work can be found in the preparation and characterization of novel biodegradable PLA-based porous systems modified with inorganic agents in the form of:

- Microcellular antibacterial polylactide-based systems prepared by additive extrusion with ALUM for medical applications.
- Polylactide-polyvinyl alcohol-based porous systems loaded with gentamicin for wound dressing applications.

The results presented in this thesis have been published in reputed international journals.

REFERENCES

1. Richbourg, N.R., N.A. Peppas, and V.I. Sikavitsas, *Tuning the Biomimetic Behavior of Scaffolds for Regenerative Medicine Through Surface Modifications*. Journal of tissue engineering and regenerative medicine, 2019.
2. Sevim, K., *Modelling of Drug Release from Biodegradable Polymers*. 2017, Department of Engineering.
3. Albertsson, A.-C. and I.K. Varma, *Aliphatic polyesters: synthesis, properties and applications*, in *Degradable Aliphatic Polyesters*. 2002, Springer. p. 1-40.
4. Russell, J., *A General Approach Towards the Synthesis of Amido-Functionalized Biodegradable Polyesters*. 2010.
5. Gigli, M., et al., *Poly (butylene succinate)-based polyesters for biomedical applications: A review*. European Polymer Journal, 2016. **75**: p. 431-460.
6. Fradet, A. and M. Tessier, *Polyesters*. Synthetic Methods in Step-Growth Polymers, 2003: p. 17-134.
7. Telegdi, L. and L. Trif, *Biodegradable Polyesters for Medical Applications*. 2018.
8. Manavitehrani, I., et al., *Biomedical applications of biodegradable polyesters*. Polymers, 2016. **8**(1): p. 20.
9. N'Goala, K.L., *The synthesis of novel biodegradable polyesters and copolyesters from anhydrosulfites*. 1996, Aston University.
10. Liu, Q., *Structure-Property Relationship of "Peptide-like" Polyesters*. 2015, University of Akron.
11. Tokiwa, Y. and B.P. Calabia, *Biodegradability and biodegradation of polyesters*. Journal of Polymers and the Environment, 2007. **15**(4): p. 259-267.
12. Li, S. and M. Vert, *Biodegradation of aliphatic polyesters*, in *Degradable polymers*. 2002, Springer. p. 71-131.
13. Vert, M., et al., *Bioresorbability and biocompatibility of aliphatic polyesters*. Journal of materials science: Materials in medicine, 1992. **3**(6): p. 432-446.
14. Teo, S.Y., et al., *Polymeric materials as platforms for topical drug delivery: a review*. Int Pharm Pharm Sci, 2017. **9**: p. 14-20.
15. Genovese, L., *Synthesis and Characterization of New Aliphatic Biodegradable Polyesters for Packaging Applications*. 2016, alma.
16. Seyednejad, H., et al., *Functional aliphatic polyesters for biomedical and pharmaceutical applications*. Journal of Controlled release, 2011. **152**(1): p. 168-176.
17. Larsen, E., et al., *Tensile and compressive properties of cancellous bone*. Journal of Biomechanics, 1991. **24**(6): p. 459.
18. Little, C.J., N.K. Bawolin, and X. Chen, *Mechanical properties of natural cartilage and tissue-engineered constructs*. Tissue Engineering Part B: Reviews, 2011. **17**(4): p. 213-227.
19. Ebrahimi, A.P., *Mechanical properties of normal and diseased cerebrovascular system*. Journal of vascular and interventional neurology, 2009. **2**(2): p. 155.
20. Salahshoor, M. and Y. Guo, *Biodegradable orthopedic magnesium-calcium (MgCa) alloys, processing, and corrosion performance*. Materials, 2012. **5**(1): p. 135-155.
21. Haghghat, F. and S.A.H. Ravandi, *Mechanical properties and in vitro degradation of PLGA suture manufactured via electrospinning*. Fibers and Polymers, 2014. **15**(1): p. 71-77.
22. Pott, P.P., et al., *Mechanical properties of mesh materials used for hernia repair and soft tissue augmentation*. PLoS One, 2012. **7**(10): p. e46978.
23. Jamshidian, M., et al., *Poly-Lactic Acid: production, applications, nanocomposites, and release studies*. Comprehensive reviews in food science and food safety, 2010. **9**(5): p. 552-571.
24. Middleton, J.C. and A.J. Tipton, *Synthetic biodegradable polymers as orthopedic devices*. Biomaterials, 2000. **21**(23): p. 2335-2346.
25. Gentile, P., et al., *An overview of poly (lactic-co-glycolic) acid (PLGA)-based biomaterials for bone tissue engineering*. International journal of molecular sciences, 2014. **15**(3): p. 3640-3659.

26. Sin, L.T., A.R. Rahmat, and W.A. Rahman, *Overview of poly (lactic Acid)*, in *Handbook of biopolymers and biodegradable plastics*. 2013, Elsevier. p. 11-54.
27. Jiang, L. and J. Zhang, *Biodegradable polymers and polymer blends*. Handbook of Biopolymers and Biodegradable Plastics: Properties, Processing and Applications, 2012: p. 109-128.
28. Armentano, I., et al., *Biodegradable polymer matrix nanocomposites for tissue engineering: a review*. Polymer degradation and stability, 2010. **95**(11): p. 2126-2146.
29. Shi, X., et al., *Rheological behaviour and mechanical characterization of injectable poly (propylene fumarate)/single-walled carbon nanotube composites for bone tissue engineering*. Nanotechnology, 2005. **16**(7): p. S531.
30. Gao, Q., et al., *A primary study of poly (propylene fumarate)-2-hydroxyethyl methacrylate copolymer scaffolds for tarsal plate repair and reconstruction in rabbit eyelids*. Journal of Materials Chemistry B, 2015. **3**(19): p. 4052-4062.
31. Du, L., et al., *Structural characterization and thermal and mechanical properties of poly (propylene carbonate)/MgAl-LDH exfoliation nanocomposite via solution intercalation*. Composites Science and Technology, 2006. **66**(7-8): p. 913-918.
32. Liu, L., et al., *Mechanical properties of poly (butylene succinate)(PBS) biocomposites reinforced with surface modified jute fibre*. Composites Part A: Applied Science and Manufacturing, 2009. **40**(5): p. 669-674.
33. Nagahata, R., et al., *Microwave-Assisted Single-Step Synthesis of Poly (lactic acid) by Direct Polycondensation of Lactic Acid*. Macromolecular rapid communications, 2007. **28**(4): p. 437-442.
34. Fukushima, K. and Y. Kimura, *An efficient solid-state polycondensation method for synthesizing stereocomplexed poly (lactic acid) s with high molecular weight*. Journal of Polymer Science Part A: Polymer Chemistry, 2008. **46**(11): p. 3714-3722.
35. Lasprilla, A.J., et al., *Poly-lactic acid synthesis for application in biomedical devices—A review*. Biotechnology advances, 2012. **30**(1): p. 321-328.
36. Farah, S., D.G. Anderson, and R. Langer, *Physical and mechanical properties of PLA, and their functions in widespread applications—A comprehensive review*. Advanced drug delivery reviews, 2016. **107**: p. 367-392.
37. Kucharczyk, P., *Preparation and modifications of biodegradable polyesters for medical applications*. 2013, Doctoral Thesis.-Zlín, Czech Republic.
38. Rasal, R.M., A.V. Janorkar, and D.E. Hirt, *Poly (lactic acid) modifications*. Progress in polymer science, 2010. **35**(3): p. 338-356.
39. Singhvi, M., S. Zinjarde, and D. Gokhale, *Poly-Lactic acid (PLA): synthesis and biomedical applications*. Journal of applied microbiology, 2019.
40. Auras, R.A., et al., *Mechanical, physical, and barrier properties of poly(lactide) films*. Journal of Plastic Film and Sheeting, 2003. **19**(2): p. 123-135.
41. Karamanlioglu, M., R. Preziosi, and G.D. Robson, *Abiotic and biotic environmental degradation of the bioplastic polymer poly (lactic acid): a review*. Polymer Degradation and stability, 2017. **137**: p. 122-130.
42. Rujnić-Sokele, M. and A. Pilipović, *Challenges and opportunities of biodegradable plastics: A mini review*. Waste Management & Research, 2017. **35**(2): p. 132-140.
43. Gan, I. and W. Chow, *Antimicrobial poly (lactic acid)/cellulose bionanocomposite for food packaging application: A review*. Food packaging and shelf life, 2018. **17**: p. 150-161.
44. Amass, W., A. Amass, and B. Tighe, *A review of biodegradable polymers: uses, current developments in the synthesis and characterization of biodegradable polyesters, blends of biodegradable polymers and recent advances in biodegradation studies*. Polymer international, 1998. **47**(2): p. 89-144.
45. Agrawal, C.M., G.G. Niederauer, and K.A. Athanasiou, *Fabrication and characterization of PLA-PGA orthopedic implants*. Tissue engineering, 1995. **1**(3): p. 241-252.
46. Zeng, F.-R., Y. Liang, and Z.-L. Li, *Precision Aliphatic Polyesters via Segmer Assembly Polymerization*. Molecules, 2018. **23**(2): p. 452.

47. Tokiwa, Y., et al., *Biodegradability of plastics*. International journal of molecular sciences, 2009. **10**(9): p. 3722-3742.
48. Leja, K. and G. Lewandowicz, *Polymer Biodegradation and Biodegradable Polymers-a Review*. Polish Journal of Environmental Studies, 2010. **19**(2).
49. Gross, R.A. and B. Kalra, *Biodegradable polymers for the environment*. Science, 2002. **297**(5582): p. 803-807.
50. Hazer, D.B., E. Kılıçay, and B. Hazer, *Poly (3-hydroxyalkanoate) s: diversification and biomedical applications: a state of the art review*. Materials Science and Engineering: C, 2012. **32**(4): p. 637-647.
51. Yoon, H., *Strength of fibers from wholly aromatic polyesters*. Colloid and Polymer Science, 1990. **268**(3): p. 230-239.
52. Manami, H., et al., *Preparation and properties of aromatic polyamides and aromatic polyesters derived from 4, 4'-sulfonyldibenzoic acid*. Journal of Polymer Science Part A: Polymer Chemistry, 1990. **28**(3): p. 465-477.
53. Sathiskumar, P. and G. Madras, *Synthesis, characterization, degradation of biodegradable castor oil based polyesters*. Polymer degradation and stability, 2011. **96**(9): p. 1695-1704.
54. Ikada, Y. and H. Tsuji, *Biodegradable polyesters for medical and ecological applications*. Macromolecular rapid communications, 2000. **21**(3): p. 117-132.
55. Vert, M., *Bioresorbable polymers for temporary therapeutic applications*. Die Angewandte Makromolekulare Chemie, 1989. **166**(1): p. 155-168.
56. Pertici, G., *Introduction to bioresorbable polymers for biomedical applications*, in *Bioresorbable polymers for biomedical applications*. 2017, Elsevier. p. 3-29.
57. Guo, B., A. Finne-Wistrand, and A.C. Albertsson, *Versatile functionalization of polyester hydrogels with electroactive aniline oligomers*. Journal of Polymer Science Part A: Polymer Chemistry, 2011. **49**(9): p. 2097-2105.
58. Parrish, B., J.K. Quansah, and T. Emrick, *Functional polyesters prepared by polymerization of α -allyl (valerolactone) and its copolymerization with ϵ -caprolactone and δ -valerolactone*. Journal of Polymer Science Part A: Polymer Chemistry, 2002. **40**(12): p. 1983-1990.
59. Thire, R.M., et al. *Functionalization of biodegradable polyester for tissue engineering applications*. in *Macromolecular symposia*. 2007. Wiley Online Library.
60. Williams, C.K., *Synthesis of functionalized biodegradable polyesters*. Chemical Society Reviews, 2007. **36**(10): p. 1573-1580.
61. Jiao, Y.-P. and F.-Z. Cui, *Surface modification of polyester biomaterials for tissue engineering*. Biomedical materials, 2007. **2**(4): p. R24.
62. Fabbri, P. and M. Messori, *Surface modification of polymers: chemical, physical, and biological routes*, in *Modification of Polymer Properties*. 2017, Elsevier. p. 109-130.
63. Hu, Y., et al., *Newly developed techniques on polycondensation, ring-opening polymerization and polymer modification: Focus on poly (lactic acid)*. Materials, 2016. **9**(3): p. 133.
64. McManus, N. and G. Rempel, *Chemical modification of polymers: catalytic hydrogenation and related reactions*. Journal of Macromolecular Science, Part C: Polymer Reviews, 1995. **35**(2): p. 239-285.
65. Soutif, J.-C. and J.-C. Brosse, *Chemical modification of polymers I. Applications and synthetic strategies*. Reactive polymers, 1990. **12**(1): p. 3-29.
66. Wang, S., W. Cui, and J. Bei, *Bulk and surface modifications of polylactide*. Analytical and Bioanalytical Chemistry, 2005. **381**(3): p. 547-556.
67. Bu, Y., J. Bei, and S. Wang, *Surface Modification of Aliphatic Polyester to Enhance Biocompatibility*. Frontiers in bioengineering and biotechnology, 2019. **7**: p. 98.
68. Aspray, T.J., M. Dimambro, and J. Steiner, *Investigation into plastic in food waste derived digestate and soil*. 2017.
69. Yi, Y., et al., *Polyester micelles for drug delivery and cancer theranostics: current achievements, progresses and future perspectives*. Materials Science and Engineering: C, 2018. **83**: p. 218-232.
70. Washington, K.E., et al., *Recent advances in aliphatic polyesters for drug delivery applications*. Wiley Interdisciplinary Reviews: Nanomedicine and Nanobiotechnology, 2017. **9**(4): p. e1446.

71. Espinoza, S.M., et al., *Poly-ε-caprolactone (PCL), a promising polymer for pharmaceutical and biomedical applications: Focus on nanomedicine in cancer*. International Journal of Polymeric Materials and Polymeric Biomaterials, 2018: p. 1-42.
72. Zilberman, M., *Active implants and scaffolds for tissue regeneration*. 2011: Springer.
73. Martina, M. and D.W. Hutmacher, *Biodegradable polymers applied in tissue engineering research: a review*. Polymer International, 2007. **56**(2): p. 145-157.
74. Pluta, K., *Scaffolds for tissue engineering*. Czasopismo Techniczne, 2015.
75. MORO, J.d.S., et al., *Tissue engineering perspectives in dentistry: review of the literature*. RGO-Revista Gaúcha de Odontologia, 2018. **66**(4): p. 361-367.
76. Guo, B. and P.X. Ma, *Synthetic biodegradable functional polymers for tissue engineering: a brief review*. Science China Chemistry, 2014. **57**(4): p. 490-500.
77. Williams, D., *Biodegradation of surgical polymers*. Journal of Materials Science, 1982. **17**(5): p. 1233-1246.
78. Törmälä, P., T. Pohjonen, and P. Rokkanen. *Ultrahigh-strength self-reinforced polylactide composites and their surgical applications*. in *Macromolecular Symposia*. 1997. Wiley Online Library.
79. Başçı, O., U. Akgun, and F.A. Barber, *Biological Properties of Suture Materials*, in *Knots in Orthopedic Surgery*. 2018, Springer. p. 11-20.
80. Baylón, K., et al., *Past, present and future of surgical meshes: a review*. Membranes, 2017. **7**(3): p. 47.
81. Annabi, N., et al., *Elastic sealants for surgical applications*. European Journal of Pharmaceutics and Biopharmaceutics, 2015. **95**: p. 27-39.
82. Saghazadeh, S., et al., *Drug delivery systems and materials for wound healing applications*. Advanced drug delivery reviews, 2018. **127**: p. 138-166.
83. Kamoun, E.A., E.-R.S. Kenawy, and X. Chen, *A review on polymeric hydrogel membranes for wound dressing applications: PVA-based hydrogel dressings*. Journal of advanced research, 2017. **8**(3): p. 217-233.
84. Rydz, J., et al., *Polyester-based (bio) degradable polymers as environmentally friendly materials for sustainable development*. International journal of molecular sciences, 2015. **16**(1): p. 564-596.
85. Pilla, S., et al., *Microcellular extrusion foaming of poly(lactide)/poly(butylene adipate-co-terephthalate) blends*. Materials Science and Engineering: C, 2010. **30**(2): p. 255-262.
86. Ding, W., et al., *Development of PLA/cellulosic fiber composite foams using injection molding: Crystallization and foaming behaviors*. Composites Part A: Applied Science and Manufacturing, 2016. **83**: p. 130-139.
87. Xu, Y., et al., *Lightweight micro-cellular plastics from polylactide/polyolefin hybrids*. Polymer, 2016. **102**: p. 73-83.
88. Kucharczyk, P., et al., *Properties enhancement of partially biodegradable polyamide/polylactide blends through compatibilization with novel polyalkenyl-poly-maleic-anhydride-amide/imide-based additives*. Journal of Reinforced Plastics and Composites, 2012. **31**(3): p. 189-202.
89. Saucéau, M., et al., *New challenges in polymer foaming: A review of extrusion processes assisted by supercritical carbon dioxide*. Progress in Polymer Science, 2011. **36**(6): p. 749-766.
90. Chauvet, M., M. Saucéau, and J. Fages, *Extrusion assisted by supercritical CO₂: A review on its application to biopolymers*. The Journal of Supercritical Fluids, 2017. **120**: p. 408-420.
91. Zhao, H. and G. Zhao, *Mechanical and thermal properties of conventional and microcellular injection molded poly (lactic acid)/poly (ε-caprolactone) blends*. Journal of the Mechanical Behavior of Biomedical Materials, 2016. **53**: p. 59-67.
92. Tor-Świątek, A., et al., *Influence of Polylactide Modification with Blowing Agents on Selected Mechanical Properties*. Advances in Science and Technology Research Journal, 2017. **11**(4): p. 206-214.
93. Nofar, M., *Effects of nano-/micro-sized additives and the corresponding induced crystallinity on the extrusion foaming behavior of PLA using supercritical CO₂*. Materials & Design, 2016. **101**: p. 24-34.
94. Fortunati, E., et al., *Multifunctional bionanocomposite films of poly(lactic acid), cellulose nanocrystals and silver nanoparticles*. Carbohydrate Polymers, 2012. **87**(2): p. 1596-1605.

95. Castro-Aguirre, E., et al., *Poly(lactic acid)—Mass production, processing, industrial applications, and end of life*. *Advanced Drug Delivery Reviews*, 2016. **107**: p. 333-366.
96. Saini, P., M. Arora, and M.N.V.R. Kumar, *Poly(lactic acid) blends in biomedical applications*. *Advanced Drug Delivery Reviews*, 2016. **107**: p. 47-59.
97. Bose, S., M. Roy, and A. Bandyopadhyay, *Recent advances in bone tissue engineering scaffolds*. *Trends in Biotechnology*, 2012. **30**(10): p. 546-554.
98. LEE H S, L.D.Y., *Cosmetic container is obtained by mixing copolymer or resin modified product chosen from e.g. polyethylene and low-density polyethylene, tea tree, alum, elvan, sodium chloride and water, drying, melting mixture and injection molding*, in S.K.C. LTD, Editor. 2016, 3SM KOREA CO LTD: korea.
99. Husárová, L., et al., *Identification of important abiotic and biotic factors in the biodegradation of poly(l-lactic acid)*. *International Journal of Biological Macromolecules*, 2014. **71**: p. 155-162.
100. Liu, L., et al., *Preparation of Antimicrobial Membranes: Coextrusion of Poly(lactic acid) and Nisaplin in the Presence of Plasticizers*. *Journal of Agricultural and Food Chemistry*, 2009. **57**(18): p. 8392-8398.
101. Erem, A.D., et al., *Antimicrobial activity of poly(l-lactide acid)/silver nanocomposite fibers*. *Textile Research Journal*, 2013. **83**(20): p. 2111-2117.
102. Stloukal, P. and P. Kucharczyk, *Acceleration of polylactide degradation under biotic and abiotic conditions through utilization of a new, experimental, highly compatible additive*. *Polymer Degradation and Stability*, 2017. **142**: p. 217-225.
103. Stloukal, P., et al., *The influence of a hydrolysis-inhibiting additive on the degradation and biodegradation of PLA and its nanocomposites*. *Polymer Testing*, 2015. **41**: p. 124-132.
104. Zhao, H., et al., *Morphology and Properties of Injection Molded Solid and Microcellular Poly(lactic Acid)/Poly(hydroxybutyrate-Valerate (PLA/PHBV) Blends*. *Industrial & Engineering Chemistry Research*, 2013. **52**(7): p. 2569-2581.
105. Matuana, L.M., *Solid state microcellular foamed poly(lactic acid): Morphology and property characterization*. *Bioresource Technology*, 2008. **99**(9): p. 3643-3650.
106. Pan, J., *5 - Modelling biodegradation of composite materials made of biodegradable polyesters and tricalcium phosphates (TCPs)*, in *Modelling Degradation of Bioresorbable Polymeric Medical Devices*, J. Pan, Editor. 2015, Woodhead Publishing. p. 71-87.
107. Stloukal, P., et al., *Carbodiimide additive to control hydrolytic stability and biodegradability of PLA*. *Polymer Testing*, 2016. **54**: p. 19-28.
108. Kucharczyk, P., et al., *Novel aspects of the degradation process of PLA based bulky samples under conditions of high partial pressure of water vapour*. *Polymer Degradation and Stability*, 2013. **98**(1): p. 150-157.
109. Lu, L., et al., *In vitro degradation of porous poly(l-lactic acid) foams*. *Biomaterials*, 2000. **21**(15): p. 1595-1605.
110. Kim, J.S., et al., *Antimicrobial effects of silver nanoparticles*. *Nanomedicine: Nanotechnology, Biology and Medicine*, 2007. **3**(1): p. 95-101.
111. Sondi, I. and B. Salopek-Sondi, *Silver nanoparticles as antimicrobial agent: a case study on E. coli as a model for Gram-negative bacteria*. *Journal of Colloid and Interface Science*, 2004. **275**(1): p. 177-182.
112. Gupta, D. and A. Laha, *Antimicrobial activity of cotton fabric treated with Quercus infectoria extract*. 2007.
113. Panagiotis, D., et al., *Cornet-Like Phosphotriazine/Diamine Polymers as Reductant and Matrix for the Synthesis of Silver Nanocomposites with Antimicrobial Activity*. *Macromolecular Materials and Engineering*, 2010. **295**(2): p. 108-114.
114. CORRAL, L.G., L.S. POST, and T.J. MONTVILLE, *Antimicrobial Activity of Sodium Bicarbonate: A Research Note*. *Journal of food science*, 1988. **53**(3): p. 981-982.
115. Boateng, J.S., et al., *Wound Healing Dressings and Drug Delivery Systems: A Review*. *Journal of Pharmaceutical Sciences*, 2008. **97**(8): p. 2892-2923.
116. Zilberman, M., et al., *Hybrid wound dressings with controlled release of antibiotics: Structure-release profile effects and in vivo study in a guinea pig burn model*. *Acta Biomaterialia*, 2015. **22**: p. 155-163.

117. Lin, Z., et al., *Biofunctions of antimicrobial peptide-conjugated alginate/hyaluronic acid/collagen wound dressings promote wound healing of a mixed-bacteria-infected wound*. International Journal of Biological Macromolecules, 2019. **140**: p. 330-342.
118. Shemesh, M. and M. Zilberman, *Structure–property effects of novel bioresorbable hybrid structures with controlled release of analgesic drugs for wound healing applications*. Acta Biomaterialia, 2014. **10**(3): p. 1380-1391.
119. Zou, F., X. Sun, and X. Wang, *Elastic, hydrophilic and biodegradable poly (1, 8-octanediol-co-citric acid)/polylactic acid nanofibrous membranes for potential wound dressing applications*. Polymer Degradation and Stability, 2019. **166**: p. 163-173.
120. Ghafari, R., et al., *Processing-structure-property relationships of electrospun PLA-PEO membranes reinforced with enzymatic cellulose nanofibers*. Polymer Testing, 2020. **81**: p. 106182.
121. Zhang, Y., et al., *Novel thymopentin release systems prepared from bioresorbable PLA–PEG–PLA hydrogels*. International Journal of Pharmaceutics, 2010. **386**(1): p. 15-22.
122. Gomaa, S.F., et al., *New polylactic acid/ cellulose acetate-based antimicrobial interactive single dose nanofibrous wound dressing mats*. International Journal of Biological Macromolecules, 2017. **105**: p. 1148-1160.
123. Park, J.-Y. and I.-H. Lee, *Controlled release of ketoprofen from electrospun porous polylactic acid (PLA) nanofibers*. Journal of Polymer Research, 2011. **18**(6): p. 1287-1291.
124. Inphonlek, S., et al., *Chitosan/xanthan gum porous scaffolds incorporated with in-situ-formed poly(lactic acid) particles: Their fabrication and ability to adsorb anionic compounds*. Colloids and Surfaces A: Physicochemical and Engineering Aspects, 2020. **603**: p. 125263.
125. Bi, H., et al., *In Vitro and In Vivo Comparison Study of Electrospun PLA and PLA/PVA/SA Fiber Membranes for Wound Healing*. Polymers, 2020. **12**(4): p. 839.
126. Ribba, L., et al., *Asymmetric biphasic hydrophobic/hydrophilic poly (lactic acid)–polyvinyl alcohol meshes with moisture control and noncytotoxic effects for wound dressing applications*. Journal of Applied Polymer Science, 2019. **136**(17): p. 47369.
127. Tang, H., et al., *Application of a novel approach to prepare biodegradable polylactic-co-glycolic acid microspheres: Surface liquid spraying*. Yakugaku Zasshi, 2007. **127**(11): p. 1851-1862.
128. Tang, H., et al., *Optimization of a novel method: surface liquid spraying to prepare poly (d, l-lactide-co-glycolide) microspheres using central composite design experiment*. Journal of Analytical Bio-Science Vol, 2008. **31**(4).
129. Ali, M., et al., *Influence of formulation parameters on encapsulation of doxycycline in PLGA microspheres prepared by double emulsion technique for the treatment of periodontitis*. Journal of Drug Delivery Science and Technology, 2019. **52**: p. 263-271.
130. Molavi, F., M. Barzegar-Jalali, and H. Hamishehkar, *Polyester based polymeric nano and microparticles for pharmaceutical purposes: A review on formulation approaches*. Journal of Controlled Release, 2020. **320**: p. 265-282.
131. Dinarvand, R., et al., *Effect of surfactant HLB and different formulation variables on the properties of poly-D,L-lactide microspheres of naltrexone prepared by double emulsion technique*. Journal of Microencapsulation, 2005. **22**(2): p. 139-151.
132. K. F. Pistel, T.K., *Effects of salt addition on the microencapsulation of proteins using W/O/W double emulsion technique*. Journal of Microencapsulation, 2000. **17**(4): p. 467-483.
133. Azarmi, S., et al., *Mechanistic evaluation of the effect of thermal-treating on Eudragit RS matrices. II* Farmaco, 2005. **60**(11): p. 925-930.
134. Billa, N., K.-H. Yuen, and K.-K. Peh, *Diclofenac Release from Eudragit-Containing Matrices and Effects of Thermal Treatment*. Drug Development and Industrial Pharmacy, 1998. **24**(1): p. 45-50.
135. Azarmi, S., et al., *Thermal treating as a tool for sustained release of indomethacin from Eudragit RS and RL matrices*. International Journal of Pharmaceutics, 2002. **246**(1): p. 171-177.
136. Castro, A.G.B., et al., *Incorporation of simvastatin in PLLA membranes for guided bone regeneration: effect of thermal treatment on simvastatin release*. Rsc Advances, 2018. **8**(50): p. 28546-28554.

137. Delgado-Enciso, I., et al., *Topical 5% potassium permanganate solution accelerates the healing process in chronic diabetic foot ulcers*. Biomed Rep, 2018. **8**(2): p. 156-159.
138. Hollingworth, H., *Professional concerns in wound care: a discussion of questionable practice recorded by nurses*. British Journal of Community Nursing, 2002. **7**(Sup2): p. 36-42.
139. Amini Moghaddam, M., et al., *Microcellular antibacterial polylactide-based systems prepared by additive extrusion with ALUM*. Polymers for Advanced Technologies, 2019. **30**(8): p. 2100-2108.
140. Gonzaga, V.d.A.M., et al., *Chitosan-laponite nanocomposite scaffolds for wound dressing application*. Journal of Biomedical Materials Research Part B: Applied Biomaterials, 2020. **108**(4): p. 1388-1397.
141. Cai, N., et al., *Tailoring mechanical and antibacterial properties of chitosan/gelatin nanofiber membranes with Fe₃O₄ nanoparticles for potential wound dressing application*. Applied Surface Science, 2016. **369**: p. 492-500.
142. Kavooosi, G., S.M.M. Dadfar, and A.M. Purfard, *Mechanical, physical, antioxidant, and antimicrobial properties of gelatin films incorporated with thymol for potential use as nano wound dressing*. Journal of Food Science, 2013. **78**(2): p. E244-E250.
143. De Cicco, F., et al., *Nanospray technology for an in situ gelling nanoparticulate powder as a wound dressing*. International journal of pharmaceutics, 2014. **473**(1-2): p. 30-37.
144. Adeli, H., M.T. Khorasani, and M. Parvazinia, *Wound dressing based on electrospun PVA/chitosan/starch nanofibrous mats: Fabrication, antibacterial and cytocompatibility evaluation and in vitro healing assay*. International journal of biological macromolecules, 2019. **122**: p. 238-254.
145. Motiei, M., et al., *Stabilization of chitosan-based polyelectrolyte nanoparticle cargo delivery biomaterials by a multiple ionic cross-linking strategy*. Carbohydrate Polymers, 2020. **231**: p. 115709.
146. Smelá, D., et al., *Chromatographic determination of biogenic amines in meat products during fermentation and long-term storage*. Chemická listy, 2004. **98**(7).
147. Liu, Y., et al., *Simultaneous Enhancement of Strength and Toughness of PLA Induced by Miscibility Variation with PVA*. Polymers, 2018. **10**(10): p. 1178.
148. Li, T.-T., et al., *Manufacture and characteristics of HA-Electrodeposited polylactic acid/polyvinyl alcohol biodegradable braided scaffolds*. Journal of the Mechanical Behavior of Biomedical Materials, 2020. **103**: p. 103555.
149. Li, T.-T., et al., *Properties and Mechanism of Hydroxyapatite Coating Prepared by Electrodeposition on a Braid for Biodegradable Bone Scaffolds*. Nanomaterials, 2019. **9**(5): p. 679.
150. Abdullah, O.G., S.B. Aziz, and M.A. Rasheed, *Structural and optical characterization of PVA:KMnO₄ based solid polymer electrolyte*. Results in Physics, 2016. **6**: p. 1103-1108.
151. Hassan, R.M. and M.A. Abd-Alla, *New coordination polymers. Part 1.—Novel synthesis of poly (vinyl ketone) and characterization as chelating agent*. Journal of Materials Chemistry, 1992. **2**(6): p. 609-611.
152. Ali, H.E., *A novel optical limiter and UV-Visible filters made of Poly (vinyl alcohol)/KMnO₄ polymeric films on glass-based substrate*. Journal of Materials Science: Materials in Electronics, 2019. **30**(7): p. 7043-7053.
153. Dai, L., et al., *Gelation of a new hydrogel system of atactic-poly(vinyl alcohol)/NaCl/H₂O*. Polymer International, 2002. **51**(8): p. 715-720.
154. Yang, H., et al., *Thermal decomposition behavior of poly (vinyl alcohol) with different hydroxyl content*. Journal of Macromolecular Science, Part B, 2012. **51**(3): p. 464-480.
155. Zhang, D., et al., *Carboxyl-modified poly(vinyl alcohol)-crosslinked chitosan hydrogel films for potential wound dressing*. Carbohydrate Polymers, 2015. **125**: p. 189-199.
156. Doménech-Carbó, M.T., et al., *Study of ageing of ketone resins used as picture varnishes by FTIR spectroscopy, UV-Vis spectrophotometry, atomic force microscopy and scanning electron microscopy X-ray microanalysis*. Analytical and Bioanalytical Chemistry, 2008. **391**(4): p. 1351-1359.
157. Omelczuk, M.O. and J.W. McGinity, *The Influence of Thermal Treatment on the Physical-Mechanical and Dissolution Properties of Tablets Containing Poly(DL-Lactic Acid)*. Pharmaceutical Research, 1993. **10**(4): p. 542-548.
158. Yin, H.-M., et al., *Engineering Porous Poly(lactic acid) Scaffolds with High Mechanical Performance via a Solid State Extrusion/Porogen Leaching Approach*. Polymers, 2016. **8**(6): p. 213.

159. Sabino, M.A., *Oxidation of polycaprolactone to induce compatibility with other degradable polyesters*. Polymer Degradation and Stability, 2007. **92**(6): p. 986-996.
160. Stocco, E., et al., *Partially oxidized polyvinyl alcohol as a promising material for tissue engineering*. Journal of tissue engineering and regenerative medicine, 2017. **11**(7): p. 2060-2070.
161. Ranganath, M., R.V. Patil, and B. Lobo. *Morphological modifications in potassium permanganate doped poly (vinyl alcohol) films*. in *Proceedings of the International Workshop on Applications of Nanotechnology to Energy, Environment and Biotechnology (NANOEEB)*. 2010.
162. Poonguzhali, R., S.K. Basha, and V.S. Kumari, *Novel asymmetric chitosan/PVP/nanocellulose wound dressing: In vitro and in vivo evaluation*. International journal of biological macromolecules, 2018. **112**: p. 1300-1309.
163. Hasanzadeh, D., et al., *Thermal Treating of Acrylic Matrices as a Tool for Controlling Drug Release*. Chemical and Pharmaceutical Bulletin, 2009. **57**(12): p. 1356-1362.
164. Ungaro, F., et al., *Cyclodextrins in the production of large porous particles: Development of dry powders for the sustained release of insulin to the lungs*. European Journal of Pharmaceutical Sciences, 2006. **28**(5): p. 423-432.
165. Archana, D., J. Dutta, and P.K. Dutta, *Evaluation of chitosan nano dressing for wound healing: Characterization, in vitro and in vivo studies*. International Journal of Biological Macromolecules, 2013. **57**: p. 193-203.
166. Pantani, R. and A. Sorrentino, *Influence of crystallinity on the biodegradation rate of injection-moulded poly(lactic acid) samples in controlled composting conditions*. Polymer Degradation and Stability, 2013. **98**: p. 1089-1096.
167. Ivanets, A.I., et al., *Physicochemical properties of manganese oxides obtained via the sol-gel method: The reduction of potassium permanganate by polyvinyl alcohol*. Russian Journal of Physical Chemistry A, 2017. **91**(8): p. 1486-1492.
168. McMurry, J.E., *Organic Chemistry*. 2015: Cengage Learning.
169. Koosehbol, S., et al., *Preparation and characterization of in situ chitosan/polyethylene glycol fumarate/thymol hydrogel as an effective wound dressing*. Materials Science and Engineering: C, 2017. **79**: p. 66-75.
170. Akhavan-Kharazian, N. and H. Izadi-Vasafi, *Preparation and characterization of chitosan/gelatin/nanocrystalline cellulose/calcium peroxide films for potential wound dressing applications*. International journal of biological macromolecules, 2019. **133**: p. 881-891.
171. Alippilakkotte, S., S. Kumar, and L. Sreejith, *Fabrication of PLA/Ag nanofibers by green synthesis method using Momordica charantia fruit extract for wound dressing applications*. Colloids and Surfaces A: Physicochemical and Engineering Aspects, 2017. **529**: p. 771-782.
172. Khorasani, M.T., et al., *Incorporation of ZnO nanoparticles into heparinised polyvinyl alcohol/chitosan hydrogels for wound dressing application*. International journal of biological macromolecules, 2018. **114**: p. 1203-1215.
173. Al-Maaieh, A. and D.R. Flanagan, *Salt and cosolvent effects on ionic drug loading into microspheres using an O/W method*. Journal of Controlled Release, 2001. **70**(1): p. 169-181.
174. Al-Sokanee, Z.N., et al., *The Drug Release Study of Ceftriaxone from Porous Hydroxyapatite Scaffolds*. AAPS PharmSciTech, 2009. **10**(3): p. 772-779.
175. Zare, M., et al., *Effect of additives on release profile of leuprolide acetate in an in situ forming controlled-release system: In vitro study*. Journal of Applied Polymer Science, 2008. **107**(6): p. 3781-3787.
176. Javadzadeh, Y., L. MUSAALREZAEI, and A. NOKHODCHI, *Liquisolid technique as a new approach to sustain propranolol hydrochloride release from tablet matrices*. International Journal of Pharmaceutics, 2008. **362**(1): p. 102-108.
177. Tamboli, V., G.P. Mishra, and A.K. Mitra, *Novel pentablock copolymer (PLA-PCL-PEG-PCL-PLA)-based nanoparticles for controlled drug delivery: effect of copolymer compositions on the crystallinity of copolymers and in vitro drug release profile from nanoparticles*. Colloid and Polymer Science, 2013. **291**(5): p. 1235-1245.

LIST OF FIGURES

Figure 1. Scheme of chemical structure of ester group [7]	8
Figure 2. Chemical structure of PLA [37].....	10
Figure 3. Main routes for the synthesis of PLA [14].....	11
Figure 4. Chemical structure of PGA [37]	12
Figure 5. Chemical structure of PLGA [7].....	12
Figure 6. Chemical structure of PCL [7].....	13
Figure 7. Chemical structure of PHAs [50].....	14
Figure 8. Chemical structure of PDO [37]	15
Figure 9. Diagrammatic representation of the chemistry of biodegradation [40].....	16
Figure 10. Hydrolytic degradation of polyesters [9]	16
Figure 11. (A) Scheme of formation of N-containing polar groups on surface of polylactone-type polymer using ammonia plasma treatment; (B) the influence of plasma-treating time under power 20W and 30 Pa of NH ₃ atmosphere on treated depth of PLGA scaffold [67].....	20
Figure 12. The modification of PLLA by the entrapment method [61].....	21
Figure 13. Esterification between carboxylic acid and alcoholic group [6].	22
Figure 14. Type and sizes of common nanocarriers used for drug delivery [70].	25
Figure 15. Basic steps in tissue engineering [75].....	27
Figure 16. Scheme of Surface liquid spraying process	37
Figure 17. SEM micrographs of the microstructures of (A) PLA, (B) PLA-ALUM, (C) PLA/MSS3, (D) PLA/MSS5, (E) PLA/ALUM/MSS3, (F) PLA/ALUM/MSS5.....	41
Figure. 18. Molecular weight evolution of the materials during abiotic hydrolysis	44
Figure. 19. Release of ALUM in phosphate buffer saline (PBS) buffer (pH = 7.4) at 37°C	48
Figure. 20. FT-IR spectra of PLA-PVA (a), PLA-PVA (T) (b), PLA-PVA/KMnO ₄ (c), PLA-PVA/KMnO ₄ (T) (d), PLA-PV/NaCl (e), PLA-PVA/NaCl (T) (f) mats	54

Figure. 21. DSC curves of porous PLA mats	55
Figure. 22. Photographic appearance of the PLA-PVA porous mat	57
Figure. 23. SEM image of PLA-PVA porous mat	57
Figure. 24. SEM images of the porous mats: (a) PLA-PVA, (b) PLA-PVA/NaCl, (c) PLA-PVA/KMnO ₄ , (d) PLA-PVA (T), (e) PLA-PVA/NaCl (T), and (f) PLA-PVA/KMnO ₄ (T)	58
Figure. 25. Swelling studies of the porous mats in PBS with pH 7.4 at 37°C	59
Figure. 26. In-vitro release profiles of porous mats loaded GS in pH 7.4 at 37°C	63

LIST OF TABLES

Table 1. Mechanical properties of the biodegradable polyesters and a few tissues and commercially available biomaterials [8].	9
Table 2. Biodegradable polyesters [44].....	18
Table 3. Commercial products made from biodegradable polyesters and their applications [8]	22
Table 4. Summary of scaffold design criteria and related functions in tissue engineering [72].....	26
Table 5. Representative synthetic biodegradable polymers currently used or under investigation for medical application [54, 80-83].	28
Table 6. Ecological applications of biodegradable polymers [54].	29
Table. 7. Compositions of the investigated samples	33
Table. 8. Selected material-related properties of samples after preparation and before degradation experiments	38
Table. 9. Initial mechanical properties of neat PLA and microcellular PLA	40
Table. 10. Thermal properties of samples prior to and after abiotic hydrolysis at various times	42
Table. 11. Reduction in colony forming units (CR) effected by of pure PLA-ALUM, microcellular PLA/ALUM/MSS3, and microcellular PLA/ALUM/MSS5	45
Table. 12. Selected material-related properties of the mats before and after thermal treatment	55
Table. 13. Porosity measurements of porous mats after 24 h of immersion in ethanol at room temperature	56
Table. 14. Water solubility measurements of the porous mats in DI water after 24 h at 37°C	60
Table. 15. Water vapor transmission rate of the porous mats	60
Table. 16. EE and LC of the porous mats before and after thermal treatment	61

LIST OF SYMBOLS AND ABBREVIATIONS

ALUM	Potassium aluminum sulfate dodecahydrate
ATR-FTIR	Attenuated Total Reflection Fourier-transform infrared
CBAs	Chemical blowing agents
CFU	Number of the colony forming units
C ₂ H ₅	Ethyl
CO	Carbon monoxide
CO ₂	Carbon dioxide
COOH	Carboxylic acid
CR	Reduction
DDS	Drug delivery systems
DI	Deionized water
ECM	Extracellular Matrix
EE	Encapsulation efficiency
FDA	Food and Drug Administration
GA	Glycolic acid
GS	Gentamicin
KMnO ₄	Potassium permanganate
LC	Loading capacity
LC	Liquid crystalline
LA	Lactic acid
NaCl	Sodium chloride
O/W	Oil in water
PBS	Phosphate buffer saline
PCL	Poly(ϵ -caprolactone)
PDLA	Poly (D-lactide)
PDLLA	Poly (D,L-lactic acid)
PDO	Poly (dioxanone)
PEG	Poly (ethylene glycol)
PGA	Poly (glycolic acid)
PHA	polyhydroxyalkanoates
PHB	Polyhydroxybutyrate
PHBV	Poly(hydroxybutyrate-co-hydroxyvalerate)
PLA	Poly(lactic acid)
PLLA	Poly (L-lactide)
PLGA	Poly Lactic-co-Glycolic Acid
PPC	Polypropylene carbonate
PPF	Poly (propylene fumarate)
PVA	Poly (vinyl alcohol)

PVK	polyvinyl ketone
R	Radicals
SCFs	Supercritical fluids
T_g	Glass transition temperature
T_m	Melting temperature
WVTR	Water vapor transmission rate
χ_c	Crystallinity

CURRICULUM VITAE

Contact information

Name: Maliheh Amini Moghaddam

Email: Amini@utb.cz

Address: T. G. Masaryka 1281, Zlin, Czech Republic.

Education

2016-2021	Ph.D. student at Tomas Bata University, Zlin, Czech Republic.
2010-2013	M.Eng. Chemical Engineering at Azad University, Shahrood Branch, Iran.
2004-2010	B.Eng. Chemical Engineering at Azad University, Quchan Branch, Iran.

Significant projects in PhD

- Development and characterization of microcellular antibacterial polylactide-based systems for medical applications.
- Poly lactide-polyvinyl alcohol-based porous systems loaded with gentamicin for wound dressing applications.
- Preparation and characterization of gold nanoclusters stabilized with chitosan and investigation of hyperthermic effects of gold nanoclusters-chitosan composites on cells for cancer therapy
- Preparation and modification of polyclay.

Research Experience

- 2016-2021 Doctoral research at Centre of Polymer Systems (CPS), Tomas Bata University, focuses on polymers for medical applications.
- Feb 2019-Aug2019 ‘Free mover mobility’ – Monash University (Australia)
Preparation and characterization of chitosan functionalized gold nanocluster and investigation of hypothermia effects on cells for cancer therapy application.
- 2016-2020 Internal Grant Agency of FT TBU, Research team member.

LIST OF PUBLICATIONS

1. Maliheh Amini Moghaddam, Petr Stloukal, Pavel Kucharczyk, Aneta Tor-Swiatek, Tomasz Garbacz, Martina Pummerová, Tomasz Klepka, Vladimír Sedlařík. *Microcellular antibacterial polylactide-based systems prepared by additive extrusion with ALUM*. *Polymers for Advanced Technologies*, 2019. **30**(8): p. 2100-2108.
2. Maliheh Amini Moghaddam, Antonio Di Martino, Tomáš Šopík, Haojie Fei, Jaroslav Císař, Vladimír Sedlařík. *Polylactide/Polyvinylalcohol-Based Porous Bioscaffold Loaded with Gentamicin for Wound Dressing Applications*. *Polymers*, 2021. **13**(6): p. 921.
3. Maliheh Amini Moghaddam, Antonio Di Martino, Kadir Ozaltin, Pavel S.Postnikov, Marina E.Trusova, Vladimir Sedlarik. Nanoencapsulation as approach to improve shelf-life and stability of a hydrophilic and hydrophobic vitamin, submitted in *Food Science and Technology*.
4. Maliheh Amini Moghaddam, Ishdeep Kaur, Anna Cifuentes-Rius, Antonio Di Martino, Deepagan Veerasikku Gopal, Vladimír Sedlařík, Nicolas H. Voelcker. Hyperthermic effects of gold nanoclusters-chitosan composite on tumour cells, submitted to *biointerphases*.

Conference Contribution

1. Maliheh Amini Moghaddam, “Optimization Nano-and Submicro-sized Mesoporous Silica particles with tunable size” Nanocon, Brno, Czech Republic, 2017.



Received: 27 February 2019 | Revised: 14 April 2019 | Accepted: 15 April 2019

DOI: 10.1002/pat.4643

RESEARCH ARTICLE

WILEY polymers
advanced
technologies

Microcellular antibacterial polylactide-based systems prepared by additive extrusion with ALUM

Maliheh Amini Moghaddam¹ | Petr Stloukal¹ | Pavel Kucharczyk¹ | Aneta Tow-Swiatek² | Tomasz Garbacz² | Martina Pummerova¹ | Tomasz Klepka² | Vladimír Sedlařík¹

¹Centre of Polymer Systems, University Institute, Tomas Bata University in Zlin, tr. Tomase Bati 5678, Zlin 760 01, Czech Republic

²Faculty of Mechanical Engineering, Department of Technology and Polymer Processing, Lublin University of Technology, ul. Nadbystrzycka 36D, Lublin 20-618, Poland

Correspondence

Vladimír Sedlařík, Centre of Polymer Systems, University Institute, Tomas Bata University in Zlin, tr. Tomase Bati 5678, Zlin 760 01, Czech Republic.
Email: sedlarik@utb.cz

Funding information

Ministerstvo Školství, Mládeže a Tělovýchovy, Grant/Award Numbers: 7AMB16PL070 and LO1504; Internal Grant Agency of TBU in Zlin, Grant/Award Number: IGA/CPS/2018/003; Ministry of Education, Youth and Sports of the Czech Republic, Grant/Award Numbers: LO1504 and 7AMB16PL070

This work investigates preparation by extrusion of microcellular antimicrobial polylactide (PLA) with an additive, the latter comprising 1% potassium aluminum sulfate dodecahydrate (ALUM), and 3% or 5% of a mixture of sodium hydrogen carbonate and sodium dihydrogen phosphate (1:1). Study was made as to the properties of the materials, their hydrolysis, release profiles, and antimicrobial properties in comparison with the pure polymer. Measuring the molecular weight of samples by gel permeation chromatography revealed that, during thermal processing, the molecular weight of the PLA prepared with additives mentioned above had reduced by approximately 43%. A mechanical test confirmed a decline in mechanical properties after processing as compared with the pure PLA. Release of the antimicrobial compound and the subsequent antimicrobial activity against *Staphylococcus aureus* and *Escherichia coli* was evaluated according to ISO 22196:2007. The release of ALUM from the microcellular specimens took place in two steps. During the first 10 days, the rate of release was extremely high in contrast with the remaining period. However, the release rate of the nonporous sample was seen to equal less than 1% in the first 10 days, a phenomenon probably arising through its less active surface.

KEYWORDS

polylactide, ALUM, antimicrobial, sodium hydrogen carbonate, microcellular structure

1 | INTRODUCTION

In recent years, polylactide (PLA), an environmentally friendly biopolymer, has been widely applied in the biomedical sphere (eg, as sutures, implants, and porous scaffolds) because of its appropriate mechanical, biodegradable, and biocompatible properties.¹⁻⁴ The three-dimensional porous structures of these materials make them suitable for use in tissue engineering as implants for regenerating certain types of tissue, such as skin and bones.^{5,6}

Fundamentally, PLA has the potential to be processed into microcellular form through various conventional techniques, including compression molding, extrusion, and injection molding.^{1,2,7,8} Microcellular extrusion is considered one of the most promising procedures for decreasing density for biomedical application.^{3,9} Essentially,

two methods for manufacturing microcellular materials exist. The first approach utilizes supercritical fluids (SCFs) typified by CO₂ and N₂, while the other pertains to chemical blowing agents (CBAs), such as carbonated salts; the latter results in creation of CO₂ because of the occurrence of thermal decomposition.⁶ SCFs are commonly employed as a consequence of their qualities of nontoxicity and nonflammability.⁵ Nonetheless, maintaining a critical condition is no simple matter, since it is necessary to apply an accurate and precise pressure of CO₂ to control the expansion and structure of products in the extruder barrel.¹⁰ In contrast, CBAs possess the advantages of being used without such consideration of pressure and at less financial cost than SCFs.⁶ It is only recently that studies have appeared in the literature on the microcellular extrusion of PLA. The majority of these describe the process of utilizing supercritical CO₂ for this purpose^{11,12}; hence, there is a

significant lack of research on CBAs. Moreover, attention in such works should be paid to investigating the change in hydrolytic degradability that often accompanies formation of a microcellular structure. Indeed, the kinetics of degradation (bioresorption) of the implant material constitute a key factor in medical applications.¹³

In recent years, it has become a commonplace to prevent the spread of microbial infections associated with medical devices through antimicrobial treatment of materials. In addition, due to the rise in drug-resistant pathogens witnessed over the past few decades, enhancing the antimicrobial properties of materials is a matter that has gained in importance. Inhibiting microbial growth on the surface of a polymer and its surroundings is achievable by mixing an organic or inorganic agent into the polymer matrix.^{14–16} Several papers have been published on the subject in the literature, wherein organic agents are added into a PLA matrix; examples of the former include cellulose, chitosan, and silver.^{10,17} Turalija et al showed that incorporating silver or chitosan into PLA resulted in them acting as antimicrobial agents effective against gram-positive and gram-negative bacteria.

Out of all the possible antimicrobial additives, aluminum potassium sulfate (ALUM) stands out as possessing particularly advantageous characteristics, such as ease of availability and low price. In addition, it is environmentally friendly and has been approved by the Food and Drug Administration (FDA). Indeed, ALUM has been frequently employed for medical application as a consequence of it not being absorbed by the body; thus, it is considered a harmless substance.¹⁸ Brynan et al reported that ALUM inhibits the growth of gram-positive and gram-negative bacteria and exhibits a level of antimicrobial activity comparable with cefotaxime (a commercial antibiotic)¹⁸. Despite all its undeniable advantages, ALUM has largely been overlooked by researchers as an additive for antimicrobial maintenance of a polymeric device.¹⁴

The investigation presented herein focused on the effect of the microcellular structure of PLA on the properties of the given material, as well as its hydrolysis, antimicrobial properties, and the release of an antimicrobial agent from the PLA matrix. Antimicrobial PLA foam was processed via the microcellular extrusion method, with a mixture of monobasic sodium salt (sodium hydrogen carbonate + another salt, at the ratio 1:1) applied as the CBA, and hydrated potassium aluminum sulfate (ALUM) as the antimicrobial agent. Study was made as to the thermal, tensile, and antimicrobial properties of the prepared microcellular PLA incorporated with ALUM. The hydrolytic degradation and release of the antimicrobial agent were studied in biological

buffer solutions at pH 7 by gel permeation chromatography (GPC) and elemental analysis, respectively.

2 | EXPERIMENTAL

2.1 | Materials

PLA semicrystalline PLA4042D with a weight average molecular weight (M_w) of 120 000 g mol⁻¹ was purchased from NatureWorks Ingeo, Minnetonka, Minnesota. Antimicrobial potassium aluminum sulfate dodecahydrate (ALUM) and monobasic sodium salts (MSS), based on sodium hydrogen carbonate in a mixture with sodium dihydrogen phosphate (ratio 1:1) and applied as a foaming agent, were supplied by Sigma-Aldrich, St. Louis, Missouri.

2.2 | Preparation of PLA mixtures

Prior to being compounded, PLA pellets were dried at 80°C under reduced pressure (300 mbar) for at least 8 hours. A co-rotating twin-screw microcompounder (HAAKE MiniLab II, Thermo Scientific, Waltham, Massachusetts) was utilized, equipped with two stainless steel screws and a bypass valve, thereby permitting continuous recirculation of the material at 190°C; the screw speed was set to 50 rpm for compounding operations without the bypass valve. The compositions of the resultant samples are shown in Table 1.

2.3 | Characterization

2.3.1 | Changes in molecular weight during hydrolysis by GPC

GPC analysis was conducted on an HT-GPC 220 chromatographic system (Agilent, Santa Clara, California), equipped with a dual detection set-up (refractive index and viscometric response detectors). The samples were dissolved in tetrahydrofuran (THF; approximately 3 mg mL⁻¹) overnight. Separation and detection took place on PL gel-mixed bed columns (1× Mixed-A, 300 × 7.8 mm, 15 μm particles + 1× Mixed-B, 300 × 7.8 mm, 10 μm particles + 1× Mixed-D, 300 × 7.8 mm, 5 μm particles) at 40°C in THF; the flow rate equaled 1.0 mL min⁻¹ and injection volume was 100 μL. The GPC system was calibrated through universal calibration, with narrow polystyrene

TABLE 1 Compositions of the investigated samples

Component Content (wt%)/Sample Designation	PLA	ALUM	MSS
PLA	100	-	-
PLA/ALUM	99	1	-
PLA/ALUM/MSS3	97	1	3
PLA/ALUM/MSS5	94	1	5
PLA/MSS3	97	-	3
PLA/MSS5	95	-	5

standards ranging from 580 to 271 000 g mol⁻¹ (Polymer Laboratories Ltd, UK). The weight average molar mass (M_w), number average molar mass (M_n), and molar-mass dispersity ($D = M_w/M_n$) of the tested samples were discerned from peaks corresponding to the relevant polymer fractions. All data processing was carried out in Cirrus software.

2.3.2 | Thermal properties—differential scanning calorimetry (DSC)

Thermal properties were investigated by DSC on a DSC1 STAR system (Mettler Toledo, Greifensee, Switzerland). Film samples of weight approximately 5 mg were placed in aluminum pans. Nitrogen flow was set to 50 mL min⁻¹, and the following heating program was applied: an initial heating cycle from 0°C to 200°C (10°C min⁻¹), maintaining the same for 2 minutes, and subsequent cooling to 0°C (20°C min⁻¹). Afterward, the temperature of 0°C was held for 2 minutes and a further heating scan performed at 200°C. Melting point temperature (T_m) and exothermal response relating to cold crystallization (T_c) were obtained from the first heating cycle. The region of glass-transition temperature (T_g) was determined from the second heating scan. The degree of crystallinity χ_c was calculated according to Equation (1)¹⁵:

$$\chi_c = \left(\frac{\Delta H_m - \Delta H_c}{\Delta H_m^0} \right) \times 100\%, \quad (1)$$

where ΔH_m is the enthalpy of fusion, ΔH_c represents cold crystallization enthalpy, and ΔH_m^0 is the tabulated enthalpy of fusion for a theoretically 100% crystalline PLA homopolymer (93.1 J g⁻¹).¹⁵

2.3.3 | Porosity

The porosity of the microcellular samples was calculated from the bulk density (ρ_B) of the microcellular polymers, which was computed from the weight to volume ratio (ρ_{Th}) of individual samples and the theoretical density according to the following equation:

$$\text{Porosity (\%)} = \left(1 - \frac{\rho_B}{\rho_{Th}} \right) \times 100. \quad (2)$$

2.3.4 | Morphology

The morphology of the prepared material was studied by thermionic-emission scanning electron microscopy (ESEM) (VEGA II LMU, TESCAN, Brno, Czech Republic) in order to visualize the size and distribution of particles in the PLA matrix. The specimens were prepared by cryogenically fracturing the samples in liquid nitrogen and then coating them with a thin layer of Au/Pd. The microscope, equipped with an SE detector, was operated in high-vacuum mode at an acceleration voltage of 10 kV.

2.3.5 | Tensile test

Investigations into the mechanical properties of the samples were carried out on a universal tensile testing device, an M350-5 CT Materials Testing Machine (Testometric Company, Lancashire, UK), at a cross-head speed of 5 mm min⁻¹ in accordance with ČSN EN ISO 527-1-4. The dimensions of dog-bone form specimens cut from compression molded plates measured 60 × 4 × 0.1 mm. Prior to testing, the samples were conditioned at 25°C, 50% RH for 24 hours. A minimum of eight specimens from each group were tested.

Statistical analysis was applied to process the results of mechanical properties evaluation. So as to eliminate extraneous results, the Dean-Dixon test was carried out (Q-test; confidence level $\alpha = .95$). After eliminating peripheral figures, corresponding averages and standard deviations (SD) were calculated.

2.3.6 | Abiotic hydrolysis

The extent and rate of PLA hydrolysis were monitored for 140 days at 37°C. The PLA film samples (50 mg) were cut into 0.5 × 0.5 cm specimens and then suspended in 50 mL of sodium phosphate buffer (0.1 mol L⁻¹, pH 7) amended with a microbial growth-inhibiting substance (NaN₃, 2% w/w). The experiment was carried out in three replications for each type of sample. The samples were withdrawn at appropriate intervals and analyzed by GPC and DSC.

2.3.7 | Release test

The individual samples (approximately 100 mg) were immersed in 10 mL of phosphate buffer saline (PBS, 7.4 pH) and incubated at 37°C. All experiments were carried out in triplicates. The volume of 1 mL was removed at predetermined intervals, the used PBS was replaced with 1 mL of fresh PBS, and then filtration took place through a 0.22- μ m syringe PTFE filter for subsequent analysis. The concentration of the Al related to the ALUM released was determined by atomic absorption spectroscopy (AAS).

2.3.8 | Atomic absorption spectroscopy (AAS)

The exact concentration of Al release into the buffer medium was determined by AAS, on an Agilent DUO 240FS/240Z/UltrAA unit (Agilent Technologies, Santa Clara, California) equipped with a hollow cathode lamp (Al: I = 10 mA and wavelength = 396.2 nm), including background correction by a deuterium lamp. A mixture of gasses, acetylene, and air was applied in the flame at flow rates of 2.0 and 13.5 L min⁻¹, respectively. Concentration was calculated according to a calibration gauged by standards with specified concentrations (Ag: 1000 mg/L, Agilent Technologies; Zn: 1000 mg/L, Fluka Analytical).

2.3.9 | Antimicrobial test

Antibacterial testing was carried out according to a procedure based on ISO 22196: 2007 "Measurement of antibacterial activity on plastic

surfaces". The bacteria employed in this study were *Staphylococcus aureus* CCM 4516 (gram-positive) and *Escherichia coli* CCM 4517 (gram-negative). Bacterial suspensions were prepared at concentrations of 1.0×10^6 CFU mL⁻¹ and 1.5×10^7 CFU mL⁻¹ for *E. coli* and *S. aureus*, respectively. The dimensions of each specimen equaled 25 mm x 25 mm, and the polyethylene film measured 20 mm x 20 mm.

Number of the colony forming units (CFU) was determined, and its reduction (CR) was expressed by diminishment in the number of colonies formed per cm² in percent, according to Equation 3:

$$CR = \left(\frac{N_s}{N_B} \right) 100(\%), \quad (3)$$

where NB is the number of viable colonies per cm² recovered from the material without the additive (blank) after 24 hours and NS is the number of viable colonies per cm² recovered from samples containing the antimicrobial agents after 24 hours.

3 | RESULTS AND DISCUSSION

3.1 | Characterization of materials

Investigation was made as to the properties of the materials, ie, molecular weight, thermal and mechanical qualities, and the morphology of the films, the latter having been prepared from neat PLA or microcellular PLA expanded by MSS. Recognized as being environmentally friendly and cheap CBA, MSS decomposes at low temperature and releases CO₂ easily. Antibacterial modification was mediated by another inexpensive and widely available additive (ALUM). Papers in the literature highlight that PLA degrades during melt processing methods such as extrusion,¹¹ a phenomenon that could be accelerated by enhancing the material with additives.¹⁶ Therefore, the effect of agents on the properties of the PLA was researched after the preparation process had ended, and these findings were compared with characteristics prior to commencement of said process.

Moreover, since the hydrolysis of the material, its antimicrobial effect, and release of ALUM might have been dramatically affected by the properties of the input material, in addition to the composition and processing history of the latter, the results obtained could be considered essential to interpreting data from the hydrolysis experiments.¹⁷⁻¹⁹

3.2 | Morphology

Scanning electron microscopy (SEM) was applied to investigate the morphology of samples, especially to gain data on the microstructure of the microcellular specimens. As can be observed from Figure 1, adding ALUM to neat PLA caused the specimens to develop more fracture-like characteristics than evidenced in neat PLA. As expected, the gases formed by the decomposition of MSS in the PLA during extrusion gave rise to an expanded pore structure in the majority of pores, measuring in the order of hundreds of micrometers. The higher

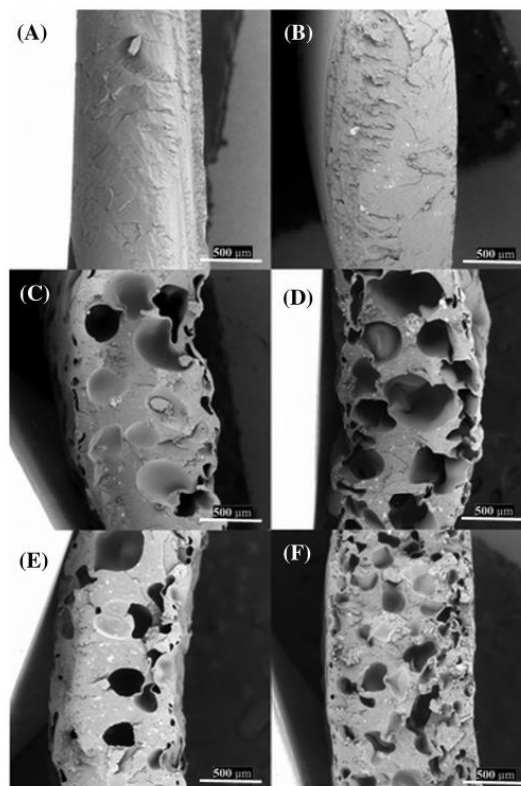


FIGURE 1 Scanning electron microscopy (SEM) micrographs of the microstructures of (A) PLA, (B) PLA-ALUM, (C) PLA/MSS3, (D) PLA/MSS5, (E) PLA/ALUM/MSS3, and (F) PLA/ALUM/MSS5

expansion ratio and density discerned of the pores were achieved by employing a greater amount of the blowing agent: (5 wt% of MSS) in the samples PLA/MSS5 (Figure 1D) and PLA/ALUM/MSS5 (Figure 1F). Additionally, incorporating ALUM and combining it with the expansion process induced by the greater concentration of MSS led to decrease in cell size and increase in the cell density of the polymer matrix, in comparison with the PLA/MSS5 sample; notably, a more uniform cell structure was also obtained. The pores in the PLA/ALUM/MSS5 specimen were roughly comparable in size with the morphological characteristics of a microcellular PLA reported in a study²⁰, which had been formed by nitrogen in a supercritical state through injection molding experiments.

Table 2 summarizes the percentage of porosity of the microcellular PLA samples. In accordance with findings from the SEM images, free-space volume was at its highest level when the greater concentration of MSS was utilized. Nevertheless, if applied in tandem with ALUM, porosity significantly diminished because of the less porous substructures formed, in addition to which the average pore size of the films reduced. These phenomena had been anticipated because of the number of bubbles nucleated, which is fully dependent on the concentration of the blowing agent dissolved in the polymer matrix.²¹

TABLE 2 Selected material-related properties of samples after preparation and before degradation experiments

Sample/property	Neat PLA Prior to Processing	Neat PLA After Processing	PLA ALUM	PLA/MSS 3	PLA/MSS5	PLA ALUM MSS3	PLA ALUM MSS5
Content of ALUM, %	-	-	1	-	-	1	1
Content of BS, %	-	-	-	3	5	3	5
M_w^a , kg mol ⁻¹	122.9	107.1	86.5	90.1	90.1	91.5	85.5
\bar{D}^b	2.44	2.12	2.43	2.53	2.42	2.34	2.24
T_m^c , °C	154.1	152.5	153.5	155.0	154.6	154.3	154.0
ΔH_m^d , J g ⁻¹	-35.9	-26.9	-24.3	16.1	-27.7	-25.3	-27.8
T_c^e , °C	-	123.2	123.5	126.2	125.7	126.2	124.5
ΔH_c^f , J g ⁻¹	-	26.2	22.0	16.6	24.5	21.1	25.0
T_g^g , °C	59.8	59.3	59.3	58.4	57.8	59.7	59.8
χ_c^h , %	38.6	0.7	2.5	0.5	3.5	4.5	3.0
Porosity	-	-	-	19.1	29.8	22.9	17.6

3.3 | Molecular weight and distribution

The weight average molecular weights of all samples measured by GPC are listed in Table 2. Neat, unprocessed PLA was used as a reference to compare the results obtained for the final film samples. As can be seen, a significant drop in M_w was detected for neat PLA after it had been processed in comparison with the same unprocessed material, caused by thermal degradation. This decline in M_w was much more pronounced for the material incorporating the antimicrobial agent ALUM and the composites expanded by MSS (PLA/ALUM, PLA/ALUM/MSS3, PLA/ALUM/MSS5). The M_w of the neat PLA and PLA with additives dropped by approximately 14% and 43%, respectively, after processing the same.

Potentially, this significant reduction in M_w could be attributed to the acidic nature of ALUM (KAl (SO₄)₂·12H₂O) and MSS, which were employed in tandem with the expansion agent. These additives act as an acid catalyst, accelerating the random hydrolysis of the ester bonds in the PLA.²² Furthermore, water molecules present in the chemical structure of ALUM could promote hydrolysis of the polymer. The concurrent effect exerted by the additives on acceleration of degradation is clearly evidenced in the M_w of the PLA/ALUM/MSS5 material, which contained ALUM and the greatest amount of the blowing agent.

3.4 | Thermal properties

The results of DSC analysis, as detailed in Table 2, demonstrate that the additives employed to prepare the antimicrobial microcellular PLA did not significantly influence the thermal properties of the given PLA, in comparison with the neat material prior to and after processing. The degree of crystallinity of the films, calculated from data obtained by thermal analysis, was very low, probably reflecting the relatively short time available for crystallization to occur during preparation of films. However, the slightly higher crystallinity of the PLA with

additives potentially indicates their nucleation effect, facilitating PLA crystallization.¹

3.5 | Mechanical properties

Tensile tests were conducted to determine the effect of the additives on mechanical properties. Table 3 details the tensile strength, elongation at break and Young modulus of the pure PLA and PLA base samples. Supplementing neat PLA with ALUM subtly enhanced all the mechanical characteristics of the material. As anticipated, the mechanical properties of the expanded samples diminished significantly in a very similar manner, regardless of their exact composition. This decline was more pronounced than in a paper in the literature²⁰, which investigated the comparable morphology of microcellular PLA specimens. Such deterioration occurred primarily because of the free-space volume contained in the expanded samples, thereby deteriorating the integrity of the same, partially reducing their molecular weight and diminishing the resultant mechanical properties.

TABLE 3 Initial mechanical properties of neat PLA and microcellular PLA

Sample	Tensile Strength, MPa	Elongation at Break, %	Young Modulus, MPa
Neat PLA after processing	50.5 ± 2.6	16.7 ± 2.1	789 ± 63
PLA-ALUM	60.6 ± 2.6	16.8 ± 0.6	907 ± 88
PLA/MSS3	27.1 ± 0.6	10.2 ± 0.5	382 ± 34
PLA/MSS5	21.4 ± 0.8	8.2 ± 0.2	322 ± 80
PLA/ALUM/MSS3	20.9 ± 0.7	9.2 ± 0.7	347 ± 68
PLA/ALUM/MSS5	21.1 ± 1.0	7.3 ± 0.2	569 ± 26

3.6 | Hydrolysis

The effects of the additives and microcellular structure on the rate of hydrolysis of the PLA-based materials were investigated by GPC and DSC in an aqueous environment at 37°C in the presence of a microbial growth inhibiting substance (NaN₃).

GPC measurement was carried out to discern changes in the PLA at a molecular level during hydrolysis (Figure 2). Reduction in M_w occurred because of random chain scission of the ester bonds, an action that participated in such hydrolysis.²³ The rate of reduction in M_w of the neat PLA was in agreement with a previous investigation²³, this having also been performed at a temperature beneath the point of glass transition. At this temperature, when PLA is in a glassy state, the polymer chains are tightly bound to one another; consequently, their mobility is very limited, thereby making it much harder for water to penetrate the polymer matrix. Moreover, the kinetics or hydrolytic scission of ester bonds by water are reduced significantly. Herein, the microcellular materials (PLA/MSS3 and PLA/MSS5) showed a slightly accelerated chain scission rate than the neat PLA. This acceleration might have been caused by two factors—the lower M_w of the microcellular samples at the beginning of hydrolysis and their porous structure enabling effective contact of the polymer material with the degradation media. As a result, there was an increase in the effective surface area of the samples, allowing water to penetrate the polymer more readily than in the neat PLA. Interestingly, the M_w of samples incorporated with ALUM remained largely unchanged for about 30 days, after which it decreased at a similar rate as the material without the additive. Hence, although the microcellular samples reached a lower M_w at the end of the observation period of 140 days, the rate of hydrolysis of the microcellular specimens was somewhat comparable with that of the nonexpanded PLA material.

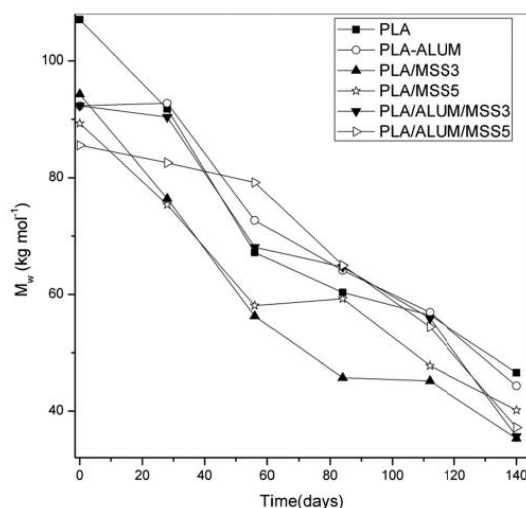


FIGURE 2 Molecular weight evolution of the materials during abiotic hydrolysis

Table 4 illustrates the effect of abiotic hydrolysis (at 0.1 mol L⁻¹, pH 7) on the thermal properties of the microcellular samples and contrasts them with those of the nonporous materials. The samples were initially highly amorphous,^{24,25} but after 12 weeks, a visible increase in crystallinity was detected in the microcellular samples only. This indicated production of a fresh degradation product, one possessing sufficient mobility to enable formation of a crystalline lattice during hydrolysis.²⁴ Notably, PLA/MSS5 showed the highest value for the degree of crystallinity, potentially attributable to the highly porous structure of the specimen. The formation of low-molecular-weight fragments, caused by chain scission of the ester bonds entrapped in the polymer matrix, brought about slight reduction in melting and glass transition temperatures. The new oligomers acted as a plasticizer, sufficiently lowering values for T_g .²³ This behavior was again more pronounced for the microcellular samples, which was in agreement with the findings obtained from GPC analysis. A split in the melting peak also appeared at certain sampling times for all the specimens. In the nonporous samples, this could be attributed to a different rate of chain scission in the cortex of the material, while in the microcellular specimens, the reason is selective degradation of the amorphous phase rather than the crystalline part.

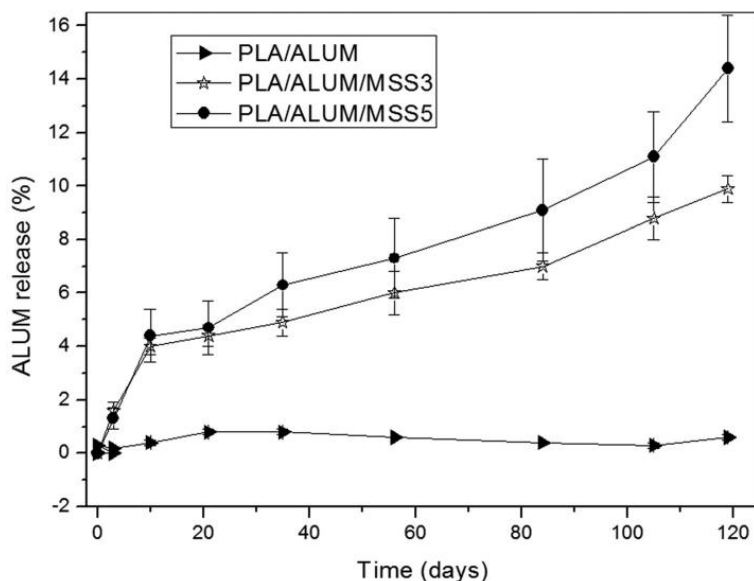
3.7 | Release of the antimicrobial compound

Release of the antimicrobial agent from the samples in phosphate buffer solution (pH = 7.4) was investigated to evaluate the effect of a porous structure on the stability of ALUM in the polymer matrix. Samples containing ALUM were incubated at 37°C for approximately 120 days in the buffer solution. The release of ALUM exhibited by the microcellular samples (PLA/ALUM/MSS) was characterized by a non-linear biphasic profile, where an initial rapid release (the first 10 days) was followed by a gradual release. The initial phase might have been due to the release of ALUM situated close to the surface. In contrast, the nonporous sample exhibited a rapid release of less than 1% of the ALUM over a few days, followed by negligible release in the subsequent period (Figure 3). The more rapid release observed from the porous material could be ascribed to the microcellular morphology of the same, hence possession of a larger active surface; this permits faster penetration of water into the polymer matrix and subsequent diffusion of ALUM onto the polymer surface. Comparing the two porous materials revealed that the initial rapid release of both was almost identical, although the release of ALUM during the following phase was slightly more pronounced for PLA/ALUM/MSS5, as it contained smaller and more numerous pores in its structure. At the end of the observation period, the cumulative release of ALUM equaled approximately 15% and 10% for PLA/ALUM/MSS5 and PLA/ALUM/MSS3, respectively, whereas for PLA-ALUM, it was only about 1%.

In point of fact, while the release of an antimicrobial agent from a medical implant might diminish the antimicrobial effect of the given material, it could still prevent microbial growth in its surroundings. Note that the tolerance of PLA/ALUM was very low, hence not visible in Figure 3.

TABLE 4 Thermal properties of samples prior to and after abiotic hydrolysis at various times

Sample	Time of Hydrolysis, wk	$T_{m,1}^a$, °C	$\Delta H_{m,1}^b$, J g ⁻¹	$T_{m,2}^c$, °C	$\Delta H_{m,2}^d$	T_c^e , °C	ΔH_c^f , J g ⁻¹	T_g^g , °C	χ_c^h , %
PLA	0	152.5	-	-	-26.9	123.2	26.2	59.3	0.7
	4	152.2	-	-	-35.9	119.2	34.5	60.0	1.5
	12	149.0	-22.4	156.5	-39.4	110.5	37.9	59.4	1.6
	20	148.1	-14.6	157.3	-40.3	104.6	40.1	58.7	0.2
PLA-ALUM	0	153.5	-	-	-24.3	123.5	22.0	59.8	2.5
	4	152.0	-	-	-33.0	117.7	31.0	59.2	2.2
	12	148.9	-19.7	156.5	-38.6	109.0	33.6	59.29	5.4
	20	148.1	-15.4	157.0	-42.5	105.1	37.7	58.93	5.2
PLA/MSS3	0	155.0	-	-	-16.1	126.2	16.6	58.4	0.5
	4	151.1	-24.01	157.4	-36.3	114.7	34.18	59.1	2.3
	12	148.9	-12.33	156.8	-38.5	107.7	30.3	59.1	8.7
	20	155.1	-	-	-41.5	95.4	28.1	56.5	14.4
PLA/MSS5	0	154.6	-	-	-27.7	125.7	24.5	57.8	3.5
	4	152.2	-16.2	158.7	-30.6	114.8	26.2	60.6	4.8
	12	148.6	-17.8	157.1	-41.8	107.7	31.5	58.7	11.1
	20	146.9	-11.0	155.8	-42.8	99.7	28.8	57.7	15.0
PLA/ALUM/MSS3	0	154.3	-	-	-25.3	126.2	21.1	59.7	4.5
	4	151.3	-28.1	157.5	-42.7	119.8	39.7	59.3	3.3
	12	148.9	-12.7	157.3	-38.0	106.5	28.7	58.8	10.0
	20	154.5	-	-	-42.3	94.0	33.4	56.2	9.6
PLA/ALUM/MSS5	0	154.0	-	-	-27.8	124.5	25.0	59.8	3.0
	4	152.2	-	155.7	-33.3	117.7	25.3	59.4	8.6
	12	155.8	-	-	-37.9	103.5	22.6	57.6	16.4
	20	155.7	-	-	-41.8	95.2	31.9	56.1	10.7

**FIGURE 3** Release of ALUM in phosphate buffer saline (PBS) buffer (pH = 7.4) at 37°C

3.8 | Antimicrobial properties

In order to inhibit microorganism growth effectively, their life cycle has to be interrupted. Table 5 shows the reduction in bacterial growth

of *S. aureus* (gram-positive) and *E. coli* (gram-negative) on the surface of the pure PLA-ALUM, microcellular PLA/ALUM/MSS3, and microcellular PLA/ALUM/MSS5 films after 24 hours of incubation at 35 ± 2°C. In general, the microcellular PLA specimens showed no

TABLE 5 Reduction in colony forming units (CR) effected by of pure PLA-ALUM, microcellular PLA/ALUM/MSS3, and microcellular PLA/ALUM/MSS5

Sample	CR (%) <i>E. coli</i> CCM 4517	CR (%) <i>S. aureus</i> CCM 4516
PLA-ALUM	100	100
PLA/ALUM/MSS3	93	98
PLA/ALUM/MSS5	64	97

alteration in bacterial growth of any significance in comparison with the pure PLA. On the contrary, it was observed that the prepared materials showed promising results at inhibiting the growth of the tested bacterial strains. Indeed, Dallas et al, who studied a hybrid organic/inorganic macromolecular matrix with silver nanoparticles, reported that this antimicrobial compound was seen to be more effective against *E. coli* than *S. aureus*.²⁶

It is in agreement with other studies dealing with antibacterial activity of Ag nanoparticles.^{27,28} This phenomenon occurs because of the differences in the membrane structure and thickness of the peptidoglycan layer in gram-positive and gram-negative microorganisms. In addition, Gupta and Laha reported that ALUM could be considered an effective antimicrobial agent against the gram-negative bacteria *E. coli*, rather than a gram-positive one.²⁹ In the literature, Corral et al stated that MSS showed antimicrobial activity against *E. coli* and *S. aureus*; therein, the value of CR rose as a consequence of increasing the amount of MSS.³⁰ It means that synergic effect of ALUM and MSS could be expected. Surprisingly, only PLA/ALUM/MSS5 against *S. aureus* evidenced a noticeable drop in percent for reduction of CFU (CR). It can be caused by the highly porous structure of the specimen that may affect the results of the applied testing procedure (ISO 22196). However, the obtained results show that antibacterial action both PLA/ALUM and PLA/ALUM/MSS samples is evident.

4 | CONCLUSIONS

This work focused on preparing and characterizing the structural, mechanical, and thermal properties of antibacterial polymeric films based on PLA, utilizing ALUM as an antimicrobial agent and monobasic sodium salts as a blowing agent. Morphological analysis of the surface of specimens revealed that adding ALUM instigated greater cell density in the polymer matrix and reduced average cell size. Tests demonstrated that mechanical properties were diminished because of microcellular morphology, and acceleration took place under circumstances of highly specific abiotic hydrolysis of the surface, thereby evidencing a rapid reduction in molecular weight by approximately 43% in comparison with neat PLA.

The microcellular PLA samples exhibited accelerated degradation, primarily due to their microcellular structure, facilitating better penetration of the buffer solution into the structure of samples. Furthermore, the release of an antimicrobial compound and subsequent antimicrobial activity against *S. aureus* and *E. coli* were evaluated. It

was confirmed that the rate of release in PLA/ALUM/MSS5 (15 %) was higher than in other samples (10 %, PLA/ALUM/MSS3), as a consequence of its microcellular morphology and larger pore size. Finally, it was demonstrated that ALUM proved effective against the gram-positive and gram-negative bacteria utilized, although its effect was greater against the latter of the two.

ACKNOWLEDGEMENTS

This work was financially supported by the Ministry of Education, Youth and Sports of the Czech Republic (grant nos. 7AMB16PL070 and LO1504), and the Internal Grant Agency of TBU in Zlin (grant no. IGA/CPS/2018/003).

ORCID

Vladimír Sedlářik  <https://orcid.org/0000-0002-7843-0719>

REFERENCES

- Pilla S, Kim SG, Auer GK, Gong S, Park CB. Microcellular extrusion foaming of poly (lactide)/poly (butylene adipate-co-terephthalate) blends. *Mater Sci Eng C*. 2010;30(2):255-262. <https://doi.org/10.1016/j.msec.2009.10.010>
- Ding W, Jahani D, Chang E, Alemdar A, Park CB, Sain M. Development of PLA/cellulosic fiber composite foams using injection molding: crystallization and foaming behaviors. *Compos Part Appl Sci Manuf*. 2016;83:130-139. <https://doi.org/10.1016/j.compositesa.2015.10.003>
- Xu Y, Delgado P, Todd AD, et al. Lightweight micro-cellular plastics from polylactide/polyolefin hybrids. *Polymer*. 2016;102:73-83. <https://doi.org/10.1016/j.polymer.2016.08.102>
- Kucharczyk P, Sedlářik V, Miskolczy N, Szakacs H, Kitano T. Properties enhancement of partially biodegradable polyamide/polylactide blends through compatibilization with novel polyalkenyl-poly-maleic-anhydride-amide/imide-based additives. *J Reinf Plast Compos*. 2012; 31(3):189-202. <https://doi.org/10.1177/0731684411434150>
- Sauceau M, Fages J, Common A, Nikitine C, Rodier E. New challenges in polymer foaming: a review of extrusion processes assisted by supercritical carbon dioxide. *Prog Polym Sci*. 2011;36(6):749-766. <https://doi.org/10.1016/j.progpolymsci.2010.12.004>
- Chauvet M, Sauceau M, Fages J. Extrusion assisted by supercritical CO₂: a review on its application to biopolymers. *J Supercrit Fluids*. 2017;120:408-420. <https://doi.org/10.1016/j.supflu.2016.05.043>
- Zhao H, Zhao G. Mechanical and thermal properties of conventional and microcellular injection molded poly (lactic acid)/poly(ε-caprolactone) blends. *J Mech Behav Biomed Mater*. 2016;53:59-67. <https://doi.org/10.1016/j.jmbbm.2015.08.002>
- Tor-Świątek A, Garbacz T, Sedlářik V, Stloukal P, Kucharczyk P. Influence of polylactide modification with blowing agents on selected mechanical properties. *Adv Sci Technol Res J*. 2017;11(4):206-214. <https://doi.org/10.12913/22998624/80850>
- Nofar M. Effects of nano-/micro-sized additives and the corresponding induced crystallinity on the extrusion foaming behavior of PLA using supercritical CO₂. *Mater Des*. 2016;101:24-34. <https://doi.org/10.1016/j.matdes.2016.03.147>
- Fortunati E, Armentano I, Zhou Q, et al. Multifunctional bionanocomposite films of poly (lactic acid), cellulose nanocrystals and silver nanoparticles. *Carbohydr Polym*. 2012;87(2):1596-1605. <https://doi.org/10.1016/j.carbpol.2011.09.066>

11. Castro-Aguirre E, Iñiguez-Franco F, Samsudin H, Fang X, Auras R. Poly (lactic acid)—mass production, processing, industrial applications, and end of life. *Adv Drug Deliv Rev.* 2016;107:333-366. <https://doi.org/10.1016/j.addr.2016.03.010>
12. Saini P, Arora M, Kumar MNVR. Poly (lactic acid) blends in biomedical applications. *Adv Drug Deliv Rev.* 2016;107:47-59. <https://doi.org/10.1016/j.addr.2016.06.014>
13. Bose S, Roy M, Bandyopadhyay A. Recent advances in bone tissue engineering scaffolds. *Trends Biotechnol.* 2012;30(10):546-554. <https://doi.org/10.1016/j.tibtech.2012.07.005>
14. LEE HS LDY, 3SM KOREA CO LTD. Cosmetic container is obtained by mixing copolymer or resin modified product chosen from e.g. polyethylene and low-density polyethylene, tea tree, alum, elvan, sodium chloride and water, drying, melting mixture and injection molding. 2016.
15. Husárová L, Pekařová S, Stloukal P, et al. Identification of important abiotic and biotic factors in the biodegradation of poly(L-lactic acid). *Int J Biol Macromol.* 2014;71:155-162. <https://doi.org/10.1016/j.ijbiomac.2014.04.050>
16. Liu L, Jin TZ, Coffin DR, Hicks KB. Preparation of antimicrobial membranes: coextrusion of poly (lactic acid) and nisaplin in the presence of plasticizers. *J Agric Food Chem.* 2009;57(18):8392-8398. <https://doi.org/10.1021/jf902213w>
17. Erem AD, Ozcan G, Erem HH, Skrifvars M. Antimicrobial activity of poly(L-lactide acid)/silver nanocomposite fibers. *Text Res J.* 2013;83(20):2111-2117. <https://doi.org/10.1177/0040517513481875>
18. Stloukal P, Kucharczyk P. Acceleration of polylactide degradation under biotic and abiotic conditions through utilization of a new, experimental, highly compatible additive. *Polym Degrad Stab.* 2017;142:217-225. <https://doi.org/10.1016/j.polymdegradstab.2017.06.024>
19. Stloukal P, Kalendova A, Mattausch H, Laske S, Holzer C, Koutny M. The influence of a hydrolysis-inhibiting additive on the degradation and biodegradation of PLA and its nanocomposites. *Polym Test.* 2015;41:124-132. <https://doi.org/10.1016/j.polymertesting.2014.10.015>
20. Zhao H, Cui Z, Sun X, Turg L-S, Peng X. Morphology and properties of injection molded solid and microcellular polylactic acid/polyhydroxybutyrate-valerate (PLA/PHBV) blends. *Ind Eng Chem Res.* 2013;52(7):2569-2581. <https://doi.org/10.1021/ie301573y>
21. Matuana LM. Solid state microcellular foamed poly (lactic acid): morphology and property characterization. *Bioresour Technol.* 2008;99(9):3643-3650. <https://doi.org/10.1016/j.biortech.2007.07.062>
22. Pan J. 5 - Modelling biodegradation of composite materials made of biodegradable polyesters and tricalcium phosphates (TCPs). In: Pan J, ed. *Modelling Degradation of Bioresorbable Polymeric Medical Devices.* Cambridge, United Kingdom: Woodhead Publishing; 2015:71-87.
23. Stloukal P, Jandikova G, Koutny M, Sedlarik V. Carbodiimide additive to control hydrolytic stability and biodegradability of PLA. *Polym Test.* 2016;54:19-28. <https://doi.org/10.1016/j.polymertesting.2016.06.007>
24. Kucharczyk P, Hnatkova E, Dvorak Z, Sedlarik V. Novel aspects of the degradation process of PLA based bulky samples under conditions of high partial pressure of water vapour. *Polym Degrad Stab.* 2013;98(1):150-157. <https://doi.org/10.1016/j.polymdegradstab.2012.10.016>
25. Lu L, Peter SJ, Lyman MD, et al. In vitro degradation of porous poly(L-lactic acid) foams. *Biomaterials.* 2000;21(15):1595-1605. [https://doi.org/10.1016/S0142-9612\(00\)00048-X](https://doi.org/10.1016/S0142-9612(00)00048-X)
26. Dallas P, Zboril R, Bourlinos AB, et al. Comet-like phosphotriazine/diamine polymers as reductant and matrix for the synthesis of silver nanocomposites with antimicrobial activity. *Macromol Mater Eng.* 2010;295(2):108-114. <https://doi.org/10.1002/mame.200900258>
27. Kim JS, Kuk E, Yu KN, et al. Antimicrobial effects of silver nanoparticles. *Nanomedicine Nanotechnol Biol Med.* 2007;3(1):95-101. <https://doi.org/10.1016/j.nano.2006.12.001>
28. Sondi I, Salopek-Sondi B. Silver nanoparticles as antimicrobial agent: a case study on *E. coli* as a model for gram-negative bacteria. *J Colloid Interface Sci.* 2004;275(1):177-182. <https://doi.org/10.1016/j.jcis.2004.02.012>
29. Gupta D, Laha A. Antimicrobial activity of cotton fabric treated with *Quercus infectoria* extract. *Indian J Fibre Text Res.* 2007;32:88-92.
30. Corral LG, Post LS, Momtville TJ. Antimicrobial activity of sodium bicarbonate: a research note. *J Food Sci.* 1988;53(3):981-982.

How to cite this article: Amini Moghaddam M, Stloukal P, Kucharczyk P, et al. Microcellular antibacterial polylactide-based systems prepared by additive extrusion with ALUM. *Polym Adv Technol.* 2019;30:2100-2108. <https://doi.org/10.1002/pat.4643>

Article

Poly lactide/Polyvinylalcohol-Based Porous Bioscaffold Loaded with Gentamicin for Wound Dressing Applications

Maliheh Amini Moghaddam, Antonio Di Martino, Tomáš Šopík , Haojie Fei, Jaroslav Císař, Martina Pummerová  and Vladimír Sedlářik *

Centre of Polymer Systems, University Institute, Tomas Bata University in Zlin, tr. Tomase Bati 5678, 760 01 Zlin, Czech Republic; Amini@utb.cz (M.A.M.); dimartino@utb.cz (A.D.M.); sopik@utb.cz (T.Š.); haojie@utb.cz (H.F.); jcisar@utb.cz (J.C.); pummerova@utb.cz (M.P.)

* Correspondence: sedlarik@utb.cz; Tel.: +420-734262658

Abstract: This study explores the feasibility of modifying the surface liquid spraying method to prepare porous bioscaffolds intended for wound dressing applications. For this purpose, gentamicin sulfate was loaded into polylactide-polyvinyl alcohol bioscaffolds as a highly soluble (hygroscopic) model drug for in vitro release study. Moreover, the influence of inorganic salts including NaCl (10 g/L) and KMnO_4 (0.4 mg/L), and post-thermal treatment (T) (80°C for 2 min) on the properties of the bioscaffolds were studied. The bioscaffolds were characterized by scanning electron microscopy, Fourier Transform infrared spectroscopy, and differential scanning calorimetry. In addition, other properties including porosity, swelling degree, water vapor transmission rate, entrapment efficiency, and the release of gentamicin sulfate were investigated. Results showed that high concentrations of NaCl (10 g/L) in the aqueous phase led to an increase of around 68% in the initial burst release due to the increase in porosity. In fact, porosity increased from 68.1 ± 1.2 to 94.1 ± 1.5 . Moreover, the thermal treatment of the Poly lactide-polyvinyl alcohol/NaCl (PLA-PVA/NaCl) bioscaffolds above glass transition temperature (T_g) reduced the initial burst release by approximately 11% and prolonged the release of the drug. These results suggest that thermal treatment of polymer above T_g can be an efficient approach for a sustained release.

Keywords: Poly lactide; porous bioscaffolds; thermal treatment; additives; sustained release; wound dressing



Citation: Amini Moghaddam, M.; Di Martino, A.; Šopík, T.; Fei, H.; Císař, J.; Pummerová, M.; Sedlářik, V. Poly lactide/Polyvinylalcohol-Based Porous Bioscaffold Loaded with Gentamicin for Wound Dressing Applications. *Polymers* **2021**, *13*, 921. <https://doi.org/10.3390/polym13060921>

Academic Editor: Iolanda De Marco

Received: 19 February 2021

Accepted: 15 March 2021

Published: 17 March 2021

Publisher's Note: MDPI stays neutral with regard to jurisdictional claims in published maps and institutional affiliations.



Copyright: © 2021 by the authors. Licensee MDPI, Basel, Switzerland. This article is an open access article distributed under the terms and conditions of the Creative Commons Attribution (CC BY) license (<https://creativecommons.org/licenses/by/4.0/>).

1. Introduction

Wound dressings have improved vastly over the past decade, from crude, traditional gauze to tissue-engineered scaffolds. An extensive variety of wound dressing formats based on their application for the wound have been investigated or made commercially available [1,2]. A desirable wound dressing should provide an optimal healing environment, which leads to rapid wound healing. It should be able to absorb exudates from the wound surface, maintain a proper moist environment in the wound bed, and, crucially, it should be able to gradually release antimicrobial active agents to ensure prolonged antimicrobial activity and sustain a healthy concentration of healing tissues [3,4]. In recent years, there has been growing attention to fabricate porous structures for wound dressing applications based on natural and synthetic polymers via different techniques. Poly lactide (PLA) is one of the biopolymers that has been widely used in wound dressing applications due to its biocompatibility, biodegradability, good mechanical durability, and non-toxicity to the human body [5,6]. However, PLA is highly hydrophobic, which severely restricts its application in the field of wound dressing due to the limitation of water uptake capacity. Moreover, hydrophobicity of PLA has a great impact on the efficiency of the release of the active agents from the polymer matrix [5,7–9]. Therefore, porous structure could be one approach in order to tackle these issues. A three-dimensional porous structure can improve the permeability of the wound dressing, and at the same time provide sufficient

space for cell growth. It has previously been reported that porous structures promote skin regeneration and wound healing [5,10]. Furthermore, porous structures offer a larger surface area that could allow active agents to diffuse outwards from the matrix in an extremely efficient manner [9].

PVA is a synthetic biocompatible polymer widely used in biomedical applications [11]. It is an excellent choice for improving the properties of PLA due to its nontoxicity, hydrophilicity, low cost, and ease of processing [12,13]. Ribba et al. fabricated PLA-PVA films for wound dressing applications, which exhibited good stability over time, humidity control, and biocompatibility [14]. Hongyan et al. developed the PLA-PVA/SA membranes and assessed their *in vivo* and *in vitro* wound healing capability. These membranes displayed an effective wound healing performance [11]. Moreover, the manufacturing of PLA-PVA scaffolds is cost-effective and easy on the large scale. Both PLA and PVA have been approved by the FDA for use in biomedical applications [13,15,16]. However, as mentioned above, tissue repair is difficult in non-porous PLA-PVA scaffolds. Therefore, there is a need to investigate the porosity of PLA-PVA scaffolds for wound dressing applications [11,17].

Surface liquid spraying is a unique and simple method for the preparation of a porous structure (porous bioscaffolds). It is similar to the emulsion freeze-drying technique. However, the only difference is that in the surface liquid spraying method, the organic phase is sprayed to the aqueous phase [18,19]. In this technique, an organic compound is dissolved in an organic solvent, which is then sprayed into an aqueous polymer solution to form an oil-in-water emulsion. The principle of the freeze-drying technique is the sublimation process, in which the frozen water in the polymer is directly converted from solid to gas state without apparent liquefaction [20,21]. Generally, the emulsion freeze-drying technique is the most widely used method due to its relative ease of use. However, this method has two major restrictions for hydrophilic drugs in the hydrophobic polymer matrix: (1) Poor encapsulation efficiency (EE), and (2) fast release of active agents occurring at the early stages [22–26]. Several studies have reported that the addition of salts to the polymer could enhance the efficiency of encapsulation by depressing drug aqueous solubility, while simultaneously depressing organic solvent solubility in the aqueous phase [22–24]. Pistel et al. demonstrated that the addition of inorganic additives, such as salts, to the aqueous phase increases porosity and the specific surface area of the polymer [27]. One approach to overcome the drug release in early stages is thermal treatment, which occurs by heating the polymer matrixes above the (T_g). Thermal treatment above T_g could change the physical-mechanical properties of polymer and therefore prolong the drug release [28–30]. Castro et al. reported sustained release of simvastatin from polylactide acid (PLA) membranes after thermal treatment [31].

In this study, PLA-PVA porous bioscaffolds were fabricated by the surface liquid spraying method for potential wound dressing application. Sodium chloride (NaCl) and potassium permanganate ($KMnO_4$) salts were added to the aqueous phase of an oil in water (O/W) emulsion. NaCl is a neutral salt while $KMnO_4$ is a strong oxidizing agent and has mild antiseptic and astringent properties, which traditionally has been used to treat exuding wounds [32,33]. Finally, after a short thermal treatment (80 °C, 2 min) of the bioscaffolds, the effect of the salts (NaCl, $KMnO_4$) and the thermal treatment on the *in vitro* release profile, entrapment efficiency and physicochemical properties of the bioscaffolds were investigated.

2. Materials and Methods

Poly(lactide semi-crystalline PLA6202D with M_W of 97 k Da was purchased from NatureWorks® Ingeo™ (Minnetonka, MN, USA). Chloroform was purchased from VWR (14 Media Village, Leighton Buzzard, LU7 0GA, UK). Gentamicin sulfate salt (G-1264) and polyvinyl alcohol with M_W of 47 k Da, degree of hydrolysis: 98.0–98.8, were supplied by Sigma-Aldrich (St. Louis, MO, USA). Sodium chloride was purchased from Mikrochem (Slovak Republic). Potassium permanganate was purchased from Penta Prague (Czech Republic).

2.1. Preparation of the Porous Bioscaffolds

The organic phase was 2% (*w/v*) PLA in chloroform solution and the aqueous phase was 0.1% (*w/v*) PVA aqueous solution. Different salt concentrations were added to the aqueous phase (10 g/L NaCl and 0.4 mg/L KMnO_4). The resultant organic solution was sprayed onto the PVA aqueous solution at the rate of 4 mL/min under moderate magnetic stirring (600 rpm) and 1 bar air-pressure at room temperature to form an oil in water (O/W) emulsion. Subsequently, stirring was maintained overnight in order to evaporate the chloroform. Next, the product was washed three times with deionized water (DI) and filtered. The loading of GS was performed by dissolving GS in DI water and dispersing the filtered product into the solution of GS and DI water. The final product was then frozen. In the final step, the frozen sample was lyophilized. Figure 1 shows the schematic diagram of the surface liquid spraying process.

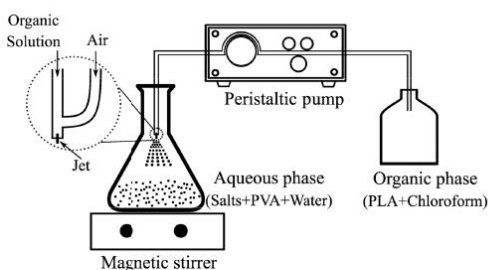


Figure 1. Scheme of the surface liquid spraying process.

2.2. Thermal Treatment of the Porous Bioscaffolds

In order to study the effects of thermal treatment, the porous bioscaffolds were placed in an oven (Memmert, Germany) at 80 °C for 2 min. The bioscaffolds were then kept in the silica gel containing desiccator. Subsequently, thermal treated bioscaffolds were then subjected to various characterization tests as described below.

2.3. Attenuated Total Reflection-Fourier-Transform Infrared (ATR-FTIR) Spectroscopy

The ATR-FTIR test is an appropriate approach to identify functional groups of polymers and molecular structures of the chemicals. The FT-IR spectra were obtained on a Nicolet iS10 instrument equipped with a Zn/Se crystal (Thermo Fisher Scientific, Waltham, MA). The collected spectra in the wavenumber range from 400 to 4000 cm^{-1} represented the average of 64 scans at a spectral resolution of 4 cm^{-1} . The spectra for bioscaffolds before and after the thermal treatment were recorded.

2.4. Differential Scanning Calorimetry (DSC)

Thermal properties of bioscaffolds before and after thermal treatment were investigated by DSC on a DSC1 STAR system (Mettler Toledo, Greifensee, Switzerland). The preparation of samples has been adopted from our previous paper [34]. In brief, approximately 5 mg of each bioscaffold was placed in an aluminum pan. The following heating program was applied in the presence of Nitrogen with the flow rate of 50 mL min^{-1} : In an initial heating cycle, bioscaffolds were heated from 25 °C to 180 °C (10 °C min^{-1}), with the highest temperature maintained for 5 min. This was followed by a subsequent cooling to −35 °C (10 °C min^{-1}). The temperature of −35 °C was maintained for 5 min, and a further heating scan was performed at 220 °C (10 °C min^{-1}). The melting temperature (T_m) and exothermal response related to cold crystallization temperature (T_c) were obtained from the second heating cycle. The region of glass-transition temperature (T_g) was determined

from the second heating scan. The degree of crystallinity (χ_c) was calculated according to the Equation (1) [34]:

$$\chi_c = \left(\frac{\Delta H_m - \Delta H_c}{\Delta H_m^0} \right) \times 100\% \quad (1)$$

where ΔH_m is the heat of fusion, ΔH_c represents the enthalpy of cold crystallization, and ΔH_m^0 is the tabulated heat of fusion for a theoretically 100% crystalline PLA homopolymer (93.1 J g⁻¹) [34].

2.5. Morphological Analysis

The morphology of the bioscaffolds was investigated by thermionic-emission scanning electron microscopy (ESEM) (VEGA-II LMU, TESCAN, Brno, Czech Republic) in order to visualize the porosity of the bioscaffolds. The bioscaffolds were prepared by cryogenic fracturing of the bioscaffolds in liquid nitrogen. This was followed by coating bioscaffolds with a thin layer of Au/Pd. The microscope equipped with an SE detector was operated at an acceleration voltage of 10kV in the high-vacuum mode [34].

2.6. Porosity Measurement

The porosity of the bioscaffolds was determined by liquid displacement method [35]. The weight (W_1) and volume (V) of bioscaffolds were measured before the immersion into ethanol. After the saturation of bioscaffolds by the absorption of ethanol, the weight of bioscaffolds were measured again (W_2). The porosity of the bioscaffolds was calculated according to the Equation (2) (ρ represents the density of the ethanol) [35]. All experiments were performed in triplicate.

$$\text{Porosity}(\%) = \left(\frac{W_2 - W_1}{\rho V} \right) \times 100 \quad (2)$$

2.7. Swelling Test

The swelling test was performed by immersing pre-weighted samples, which had been cut into 1 cm² square pieces, in phosphate-buffered saline (PBS) solution of pH 7.4 at 37 °C. Subsequently, the samples were removed at specific time intervals and the excess water on the surface was carefully absorbed by using filter paper, after which the samples were weighted. The degree of swelling was calculated according to the following Equation [36].

$$\text{degree of swelling}(\%) = (W_t - W_i) / W_i \times 100 \quad (3)$$

where W_t is the weight of the swollen sample, and W_i is the sample at time zero (starting time).

2.8. Water Solubility

To determine the water solubility of the PVA fraction presented in bioscaffolds, samples (samples were cut into 1 cm² square pieces) were placed in an oven at 37 °C for 24 h. Then, the dried bioscaffolds were immersed in DI water for 24 h and dried again at 37 °C for 24 h. The solubility of the bioscaffolds was evaluated using the following Equation [37]:

$$S = \left(\frac{W_0 - W_d}{W_0} \right) \times 100 \quad (4)$$

where W_0 and W_d represent the weights of the dry sample and the weight of the dried sample at 37 °C after immersion in distilled water, respectively [37].

2.9. Water Vapor Transmission Rate (WVTR)

The moisture permeability of the bioscaffolds was determined by measuring the WVTR according to the standard ASTM test method (E96-90) as follows [38]. The samples were cut into discs with a diameter of 15 mm, and mounted on top of a plastic tube

containing 10 mL of distilled water. These assemblies were sealed with Teflon tape in order to avoid boundary loss and then placed in a straight position at 37 °C inside an oven containing 1 kg of freshly dried silica gel, to maintain relatively low humidity conditions. After regular intervals of time, the weights of the assemblies were measured. The WVTR of the samples was calculated according to the following Equation [39]:

$$\text{WVTR (gr/m}^2 \cdot \text{Day)} = (W_i - W_f)/A \quad (5)$$

where A is the exposure area, and W_i and W_f are the initial and final weights of the assemblies respectively.

2.10. Solvent Residue Analysis

Chloroform residue was measured by a headspace autosampler AOC-5000 connected to the GCMS-QP2010 Ultra device (Shimadzu, Kyoto, Japan) equipped with a fused silica capillary column (Stabilwax, 30 m × 0.25 mm × 0.25 μm, Restek, PA, USA). Headspace samples were prepared in 20 mL gas tied vials filled with cca 0.05 mg of sample for an equilibrium time of 30 min at 95 °C. Helium was used as the carrier gas, at a flow rate of 1.26 mL/min. The temperature of the injection was maintained at 230 °C at a split ratio of 1:20, the volume of the injected sample equalling 1 mL. The temperature of the column was held at 50 °C for 1 min, and then increased to 70 °C at a rate of 25 °C/min, and increased to 240 °C for additional 2 min. The temperatures of the ion source (EI, 70 eV) and the interface were set at 200 °C and 240 °C, respectively. The range of the scan was 25–250 (m/z) at event time 0.3. The peaks obtained in the resulting TIC spectrum were identified with the help of the NIST11 Spectra Library.

2.11. Drug Loading and In Vitro Release Study

The gentamicin sulfate (GS) loading efficiency and in vitro release behavior of the drug was carried out in the presence of a non-toxic and isotonic release medium, PBS. The entrapment efficiency (EE) and loading capacity (LC) of GS were evaluated by immersing the bioscaffolds into 50 mL of PBS 10 mM at pH 7.4 in capped glass flasks. The glass flasks were kept in an orbital incubator (Stuart SI500, UK) at 37 ± 0.5 °C, set to 40 rpm for 1 h. Equations (6) and (7) were applied to calculate EE (%) and LC (%), respectively [40].

$$\text{EE(\%)} = \frac{\text{Total}_{\text{GS}} - \text{Free}_{\text{GS}}}{\text{Total}_{\text{GS}}} \times 100 \quad (6)$$

$$\text{LC(\%)} = \frac{\text{Total}_{\text{GS}} - \text{Free}_{\text{GS}}}{\text{matsweight}} \times 100 \quad (7)$$

where Total_{GS} was the amount of primary GS added to the solution, and Free_{GS} was assessed through high-performance liquid chromatography (HPLC), on a Dionex UltiMate 3000 Series device (Thermo Fisher Scientific, Germany) using o-phthalaldehyde (OPA) as a derivatizing agent. The methodology was adapted from Smělá et al., [41] with minor modifications, as described below. The reducing solution was prepared by adding 250 μL of 2-mercaptoethanol and 10 mL of 0.04 M sodium borate (pH 11). Separately, a solution of OPA was prepared by dissolving 2.5 g of OPA in a mixture composed of 400 μL methanol, 200 μL reducing solution and 4.4 mL of 0.04 M sodium borate (pH 11). The OPA solution was stored in the dark and utilized within 24 h after preparation. The separation after OPA in needle derivatization was performed on a reversed-phase column XSELECT CSH C18 5 μm (4.6 × 250 mm; Waters, USA), equipped with a security guard column (Phenomenex, USA) at 30 °C. A mixture of 100 mM Acetate buffer (A; pH 5.8) and HPLC grade Acetonitrile (ACN; B) was applied as the mobile phase (55:45, v/v) at a flow rate of 0.4 mL/min. The volume of the injection was defined by user defined program (UDP) settings, a volume of 10 μL was injected into the column originating from a drawn sample volume of 1 μL. The eluted OPA derivatives were detected by fluorescence using 330 nm and 440 nm as

excitation and emission wavelengths, respectively. All measurements were performed in triplicate.

In the next stage, to evaluate the *in vitro* release rate, the medium was replaced with 50 mL fresh PBS 10mM (pH 7.4), and glass flasks were kept in an orbital incubator at 37 ± 0.5 °C, 40 rpm. At predefined time intervals, 2 mL of the medium was taken, and the same volume of the fresh medium was replaced in the glass flasks. The amount of GS in the medium was evaluated by HPLC apparatus, and OPA was used as a derivatizing agent [41]. The cumulative percentage release of GS from the bioscaffolds was calculated and plotted against time ($n = 3$).

2.12. Statistical Analysis

All experiments were done in triplicates, and the data were presented as mean \pm standard deviation. One-way ANOVA analysis was carried out using the Graph Pad Prism [version 8.00, Graph Pad Software, La Jolla, CA, USA], with $p < 0.05$ considered as statistically significant.

3. Results and Discussion

3.1. Chemical Characteristic

3.1.1. Attenuated Total Reflection Fourier-Transform Infrared (ATR-FTIR) Spectroscopy

The ATR-FTIR spectroscopy analysis was carried out to investigate the structural changes of bioscaffolds based on PLA, PVA, and different salts before and after thermal treatment at the molecular level. The FT-IR spectra of bioscaffolds are shown in Figure 2A. The PLA-PVA bioscaffolds show some characteristic peaks identified by the strong infrared absorption band in the region of $1650\text{--}1754$ cm^{-1} , which corresponds to the stretching vibration of the carbon-oxygen double bond (C=O). The band at 1187 cm^{-1} is assigned to the stretching vibration of the carbon-oxygen bond (C-O). The two peaks around 1448 and 1373 cm^{-1} correspond to the methyl groups of the PLA-PVA bioscaffolds. Moreover, the high-intensity peak that is positioned at 3399 cm^{-1} corresponds to the stretching vibration of the oxygen-hydrogen bond (O-H) [12,42,43]. Figure 2A, illustrates that the intensity and position of the absorption peak of the hydroxyl group changed with the addition of salts and thermal treatment. Addition of KMnO_4 to the bioscaffolds caused the disappearance of the O-H peak in the FT-IR spectra, which indicates the oxidation of PVA to polyvinyl ketone (PVK). The formation of corresponding ketone is due to the fact that KMnO_4 is a strong oxidizing agent [44–46].

In the case of the addition of NaCl, the hydroxyl peak in PLA-PVA/NaCl bioscaffold is weaker than it is in PLA-PVA bioscaffold and its position shifted slightly towards a higher frequency (3430 cm^{-1}). This can be attributed to a higher degree of hydrogen bonding in the PLA-PVA bioscaffold, because hydrogen bonding is disrupted by the addition of NaCl [47]. The thermal treated PLA-PVA and PLA-PVA/NaCl bioscaffolds show that the hydroxyl peak has a lower intensity in comparison with the non-thermal treated bioscaffolds [48]. In case of the thermal treated PLA-PVA/ KMnO_4 bioscaffold, the O-H peak in the FT-IR spectra appear and it shifted to a higher wavelength from (3353 cm^{-1}). This can be explained by the partial formation of the carboxylic acid group due to the elevated temperature in the presence of KMnO_4 [49,50]. Moreover, oxidation process led to an increase in the carbon-oxygen double bond (C=O) peak as can be seen in Figure 2B [51,52].

3.1.2. Thermal Properties

DSC analysis of the porous bioscaffolds was carried out to study the effects of the thermal treatment and salts on the thermal behavior of the bioscaffolds. The correlated thermal properties of the bioscaffolds are summarized in Table 1. As expected, crystallinity (χ_c) increased after the thermal treatment of the bioscaffolds [31]. The T_g of the bioscaffolds did not demonstrate any significant changes after the thermal treatment, as shown in Figure 3. Furthermore, T_m and T_c values were not affected by the thermal treatment and were in agreement with the published literature values [31,53]. Increase in the concentration of

NaCl caused significant reduction in crystallinity, which could be attributed to the fact that high NaCl content impedes PLA chain mobility and thereby prohibits crystallization [54]. According to the literature, the oxidation of PLA and PVA by KMnO_4 caused a decrease in crystallinity [55,56]. Moreover, the addition of salts induced a decrease in T_c , an increase in T_m (consistent with the results given in [57]), and showed no difference in the T_g values.

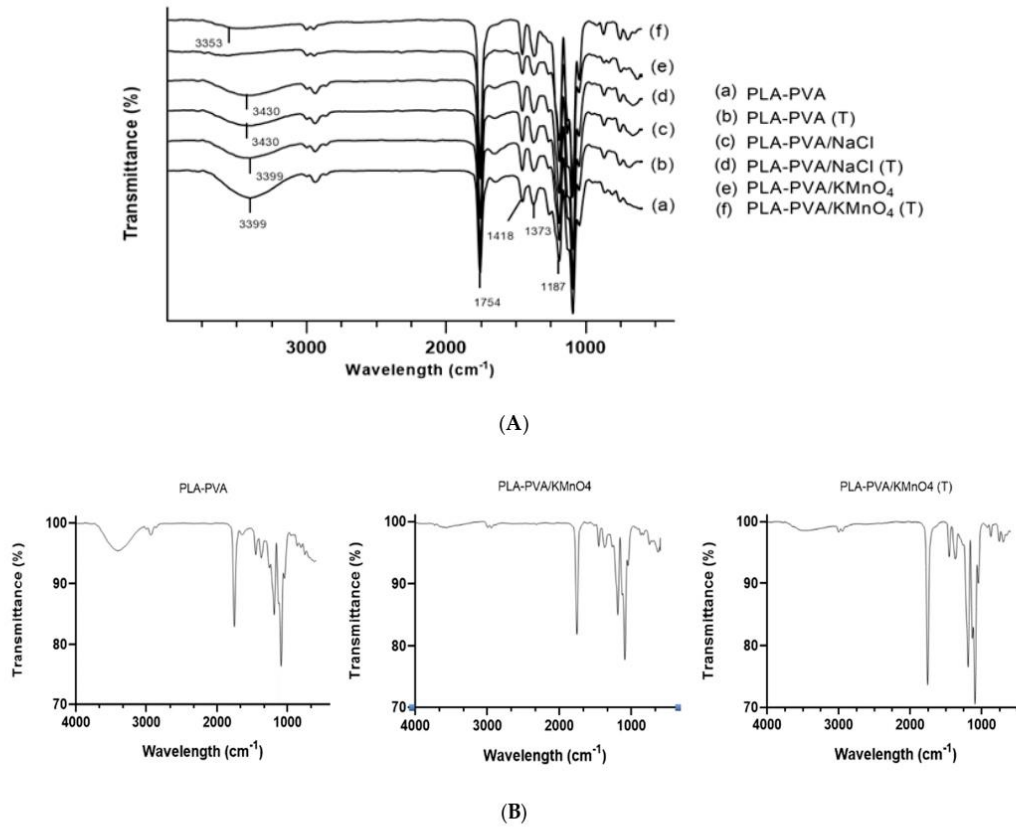


Figure 2. (A). FT-IR spectra of PLA-PVA (a), PLA-PVA (T) (b), PLA-PVA/ KMnO_4 (c), PLA-PVA/ KMnO_4 (T) (d), PLA-PV/ NaCl (e), PLA-PVA/ NaCl (T) (f) bioscaffolds. (B). FT-IR spectra of PLA-PVA, PLA-PVA/ KMnO_4 , and PLA-PVA/ KMnO_4 (T) of bioscaffolds.

Table 1. Selected material-related properties of the bioscaffolds before and after thermal treatment.

Sample/Property	Untreated			After Thermal Treatment		
	PLA-PVA	PLA-PVA/ KMnO_4	PLA-PVA/ NaCl	PLA-PVA	PLA-PVA/ KMnO_4	PLA-PVA/ NaCl
χ_c	5.1	4.9	0.7	8.8	5.3	3.0
T_g	61.9	62.0	62.0	61.1	61.7	61.2
T_c	129.9	118.3	115.4	130.4	118.1	114.4
T_m	164.3	167.4	168.0	164.6	167.5	167.0

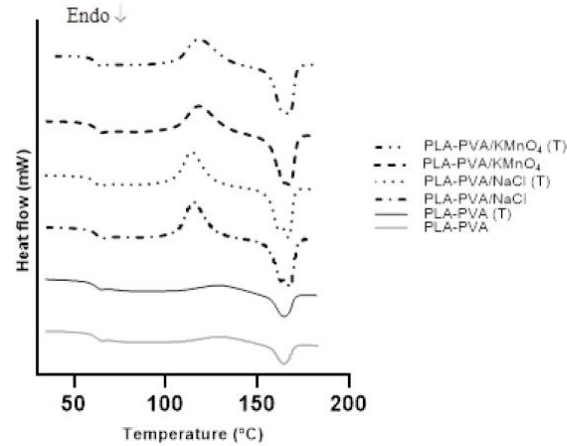


Figure 3. DSC curves of porous PLA bioscaffolds.

3.1.3. Measurement of Porosity

The study of the porosity of wound dressings is a very important factor as it affects the absorption capacity of exudates from the wound, which can reduce the probability of infection [58]. As shown in Table 2, all the bioscaffolds showed a porosity ranging between 68.1 ± 1.2 and $94.1 \pm 1.5\%$ with statistical significance ($p < 0.05$). These results indicate that the porosity was increased with the addition of the salts. A higher salt concentration led to an increase in the porous structure, resulting in an irregular and spongier shape [27]. However, the total porosity of the bioscaffolds slightly decreased after the thermal treatment [29,30,59]. The graph clearly shows that non-thermal treated bioscaffolds with the highest concentration (10 g/L) of NaCl possessed the highest porosity (94%), whereas there was a reduction of porosity (92%) for thermal treated bioscaffolds with the same concentration of NaCl. Addition of KMnO_4 to the bioscaffolds also followed the same trend as NaCl in terms of porosity. It is worth noting that the thermal treated bioscaffolds without salt (neat bioscaffolds) showed the lowest levels of porosity (68%).

Table 2. Porosity measurements of porous bioscaffolds after 24 h of immersion in ethanol at room temperature.

Sample	Untreated			After Thermal Treatment		
	PLA-PVA	PLA-PVA/ KMnO_4	PLA-PVA/NaCl	PLA-PVA	PLA-PVA/ KMnO_4	PLA-PVA/NaCl
Porosity	69.87 ± 2.1	78.77 ± 4.2	94.1 ± 1.5	68.1 ± 1.2	75 ± 0.94	92.86 ± 0.54

p value < 0.05.

3.1.4. Morphology of the Porous Bioscaffolds

The optical photographs PLA-PVA porous bioscaffolds is shown in Figure 4. PLA-PVA has a white appearance with a smooth surface. The final dimension of produced samples is a circle with a diameter of 40 mm and a thickness of 5 mm. Scanning electron microscopy (SEM) was used to investigate the effects of the addition of salts and thermal treatment on the morphology of porous bioscaffolds. As can be observed from Figure 5, the PLA-PVA bioscaffold shows a disordered, interconnected pore-like structure with a rough surface. However, high resolution SEM analysis (Figure 6a shows that the neat PLA-PVA bioscaffold has fracture-like characteristics with almost no holes or pores. The addition of 10 g/L NaCl to the bioscaffolds led to the formation of more porous structures with interconnected pores with varying pore sizes in the range of 0.2–7 μm (Figure 6b). As can be seen from Figure 6c, the addition of 0.4 mg/L KMnO_4 to the bioscaffolds led to the formation of a

porous structure in the range of 0.4–4 μm . However, comparing Figure 6b,c leads to two main observations: (1) The addition of 10 g/L NaCl to the bioscaffolds led to the formation of more porous structures compared to the addition of 0.4 mg/L KMnO_4 to the bioscaffolds; and (2) the addition of different salts led to the formation of different shapes and sizes of the pores. It is likely that the size and shape of the pores differ due to the oxidation of PVA by KMnO_4 (discussed in FT-IR analysis section) in the case of PLA-PVA/ KMnO_4 bioscaffolds. Pore formation of the bioscaffolds containing salts can be attributed to its osmotic properties in the aqueous phase, which has already been demonstrated by other authors [27,60]. The bioscaffolds that have been subjected to thermal treatment present smoother surfaces with fewer fractures and less porosity (Figure 6). These results were consistent with other studies [30,59].



Figure 4. Photographic appearance of the PLA-PVA porous bioscaffold.

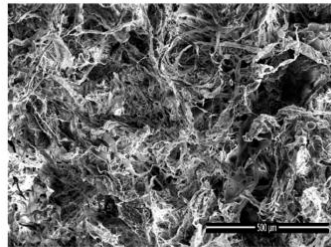


Figure 5. SEM image of PLA-PVA porous bioscaffold.

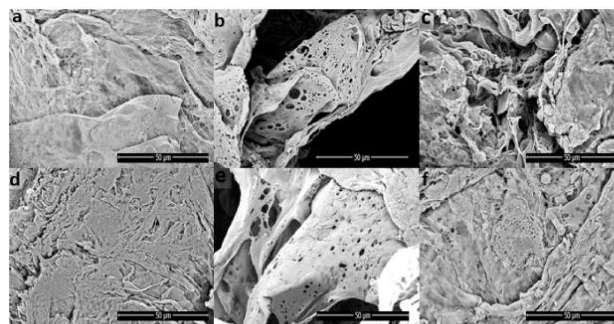


Figure 6. SEM images of the porous bioscaffolds: (a) PLA-PVA, (b) PLA-PVA/NaCl, (c) PLA-PVA/ KMnO_4 , (d) PLA-PVA (T), (e) PLA-PVA/NaCl (T), and (f) PLA-PVA/ KMnO_4 (T).

3.1.5. Swelling Test

The degree of swelling is mainly dependent on the porosity and hydrophilicity of the bioscaffolds [35,61]. This property of the bioscaffolds plays an important role in the acceleration of wound healing as it absorbs exudates and fluids secreted from the wound and provides a moist environment for the wound area [3,8]. Figure 7 shows the swelling behavior of the bioscaffolds. It was observed that increasing porosity led to an increase in the swelling degree. The highest swelling degree was obtained by the non-thermal treated PLA-PVA/NaCl bioscaffolds. This can be attributed to the high porosity percentage of PLA-PVA/NaCl compared to other bioscaffolds (Table 2). The lowest swelling degree was obtained from thermal treated neat PLA-PVA bioscaffolds due to its lowest porosity and relatively high crystallinity [62]. The higher swelling degree of thermal treated PLA-PVA/KMnO₄ bioscaffolds compared to non-thermal treated PLA-PVA/KMnO₄ bioscaffolds may be attributed to the formation of the carboxylic acid group by oxidation of PVK in the presence of KMnO₄ at an elevated temperature (80 °C). Therefore, the higher swelling degree of thermal treated PLA-PVA/KMnO₄ bioscaffolds is attributed to the higher polarity and hydrophilic character of the carboxylic acid [57,63,64]. Solvent residue analyses were performed and values of chloroform approximately 8 ppm were found.

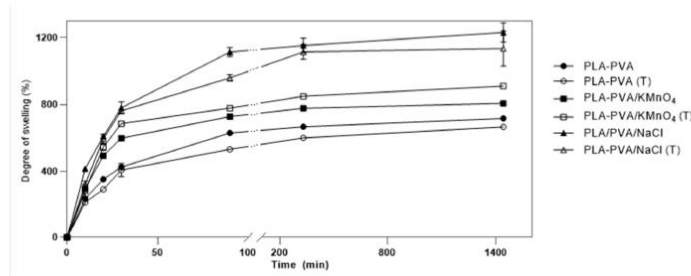


Figure 7. Swelling studies of the porous bioscaffolds in phosphate-buffered saline (PBS) with pH 7.4 at 37 °C.

3.1.6. Water Solubility

The water solubility of a polymer is a key factor in wound dressing applications, as the rate of degradation or hydrolysis takes place simultaneously with the wound healing process. If the degradation of the wound dressing occurs before the completion of the wound healing process, the wound dressing will need to be applied on the patient several times. This will not only cause discomfort but will also impose extra costs on the patient [65]. The water solubility assessment was performed by calculating the weight loss of the bioscaffolds in DI water after 24 h using Equation (4). Water solubility of the bioscaffolds ranges from 2% for thermal treated PLA-PVA and 10% for non-thermal treated PLA-PVA/NaCl as indicated in Table 3. These results reveal that water solubility increases by increasing the amount of the salts in the bioscaffolds. This increase in water solubility can be attributed to an increase in the porosity of the bioscaffolds, which is a result of the addition of salts. More porous structures allow and retain a higher number of water molecules in their structure [37,65]. It is worth noting that all the bioscaffolds kept their initial shape even after 24 h. Notably, the thermal treatment of the bioscaffolds did not significantly affect the values of water solubility.

Table 3. Water solubility measurements of the porous bioscaffolds in DI water after 24 h at 37 °C.

Sample	Untreated			After Thermal Treatment		
	PLA-PVA	PLA-PVA/KMnO ₄	PLA-PVA/NaCl	PLA-PVA	PLA-PVA/KMnO ₄	PLA-PVA/NaCl
Water solubility	4.09 ± 0.00	6.50 ± 0.20	10.87 ± 0.18	2.67 ± 0.25	7.36 ± 0.18	9.41 ± 0.50

3.1.7. Water Vapor Transmission Rate (WVTR)

Water vapor transmission rate (WVTR) is the measurement of the amount of water lost through the dressing material [58]. An ideal wound dressing material should protect the wound from dehydration, which will occur due to high WVTR. It should also protect the wound from the accumulation of exudates and the risk of bacterial growth caused by low WVTR [66,67]. To maintain a moist environment for better wound healing the optimal range of WVTR for wound dressing material is 2000–2500 (g/m²·day) [39,68]. As shown in Table 4, the measured value of WVTR of the bioscaffolds were in the range of 2115–2287 g/m²·day ($p < 0.05$). As previously mentioned, the addition of salts increased the porosity of the bioscaffolds. This increase in the porosity is the main reason for the observed increase in the values of the WVTR in PLA-PVA/NaCl and PLA-PVA/KMnO₄ bioscaffolds. The thermal treatment of the bioscaffolds did not affect the values of WVTR. The obtained WVTR results demonstrate that the bioscaffolds are suitable for wound dressing applications [39,68].

Table 4. Water vapor transmission rate of the porous bioscaffolds.

Sample	Untreated			After Thermal Treatment		
	PLA-PVA	PLA-PVA/KMnO ₄	PLA-PVA/NaCl	PLA-PVA	PLA-PVA/KMnO ₄	PLA-PVA/NaCl
WVTR	2146.01 ± 19.48	2214.16 ± 20.94	2287.61 ± 25.31	2077 ± 18.65	2207.08 ± 24.45	2259.3 ± 21.35

p value < 0.05.

3.2. In Vitro Drug Release Studies

An ideal antimicrobial wound dressing should sustain a long period of controlled drug release in order to accelerate the healing process and to avoid frequent changing of the dressing [49]. Gentamicin sulfate as an antibiotic agent was loaded into the PLA-PVA bioscaffolds. The effect of the addition of different types of salts and thermal treatment on entrapment efficiency (EE), loading capacity (LC), and in vitro were studied. Tang et al. reported that the EE of drugs in the surface liquid spraying method is higher than the EE of drugs in the traditional emulsion solvent evaporation method [18]. Therefore, the liquid spraying method was used to obtain a higher EE. As shown in Table 5, the surface liquid spraying method resulted in a high entrapment efficiency of the drug (90.11%). Furthermore, the addition of salts increased the EE. This could be attributed to the changing of the aqueous solubility of the organic solvent by salt [24,69]. This could also be explained by increasing the porosity of the bioscaffolds due to the addition of salts as mentioned in the porosity measurement section [27,70]. While the thermal treatment did not significantly impact the EE, this was not the case for the PLA-PVA/NaCl. This could be attributed to the reduced porosity of PLA-PVA/NaCl due to the thermal treatment. Table 5 demonstrates that the addition of salts and thermal treatment did not affect LC (%), which can be attributed to the strong dependency of LC on the polymer weight ratio in accordance with Equation (7).

Table 5. Encapsulation efficiency (EE) and loading capacity (LC) of the porous bioscaffolds before and after thermal treatment.

Properties	Untreated Treatment			After Thermal Treatment		
	PLA-PVA	PLA-PVA/KMnO ₄	PLA-PVA/NaCl	PLA-PVA	PLA-PVA/KMnO ₄	PLA-PVA/NaCl
EE (%)	90.11 ± 0.21	92.08 ± 0.06	97.57 ± 0.03	92.38 ± 0.49	93.52 ± 0.46	86.7 ± 0.4
LC (%)	4.5 ± 0.01	4.6 ± 0.003	4.8 ± 0.001	4.6 ± 0.02	4.7 ± 0.02	4.32 ± 0.02

p value < 0.05.

The addition of salts to the polymer has a crucial effect on the initial burst release and the porosity of the bioscaffolds. The initial burst release and the porosity of the bioscaffolds vary depending on the salt concentration [27]. The in vitro release profiles of antibiotics from the wound dressings are displayed in Figure 8. PLA-PVA/NaCl bioscaffolds exhibited

the highest initial burst release due to the highest salt concentration and porosity. The cumulative drug release was around 82%. The burst release rate during the first 24 h in PLA-PVA/NaCl bioscaffolds can be attributed to the fact that the aqueous environment washed all the drugs from the surface, and other nearby drugs were removed through the pores of the polymer matrix [70,71]. In comparison with PLA-PVA/NaCl bioscaffolds, thermal treated PLA-PVA/NaCl bioscaffolds showed an initial burst release of drugs during the first 6 h of around 11%. This clearly showed a reducing initial burst release followed by a gradual release at a decreasing rate over time, with around 50% release of the drug during 14 days. These results are consistent with the results of other groups where thermal treatment was employed as a tool for prolonging the release of the drug. Moreover, thermal treatment of polymer at temperatures above T_g reduced the drug release rate [28,72]. This can be attributed to the fact that thermal treatment increases the crystallinity of the polymer, where crystalline domains function as a physical barrier, leading to slower diffusion of the drug [31]. As a result, thermal treatment of the PLA-PVA/NaCl bioscaffolds cause the sustained release of GS. However, due to the heating of the bioscaffolds above T_g (80 °C), the drug release rate was reduced.

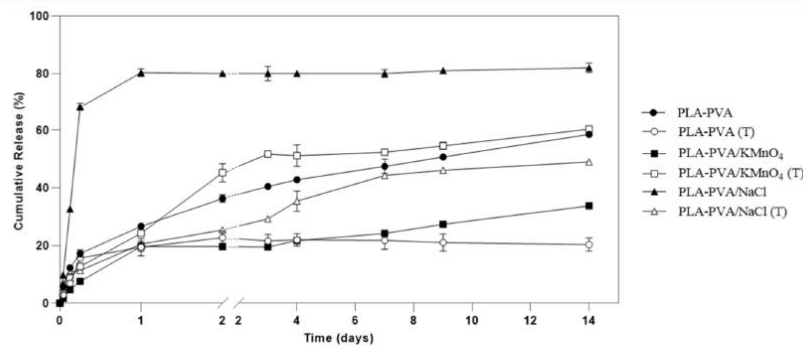


Figure 8. In vitro release profiles of porous bioscaffolds loaded gentamicin sulfate (GS) in pH 7.4 at 37 °C.

As shown in Figure 8, for PLA-PVA/KMnO₄ bioscaffolds, the initial burst release of drugs during the first 24 h was only approximately 20%, followed by a gradual and constant release of GS over 14 days. The cumulative drug release was 33%. However, thermal treated PLA-PVA/KMnO₄ bioscaffolds showed an initial burst release of around 12% during the first 6 h, followed by a fast sustained release profile around 61% over 14 days. As can be seen in the figure, the cumulative drug release rate of heat treated PLA-PVA/KMnO₄ bioscaffolds had a higher release rate in comparison with PLA-PVA/KMnO₄ bioscaffolds. This could be explained by the formation of PVK as the result of the interaction between KMnO₄ and PVA. The thermal treating of PLA-PVA/KMnO₄ bioscaffolds caused partial oxidation of the formed PVK by KMnO₄, and resulted in the formation of carboxylic acid groups. Carboxylic acids have a higher polarity and hydrophilic character in comparison with ketones (PVK) [57,63,64]. Therefore, thermally treated PLA-PVA/KMnO₄ bioscaffolds have a relatively higher hydrophilicity as compared to non-thermal treated PLA-PVA/KMnO₄ bioscaffolds. This higher hydrophilicity causes PBS to permeate more freely into thermal treated PLA-PVA/KMnO₄ bioscaffolds than it can permeate into the PLA-PVA/KMnO₄ bioscaffolds. Hence, although thermal treatment of the PLA-PVA/KMnO₄ bioscaffolds led to a decrease in porosity, its higher relative hydrophilic character caused the higher cumulative release rate.

For the neat PLA-PVA bioscaffolds, the initial burst release occurred during the first 6 h followed by a slow and gradual release at around 58% over 14 days (Figure 8). The thermally treated neat PLA-PVA bioscaffolds exhibited the initial burst release in the first 6 h at around 14% while the cumulative drug release was 20%. This means that the thermally

treated neat PLA-PVA bioscaffolds could not release the drugs and kept the drug inside the bioscaffolds. This can be attributed to the less porous structure and relatively higher crystallinity of the bioscaffolds [73].

4. Conclusions

Polymeric porous bioscaffolds of PLA-PVA were prepared in this study by a slightly modified form of surface liquid spraying method. The effects of the addition of different salts (NaCl and KMnO_4) and thermal treatment (80 °C for 2 min) on the bioscaffolds were investigated. The SEM results indicated that prepared bioscaffolds had interconnected porous structures and the addition of salts considerably enhanced the porosity of the bioscaffolds. Moreover, the swelling degree and water solubility of bioscaffolds were increased due to the increase in porosity. The *in vitro* release of gentamicin sulfate was studied and it was shown that a higher entrapment efficiency and initial burst release was achieved by the addition of salt to the aqueous phase. Additionally, the thermal treatment of the polymer above T_g reduced the initial burst release and prolonged the release of the drug. Finally, it worth noting that the procedure suggested in this study to prepare bioscaffolds is cost-efficient and non-toxic, since all the solvents can be easily and completely removed. Therefore, the novel PLA-PVA bioscaffolds developed in this work could be a potential candidate for wound dressing applications in the future.

Author Contributions: Conceptualization, M.A.M.; methodology, M.A.M. and A.D.M.; validation, M.A.M., T.Š., H.F., J.C. and M.P.; formal analysis, M.A.M.; investigation, M.A.M.; data curation, M.A.M.; writing—original draft preparation, M.A.M.; writing—review and editing, M.A.M. and V.S.; supervision, V.S.; project administration, M.A.M.; funding acquisition, V.S. All authors have read and agreed to the published version of the manuscript.

Funding: This research was funded by the Ministry of Education, Youth, and Sports of the Czech Republic (grant no. RP/CPS/2020/002), and the Internal Grant Agency of TBU in Zlín (grant No. IGA/CPS/2020/002).

Institutional Review Board Statement: Not applicable.

Informed Consent Statement: Not applicable.

Data Availability Statement: Not applicable.

Conflicts of Interest: The authors declare no conflict of interest.

References

1. Boateng, J.S.; Matthews, K.H.; Stevens, H.N.; Eccleston, G.M. Wound Healing Dressings and Drug Delivery Systems: A Review. *J. Pharm. Sci.* **2008**, *97*, 2892–2923. [[CrossRef](#)]
2. Zilberman, M.; Egozi, D.; Shemesh, M.; Keren, A.; Mazor, E.; Baranes-Zeevi, M.; Goldstein, N.; Berdicevsky, I.; Gilhar, A.; Ullmann, Y. Hybrid wound dressings with controlled release of antibiotics: Structure-release profile effects and *in vivo* study in a guinea pig burn model. *Acta Biomater.* **2015**, *22*, 155–163. [[CrossRef](#)]
3. Lin, Z.; Wu, T.; Wang, W.; Li, B.; Wang, M.; Chen, L.; Xia, H.; Zhang, T. Biofunctions of antimicrobial peptide-conjugated alginate/hyaluronic acid/collagen wound dressings promote wound healing of a mixed-bacteria-infected wound. *Int. J. Biol. Macromol.* **2019**, *140*, 330–342. [[CrossRef](#)]
4. Shemesh, M.; Zilberman, M. Structure–property effects of novel bioresorbable hybrid structures with controlled release of analgesic drugs for wound healing applications. *Acta Biomater.* **2014**, *10*, 1380–1391. [[CrossRef](#)]
5. Zou, F.; Sun, X.; Wang, X. Elastic, hydrophilic and biodegradable poly (1, 8-octanediol-co-citric acid)/polylactic acid nanofibrous membranes for potential wound dressing applications. *Polym. Degrad. Stab.* **2019**, *166*, 163–173. [[CrossRef](#)]
6. Ghafari, R.; Scaffaro, R.; Maio, A.; Gulino, E.F.; Re, G.L.; Jonoobi, M. Processing-structure-property relationships of electrospun PLA-PEO membranes reinforced with enzymatic cellulose nanofibers. *Polym. Test.* **2020**, *81*, 106182. [[CrossRef](#)]
7. Zhang, Y.; Wu, X.; Han, Y.; Mo, F.; Duan, Y.; Li, S. Novel thymopentin release systems prepared from bioresorbable PLA-PEG-PLA hydrogels. *Int. J. Pharm.* **2010**, *386*, 15–22. [[CrossRef](#)]
8. Gomaa, S.F.; Madkour, T.M.; Moghannem, S.; El-Sherbiny, I.M. New polylactic acid/ cellulose acetate-based antimicrobial interactive single dose nanofibrous wound dressing mats. *Int. J. Biol. Macromol.* **2017**, *105*, 1148–1160. [[CrossRef](#)]
9. Park, J.-Y.; Lee, I.-H. Controlled release of ketoprofen from electrospun porous polylactic acid (PLA) nanofibers. *J. Polym. Res.* **2011**, *18*, 1287–1291. [[CrossRef](#)]

10. Inphonlek, S.; Niamsiri, N.; Sunintaboon, P.; Sirisinha, C. Chitosan/xanthan gum porous scaffolds incorporated with in-situ-formed poly(lactic acid) particles: Their fabrication and ability to adsorb anionic compounds. *Colloids Surf. A Physicochem. Eng. Asp.* **2020**, *603*, 125263. [[CrossRef](#)]
11. Bi, H.; Feng, T.; Li, B.; Han, Y. In Vitro and In Vivo Comparison Study of Electrospun PLA and PLA/PVA/SA Fiber Membranes for Wound Healing. *Polymers* **2020**, *12*, 839. [[CrossRef](#)]
12. Liu, Y.; Wei, H.; Wang, Z.; Li, Q.; Tian, N. Simultaneous Enhancement of Strength and Toughness of PLA Induced by Miscibility Variation with PVA. *Polymers* **2018**, *10*, 1178. [[CrossRef](#)]
13. Augustine, R.; Zahid, A.A.; Hasan, A.; Wang, M.; Webster, T.J. CTGF loaded electrospun dual porous core-shell membrane for diabetic wound healing. *Int. J. Nanomed.* **2019**, *14*, 8573. [[CrossRef](#)]
14. Ribba, L.; Tamayo, L.; Flores, M.; Riveros, A.; Kogan, M.J.; Cerda, E.; Goyanes, S. Asymmetric biphasic hydrophobic/hydrophilic poly(lactic acid)-polyvinyl alcohol meshes with moisture control and noncytotoxic effects for wound dressing applications. *J. Appl. Polym. Sci.* **2019**, *136*, 47369. [[CrossRef](#)]
15. Bhattarai, R.S.; Das, A.; Alzhrani, R.M.; Kang, D.; Bhaduri, S.B.; Boddu, S.H. Comparison of electrospun and solvent cast polylactic acid (PLA)/poly(vinyl alcohol)(PVA) inserts as potential ocular drug delivery vehicles. *Mater. Sci. Eng. C* **2017**, *77*, 895–903. [[CrossRef](#)]
16. Cardea, S.; Baldino, L.; Scognamiglio, M.; Reverchon, E. 3D PLLA/Ibuprofen composite scaffolds obtained by a supercritical fluids assisted process. *J. Mater. Sci. Mater. Med.* **2014**, *25*, 989–998. [[CrossRef](#)]
17. Sujka, W.; Draczynski, Z.; Kolesinska, B.; Latanska, I.; Jastrzebski, Z.; Rybak, Z.; Zywicka, B. Influence of Porous Dressings Based on Butyric-Acetic Chitin Co-Polymer on Biological Processes In Vitro and In Vivo. *Materials* **2019**, *12*, 970. [[CrossRef](#)]
18. Tang, H.; Xu, N.; Meng, J.; Wang, C.; Nie, S.F.; Pan, W.S. Application of a novel approach to prepare biodegradable polylactic-co-glycolic acid microspheres: Surface liquid spraying. *Yakugaku Zasshi* **2007**, *127*, 1851–1862. [[CrossRef](#)]
19. Tang, H.; Xu, N.; Meng, J.; Wang, C.; Nie, S.F.; Pan, W. Optimization of a novel method: Surface liquid spraying to prepare poly(D, L-lactide-co-glycolide) microspheres using central composite design experiment. *J. Anal. Bio-Sci.* **2008**, *31*, 283–290.
20. Qian, L.; Zhang, H. Controlled freezing and freeze drying: A versatile route for porous and micro-/nano-structured materials. *J. Chem. Technol. Biotechnol.* **2011**, *86*, 172–184. [[CrossRef](#)]
21. do Vale Moraes, A.R.; do Nascimento Alencar, É.; Júnior, F.H.X.; De Oliveira, C.M.; Marcelino, H.R.; Barratt, G.; Fessi, H.; Do Egito, E.S.T.; Elaissari, A. Freeze-drying of emulsified systems: A review. *Int. J. Pharm.* **2016**, *503*, 102–114. [[CrossRef](#)]
22. Ali, M.; Walboomers, X.F.; Jansen, J.A.; Yang, F. Influence of formulation parameters on encapsulation of doxycycline in PLGA microspheres prepared by double emulsion technique for the treatment of periodontitis. *J. Drug Deliv. Sci. Technol.* **2019**, *52*, 263–271. [[CrossRef](#)]
23. Molavi, F.; Barzegar-Jalali, M.; Hamishehkar, H. Polyester based polymeric nano and microparticles for pharmaceutical purposes: A review on formulation approaches. *J. Control. Release* **2020**, *320*, 265–282. [[CrossRef](#)]
24. Dinarvand, R.; Moghadam, S.H.; Sheikhi, A.; Atyabi, F. Effect of surfactant HLB and different formulation variables on the properties of poly-D,L-lactide microspheres of naltrexone prepared by double emulsion technique. *J. Microencapsul.* **2005**, *22*, 139–151. [[CrossRef](#)]
25. Yin, W.; Yates, M. Encapsulation and sustained release from biodegradable microcapsules made by emulsification/freeze drying and spray/freeze drying. *J. Colloid Interface Sci.* **2009**, *336*, 155–161. [[CrossRef](#)]
26. Ong, Y.X.J.; Lee, L.Y.; Davoodi, P.; Wang, C.H. Production of drug-releasing biodegradable microporous scaffold using a two-step micro-encapsulation/supercritical foaming process. *J. Supercrit. Fluids* **2018**, *133*, 263–269. [[CrossRef](#)]
27. Pistel, K.F.; Kissel, T. Effects of salt addition on the microencapsulation of proteins using W/O/W double emulsion technique. *J. Microencapsul.* **2000**, *17*, 467–483.
28. Azarmi, S.; Ghaffari, F.; Löbenberg, R.; Nokhodchi, A. Mechanistic evaluation of the effect of thermal-treating on Eudragit RS matrices. *Il Farm.* **2005**, *60*, 925–930. [[CrossRef](#)]
29. Billa, N.; Yuen, K.-H.; Peh, K.-K. Diclofenac Release from Eudragit-Containing Matrices and Effects of Thermal Treatment. *Drug Dev. Ind. Pharm.* **1998**, *24*, 45–50. [[CrossRef](#)] [[PubMed](#)]
30. Azarmi, S.; Farid, J.; Nokhodchi, A.; Bahari-Saravi, S.M.; Valizadeh, H. Thermal treating as a tool for sustained release of indomethacin from Eudragit RS and RL matrices. *Int. J. Pharm.* **2002**, *246*, 171–177. [[CrossRef](#)]
31. Castro, A.G.; Löwik, D.W.; van Steenberg, M.J.; Jansen, J.A.; van den Beucken, J.J.; Yang, F. Incorporation of simvastatin in PLLA membranes for guided bone regeneration: Effect of thermal treatment on simvastatin release. *RSC Adv.* **2018**, *8*, 28546–28554. [[CrossRef](#)]
32. Delgado-Enciso, I.; Madrigal-Perez, V.M.; Lara-Esqueda, A.; Diaz-Sanchez, M.G.; Guzman-Esquivel, J.; Rosas-Vizcaino, L.E.; Soriano Hernández, A.D. Topical 5% potassium permanganate solution accelerates the healing process in chronic diabetic foot ulcers. *Biomed. Rep.* **2018**, *8*, 156–159. [[CrossRef](#)]
33. Hollingworth, H. Professional concerns in wound care: A discussion of questionable practice recorded by nurses. *Br. J. Community Nurs.* **2002**, *7* (Suppl. 2), 36–42. [[CrossRef](#)]
34. Amini Moghaddam, M.; Stloukal, P.; Kucharczyk, P.; Tow-Swiątek, A.; Garbacz, T.; Pummerova, M.; Klepka, T.; Sedlářik, V. Microcellular antibacterial polylactide-based systems prepared by additive extrusion with ALUM. *Polym. Adv. Technol.* **2019**, *30*, 2100–2108. [[CrossRef](#)]

35. Gonzaga, V.D.A.; Poli, A.L.; Gabriel, J.S.; Tezuka, D.Y.; Valdes, T.A.; Leitão, A.; Rodero, C.F.; Bauab, T.M.; Chorilli, M.; Schmitt, C.C. Chitosan-laponite nanocomposite scaffolds for wound dressing application. *J. Biomed. Mater. Res. Part B Appl. Biomater.* **2020**, *108*, 1388–1397. [[CrossRef](#)] [[PubMed](#)]
36. Cai, N.; Li, C.; Han, C.; Luo, X.; Shen, L.; Xue, Y.; Yu, F. Tailoring mechanical and antibacterial properties of chitosan/gelatin nanofiber membranes with Fe₃O₄ nanoparticles for potential wound dressing application. *Appl. Surf. Sci.* **2016**, *369*, 492–500. [[CrossRef](#)]
37. Kavooosi, G.; Dadfar, S.M.M.; Purfard, A.M. Mechanical, physical, antioxidant, and antimicrobial properties of gelatin films incorporated with thymol for potential use as nano wound dressing. *J. Food Sci.* **2013**, *78*, E244–E250. [[CrossRef](#)]
38. De Cicco, F.; Porta, A.; Sansone, F.; Aquino, R.P.; Del Gaudio, P. Nanospray technology for an in situ gelling nanoparticulate powder as a wound dressing. *Int. J. Pharm.* **2014**, *473*, 30–37. [[CrossRef](#)]
39. Adeli, H.; Khorasani, M.T.; Parvazinia, M. Wound dressing based on electrospun PVA/chitosan/starch nanofibrous mats: Fabrication, antibacterial and cytocompatibility evaluation and in vitro healing assay. *Int. J. Biol. Macromol.* **2019**, *122*, 238–254. [[CrossRef](#)]
40. Motiei, M.; Sedlařík, V.; Lucia, L.A.; Fei, H.; Münster, L. Stabilization of chitosan-based polyelectrolyte nanoparticle cargo delivery biomaterials by a multiple ionic cross-linking strategy. *Carbohydr. Polym.* **2020**, *231*, 115709. [[CrossRef](#)] [[PubMed](#)]
41. Smelá, D.; Pechová, P.; Komprda, T.; Klejduš, B.; Kubán, V. Chromatographic determination of biogenic amines in meat products during fermentation and long-term storage. *Chem. Listy* **2004**, *98*. [[CrossRef](#)]
42. Li, T.T.; Zhang, Y.; Ling, L.; Lin, M.C.; Wang, Y.; Wu, L.; Lin, J.H.; Lou, C.W. Manufacture and characteristics of HA-Electrodeposited polylactic acid/polyvinyl alcohol biodegradable braided scaffolds. *J. Mech. Behav. Biomed. Mater.* **2020**, *103*, 103555. [[CrossRef](#)] [[PubMed](#)]
43. Li, T.T.; Ling, L.; Lin, M.C.; Jiang, Q.; Lin, Q.; Lin, J.H.; Lou, C.W. Properties and Mechanism of Hydroxyapatite Coating Prepared by Electrodeposition on a Braid for Biodegradable Bone Scaffolds. *Nanomaterials* **2019**, *9*, 679. [[CrossRef](#)]
44. Abdullah, O.G.; Aziz, S.B.; Rasheed, M.A. Structural and optical characterization of PVA:KMnO₄ based solid polymer electrolyte. *Results Phys.* **2016**, *6*, 1103–1108. [[CrossRef](#)]
45. Hassan, R.M.; Abd-Alla, M.A. New coordination polymers. Part 1.—Novel synthesis of poly (vinyl ketone) and characterization as chelating agent. *J. Mater. Chem.* **1992**, *2*, 609–611. [[CrossRef](#)]
46. Ali, H.E. A novel optical limiter and UV-Visible filters made of Poly (vinyl alcohol)/KMnO₄ polymeric films on glass-based substrate. *J. Mater. Sci. Mater. Electron.* **2019**, *30*, 7043–7053. [[CrossRef](#)]
47. Dai, L.; Ukai, K.; Shaheen, S.M.; Yamaura, K. Gelation of a new hydrogel system of atactic-poly(vinyl alcohol)/NaCl/H₂O. *Polym. Int.* **2002**, *51*, 715–720. [[CrossRef](#)]
48. Yang, H.; Xu, S.; Jiang, L.; Dan, Y. Thermal decomposition behavior of poly (vinyl alcohol) with different hydroxyl content. *J. Macromol. Sci. Part B* **2012**, *51*, 464–480. [[CrossRef](#)]
49. Zhang, D.; Zhou, W.; Wei, B.; Wang, X.; Tang, R.; Nie, J.; Wang, J. Carboxyl-modified poly(vinyl alcohol)-crosslinked chitosan hydrogel films for potential wound dressing. *Carbohydr. Polym.* **2015**, *125*, 189–199. [[CrossRef](#)]
50. Doménech-Carbó, M.T.; Yusá-Marco, D.J.; Bitossi, G.; Silva, M.F.; Mas-Barberá, X.; Osete-Cortina, L. Study of ageing of ketone resins used as picture varnishes by FTIR spectroscopy, UV-Vis spectrophotometry, atomic force microscopy and scanning electron microscopy X-ray microanalysis. *Anal. Bioanal. Chem.* **2008**, *391*, 1351–1359. [[CrossRef](#)] [[PubMed](#)]
51. Daoud, S.; Bou-Maroun, E.; Dujourdy, L.; Waschatko, G.; Billecke, N.; Cayot, P. Fast and direct analysis of oxidation levels of oil-in-water emulsions using ATR-FTIR. *Food Chem.* **2019**, *293*, 307–314. [[CrossRef](#)] [[PubMed](#)]
52. Chelliah, A.; Subramaniam, M.; Gupta, R.; Gupta, A. Evaluation on the thermo-oxidative degradation of PET using prodegradant additives. *Indian J. Sci. Technol.* **2017**, *10*, 2–5. [[CrossRef](#)]
53. Omelczuk, M.O.; McGinity, J.W. The Influence of Thermal Treatment on the Physical-Mechanical and Dissolution Properties of Tablets Containing Poly(DL-Lactic Acid). *Pharm. Res.* **1993**, *10*, 542–548. [[CrossRef](#)]
54. Yin, H.M.; Qian, J.; Zhang, J.; Lin, Z.F.; Li, J.S.; Xu, J.Z.; Li, Z.M. Engineering Porous Poly(lactic acid) Scaffolds with High Mechanical Performance via a Solid State Extrusion/Porogen Leaching Approach. *Polymers* **2016**, *8*, 213. [[CrossRef](#)] [[PubMed](#)]
55. Sabino, M.A. Oxidation of polycaprolactone to induce compatibility with other degradable polyesters. *Polym. Degrad. Stab.* **2007**, *92*, 986–996. [[CrossRef](#)]
56. Stocco, E.; Barbon, S.; Grandi, F.; Gamba, P.G.; Borgio, L.; Del Gaudio, C.; Grandi, C. Partially oxidized polyvinyl alcohol as a promising material for tissue engineering. *J. Tissue Eng. Regen. Med.* **2017**, *11*, 2060–2070. [[CrossRef](#)]
57. Ranganath, M.; Patil, R.V.; Lobo, B. Morphological modifications in potassium permanganate doped poly (vinyl alcohol) films. In Proceedings of the International Workshop on Applications of Nanotechnology to Energy, Environment and Biotechnology (NANOEEB), Karnataka, India, 14–16 December 2010.
58. Poonguzhali, R.; Basha, S.K.; Kumari, V.S. Novel asymmetric chitosan/PVP/nanocellulose wound dressing: In vitro and in vivo evaluation. *Int. J. Biol. Macromol.* **2018**, *112*, 1300–1309. [[CrossRef](#)]
59. Hasanzadeh, D.; Ghaffari, S.; Monajjemzadeh, F.; Al-Hallak, M.K.; Soltani, G.; Azarmi, S. Thermal Treating of Acrylic Matrices as a Tool for Controlling Drug Release. *Chem. Pharm. Bull.* **2009**, *57*, 1356–1362. [[CrossRef](#)]
60. Ungaro, F.; De Rosa, G.; Miro, A.; Quaglia, F.; La Rotonda, M.I. Cyclodextrins in the production of large porous particles: Development of dry powders for the sustained release of insulin to the lungs. *Eur. J. Pharm. Sci.* **2006**, *28*, 423–432. [[CrossRef](#)]
61. Archana, D.; Dutta, J.; Dutta, P.K. Evaluation of chitosan nano dressing for wound healing: Characterization, in vitro and in vivo studies. *Int. J. Biol. Macromol.* **2013**, *57*, 193–203. [[CrossRef](#)] [[PubMed](#)]

62. Pantani, R.; Sorrentino, A. Influence of crystallinity on the biodegradation rate of injection-moulded poly(lactic acid) samples in controlled composting conditions. *Polym. Degrad. Stab.* **2013**, *98*, 1089–1096. [[CrossRef](#)]
63. Ivanets, A.I.; Prozorovich, V.G.; Krivoschapina, E.F.; Kuznetsova, T.F.; Krivoschapkin, P.V.; Katsoshvili, L.L. Physicochemical properties of manganese oxides obtained via the sol–gel method: The reduction of potassium permanganate by polyvinyl alcohol. *Russ. J. Phys. Chem. A* **2017**, *91*, 1486–1492. [[CrossRef](#)]
64. McMurry, J.E. *Organic Chemistry*; Cengage Learning: Boston, MA, USA, 2015.
65. Koosehgo, S.; Ebrahimian-Hosseiniabadi, M.; Alizadeh, M.; Zamanian, A. Preparation and characterization of in situ chitosan/polyethylene glycol fumarate/thymol hydrogel as an effective wound dressing. *Mater. Sci. Eng. C* **2017**, *79*, 66–75. [[CrossRef](#)]
66. Akhavan-Kharazian, N.; Izadi-Vasafi, H. Preparation and characterization of chitosan/gelatin/nanocrystalline cellulose/calcium peroxide films for potential wound dressing applications. *Int. J. Biol. Macromol.* **2019**, *133*, 881–891. [[CrossRef](#)] [[PubMed](#)]
67. Alippilakkotte, S.; Kumar, S.; Sreejith, L. Fabrication of PLA/Ag nanofibers by green synthesis method using Momordica charantia fruit extract for wound dressing applications. *Colloids Surf. A Physicochem. Eng. Asp.* **2017**, *529*, 771–782. [[CrossRef](#)]
68. Khorasani, M.T.; Joorabloo, A.; Moghaddam, A.; Shamsi, H.; MansooriMoghadam, Z. Incorporation of ZnO nanoparticles into heparinised polyvinyl alcohol/chitosan hydrogels for wound dressing application. *Int. J. Biol. Macromol.* **2018**, *114*, 1203–1215. [[CrossRef](#)]
69. Al-Maaieh, A.; Flanagan, D.R. Salt and cosolvent effects on ionic drug loading into microspheres using an O/W method. *J. Control. Release* **2001**, *70*, 169–181. [[CrossRef](#)]
70. Al-Sokanee, Z.N.; Toabi, A.A.H.; Al-Assadi, M.J.; Alassadi, E.A. The Drug Release Study of Ceftriaxone from Porous Hydroxyapatite Scaffolds. *AAPS PharmSciTech* **2009**, *10*, 772–779. [[CrossRef](#)]
71. Zare, M.; Mobedi, H.; Barzin, J.; Mivehchi, H.; Jamshidi, A.; Mashayekhi, R. Effect of additives on release profile of leuprolide acetate in an in situ forming controlled-release system: In vitro study. *J. Appl. Polym. Sci.* **2008**, *107*, 3781–3787. [[CrossRef](#)]
72. Javadzadeh, Y.; Musaalrezaei, L.; Nokhodchi, A. Liquesolid technique as a new approach to sustain propranolol hydrochloride release from tablet matrices. *Int. J. Pharm.* **2008**, *362*, 102–108. [[CrossRef](#)]
73. Tamboli, V.; Mishra, G.P.; Mitra, A.K. Novel pentablock copolymer (PLA–PCL–PEG–PCL–PLA)-based nanoparticles for controlled drug delivery: Effect of copolymer compositions on the crystallinity of copolymers and in vitro drug release profile from nanoparticles. *Colloid Polym. Sci.* **2013**, *291*, 1235–1245. [[CrossRef](#)] [[PubMed](#)]